Understanding Phosphorylation-Mediated Changes in the Subcellular Localization and Functioning of Siah2 Protein in the Context of *Helicobacter pylori*-Mediated Gastric Cancer

By
Pragyesh Dixit

Enrolment No LIFE11201404007

National Institute of Science Education and Research (NISER)

Bhubaneswar

A thesis submitted to the

Board of Studies in Life Sciences

In partial fulfillment of requirements

for the Degree of
DOCTOR OF PHILOSOPHY

of

HOMI BHABHA NATIONAL INSTITUTE

May, 2021

Homi Bhabha National Institute

Recommendations of the Viva Voce Committee

As members of the Viva Voce Committee, we certify that we have read the dissertation prepared by Pragyesh Dixit entitled "Understanding Phosphorylation-Mediated Changes in the Subcellular Localization and Functioning of Siah2 Protein in the Context of *Helicobacter pylori*-Mediated Gastric Cancer" and recommend that it may be accepted as fulfilling the thesis requirement for the award of Degree of Doctor of Philosophy.

|		
Chairman – Dr. Chandan Goswami		24.09.2021
Guide / Convener – Dr. Asima Bhattacharyya		24.09.2021
Examiner - Prof. Snehasikta Swarnakar		24/09/2021
Member 1- Dr. Subhasis Chattopadhyay		24/09/2021
Member 2- Dr. Harapriya Mohapatra		24.09.2021
External Member- Prof. Jagneshwar Dandapat		24/09/2021
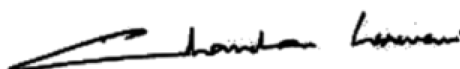
Final approval and acceptance of this thesis is contingent upon the candidate's submission of the final copies of the thesis to HBNI.

I/We hereby certify that I/we have read this thesis prepared under my/our direction and recommend that it may be accepted as fulfilling the thesis requirement.

Date: 24.09.2021   Dr. Asima Bhattacharyya

Place: NISER, Bhubaneswar   Guide

STATEMENT BY AUTHOR

This dissertation has been submitted in partial fulfillment of requirements for an advanced degree at Homi Bhabha National Institute (HBNI) and is deposited in the Library to be made available to borrowers under rules of the HBNI.

Brief quotations from this dissertation are allowable without special permission, provided that accurate acknowledgement of source is made. Requests for permission for extended quotation from or reproduction of this manuscript in whole or in part may be granted by the Competent Authority of HBNI when in his or her judgment the proposed use of the material is in the interests of scholarship. In all other instances, however, permission must be obtained from the author.

Pragyesh Dixit

DECLARATION

I, hereby declare that the investigation presented in the thesis has been carried out by me. The work is original and has not been submitted earlier as a whole or in part for a degree / diploma at this or any other Institution / University.

Pragyesh Dixit

Certificate

This is to certify that the thesis entitled "**Understanding phosphorylation-mediated changes in the subcellular localization and functioning of Siah2 protein in the context of *Helicobacter pylori*-mediated gastric cancer**", which is being submitted by Mr. Pragyesh Dixit in partial fulfilment of the degree of Doctor of Philosophy (PhD) in Life Sciences of Homi Bhabha National Institute is a record of his own research work carried by him. He has carried out his research for the last seven years on the subject matter of the thesis under my supervision at National Institute of Science Education and Research (NISER), Bhubaneswar.

To the best of our knowledge, the matter embodied in this thesis has not been submitted for the award of any other degree.

Signature of the Candidate

Pragyesh Dixit
National Institute of Science
Education and Research (NISER)
Bhubaneswar

Signature of the Supervisor

Dr. Asima Bhattacharyya
Associate Professor
National Institute of Science
Education and Research (NISER)
Bhubaneswar

List of Publications arising from the thesis

Journals

Research Articles:

1. *Helicobacter pylori*-induced gastric cancer is orchestrated by MRCKβ-mediated Siah2 phosphorylation. **Dixit P**, Kokate SB, Poirah I, Chakraborty D, Smoot DT, Ashktorab H, Rout N, Singh SP, Bhattacharyya A. J Biomed Sci. 2021 Feb; 28: 12.

2. *Siah2-GRP78 interaction regulates ROS and provides a proliferative advantage to *Helicobacter pylori*-infected gastric epithelial cancer cells. **Dixit P**, Suratkal SS, Chakraborty D, Poirah I, Samal S, Rout N, Singh SP, Sarkar A & Bhattacharyya A. (Under review, Molecular Oncology).

3. Testin and Filamin-C downregulation by acetylated Siah2 increases invasiveness of *Helicobacter pylori*-infected gastric cancer cells. Kokate SB, **Dixit P**, Poirah I, Roy AD, Chakraborty D, Rout N, Singh SP, Ashktorab H, Smoot DT, Bhattacharyya A. Int J Biochem Cell Biol. 2018 Oct; 103:14-24.

4. Acetylation-mediated Siah2 stabilization enhances PHD3 degradation in *Helicobacter pylori*-infected gastric epithelial cancer cells. Kokate SB, **Dixit P**, Das L, Rath S, Roy AD, Poirah I, Chakraborty D, Rout N, Singh SP, Bhattacharyya A. FASEB J 2018 Oct; 32 (10): 5378-5389.

5. Membrane-bound β-catenin degradation is enhanced by ETS2-mediated Siah1 induction in *Helicobacter pylori*-infected gastric cancer cells. Das L, Kokate SB, **Dixit P**, Rath S, Rout N, Singh SP, Crowe SE, Bhattacharyya A. Oncogenesis (Springer Nature) (2017) 6, e327; doi:10.oncsis.2017.26.

6. Inhibition of histone/lysine acetyltransferase activity kills CoCl2-treated and hypoxia-exposed gastric cancer cells and reduces their invasiveness. Rath S, Das L, Kokate SB, Ghosh

N, **Dixit P**, Rout N, Singh SP, Chattopadhyay S, Ashktorab H, Smoot DT, Swamy MM, Kundu TK, Crowe, SE, Bhattacharyya A. Int J Biochem Cell Biol. 2017 Jan; 82:28-40.

7. Cobalt chloride-mediated protein kinase Cα (PKCα) phosphorylation induces hypoxia-inducible factor 1α (HIF1α) in the nucleus of gastric cancer cell. Rath S, Anand A, Ghosh N, Das L, Kokate SB, **Dixit P**, Majhi S, Rout N, Singh SP, Bhattacharyya A. Biochem Biophys Res Commun. 2016 Feb 26; 471(1):205-12.

Invited Review Article:

1. Silent hypoxia in COVID-19: a gut microbiota connection. Gopal AB, Chakraborty S, Padhan PK, Barik A, **Dixit P**, Chakraborty D, Poirah I, Samal S, Sarkar A & Bhattacharyya A. Current Opinion in Physiology 2021 Oct; 23:100456.

Invited Book Chapter:

1. *Analysis of the effect of HAT/KAT inhibition on Siah2-mediated reactive oxygen species generation in Helicobacter pylori-infected gastric epithelial cells. Rath S^, **Dixit P^**, Kokate SB^, Das L, Chakraborty D & Bhattacharyya A. (To be communicated to Methods in Molecular Biology, Springer Nature).

Conferences:

1. Association between CEACAMs and hypoxia defines gastric cancer progression". I Poirah, D Chakraborty, **P Dixit**, S Samal, PK Padhan, A Barik, SP Singh, BB Singer and A Bhattacharyya, AACR Annual Meeting 2021; April 10-15, 2021 and May 17-21, 2021; Philadelphia, USA.

2. *Helicobacter pylori*-mediated gastric cancer: at the crossroads between hypoxia and inflammation. AD Roy, I Poirah, D Chakraborty, **P Dixit**, A Singh, SP Singh and A Bhattacharyya, 17th International Congress of Immunology, Beijing, China,19-23 Oct 2019.

3. *Helicobacter pylori* increases reactive oxygen species burden of infected gastric epithelial cells via involvement of Siah proteins. **P Dixit**[#], SB Kokate, I Poirah, AD Roy, D Chakraborty,

N Rout, SP Singh and A Bhattacharyya, 14th Indo Australian Biotechnology Conference, ACTREC, Navi Mumbai, India, 22-23 Oct 2018.

4. Generation of reactive oxygen species in *Helicobacter pylori*-infected gastric epithelial cells is associated with Siah proteins. **P Dixit**, SB Kokate, I Poirah, AD Roy, D Chakraborty, N Rout, SP Singh and A Bhattacharyya, 4th International Conference on Translational Research, Goa, India, 11-13 Oct 2018.

5. Siah2 acetylation regulates invasiveness of *Helicobacter pylori*-infected human gastric epithelial cells. SB Kokate, **P Dixit**, L Das, S Rath, AD Roy, I Poirah, D Chakraborty, N Rout, SP Singh and A Bhattacharyya, 13th National Research Scholars Meet (13th NRSM-2017, OP-01), ACTREC, Mumbai, India.

*Pertaining to the thesis, #Awarded a prize for poster presentation, ^Equal contributions.

Pragyesh Dixit

DEDICATIONS

This work is dedicated to my family and loved ones.

ACKNOWLEDGEMENTS

CONTENTS

SUMMARY

Helicobacter pylori infection is the prime cause of gastric cancer (GC), one of the most common malignancies of the world. *H. pylori*-induced signalling pathways modulate the outcome of GC. Siah2, a RING E3-ubiquitin ligase, is upregulated by *H. pylori* infection and leads to enhanced invasiveness and tumorigenicity of the infected gastric epithelial cells (GECs). Posttranslational modifications of Siah2 regulate its subcellular localization and functioning. Albeit, the role of acetylated Siah2 in *H. pylori*-infected GECs has been elucidated, the impact of *H. pylori*-induced phosphorylation remained unknown. Thus, this thesis aimed to explore the role of phosphorylation-mediated changes in the subcellular localization and functioning of Siah2 protein in the context of *H. pylori*-mediated GC.

This study identified that myotonic dystrophy kinase-related Cdc42-binding kinase β (MRCKβ) was responsible for Siah2 phosphorylation in *H. pylori*-infected GECs. Siah2-MRCKβ interaction was confirmed by co-immunoprecipitation assay. *H. pylori* infection significantly decreased MRCKβ protein levels. Overexpression and suppression of *siah2* established its importance in MRCKβ regulation. Further experiments confirmed that Siah2 mediated ubiquitination of MRCKβ and led to its proteasomal degradation. Overexpression of *mrckβ* significantly enhanced Siah2 phosphorylation. The most probable phosphorylatable Siah2 residues were identified by using NetPhos 3.0 software. These residues were mutated by site-directed mutagenesis to generate Siah2 phospho-null mutants. Cells stably-expressing Siah2 phospho-null mutants were generated and cotransfected with *mrckβ* to identify the residues where Siah2 were phosphorylated by MRCKβ. Ser^6 and Thr^{279} residues of Siah2 were identified to be phosphorylated by MRCKβ in *H. pylori*-infected GECs. Antibodies against Ser^6 and Thr^{279}-phosphorylated-Siah2 were custom-generated.

Siah2 modulates reactive oxygen species (ROS) generation under various conditions. The role of Siah2 and its phosphorylation on ROS generation of *H. pylori*-infected GECs was elucidated. Siah2 significantly enhanced ROS generation which was further increased in Siah2 phospho-null mutant S6A-expressing cells after *H. pylori* infection. A 78-kDa glucose-regulated antioxidant protein (GRP78) was found to interact with Siah2. Overexpression and suppression of *grp78* established it as a crucial regulator of ROS generation in *H. pylori*-infected GECs. GRP78 was significantly decreased in *H. pylori*-infected GECs and human gastric biopsies. *siah2* overexpression and suppression established that GRP78 decrease was Siah2-mediated. GRP78 decreased, whereas Siah2 and its phosphorylation were enhanced in both the cytoplasmic as well as in the mitochondrial fractions of *H. pylori*-infected GECs. Phosphorylation of Siah2 at Ser^6 was identified to be crucial for the maintenance of the tubulo-reticular mitochondrial morphology and cytoprotective aggresome formation. Through various *in vitro* assays Siah2 phosphorylation was found to significantly enhance carcinogenicity, clonogenicity, invasiveness and proliferation of *H. pylori*-infected GECs. Enhanced Ser^6- and Thr^{279}-phosphorylated-Siah2 were detected in metastatic human GC biopsies as compared to their paired normal. C57BL/6 mice also exhibited significantly enhanced P-Ser^6-Siah2 and P-Thr^{279}-Siah2 in *H. felis*-infected murine gastric tissues as compared to the uninfected ones. In summary, this research established Siah2 phosphorylation as a crucial contributor towards the progression and metastasis of *Helicobacter*-infected GC and portrayed phospho-Siah2 as an important histological marker in this malignancy.

LIST OF ABBREVIATIONS USED

AGC kinases	Protein kinases A, G and C
Ala	Alanine
AlpA/B	Adherence associated lipoprotein A/B
ANOVA	Analysis of variance
APS	Ammonium persulfate
ATCC	American Type Culture Collection
BabA	Blood group antigen-binding adhesin A
BSA	Bovine serum albumin
C. pylori	*Campylobacter pylori*
C. pyloridis	*Campylobacter pyloridis*
cag PAI	Cytotoxin-associated gene pathogenicity island
CBB	Coomassie brilliant blue
CEACAMs	Carcinoembryonic antigen-related cell adhesion molecules
cPD	Cumulative population doubling
Csk	C-terminal Src kinase
DAPI	4', 6-diamidino-2-phenylindole
DCFDA	2,7-dichlorodihydrofluorescein diacetate
DMSO	Dimethyl sulfoxide
EDTA	Ethylenediamine tetraacetic acid

EGTA	Ethylene glycol tetraacetic acid
EMT	Epithelial-mesenchymal transition
EPIYA	Glutamate-proline-isoleucine-tyrosine-alanine
ETS2	E26 transformation-specific sequence 2
FBS	Fetal bovine serum
GC	Gastric cancer
GECs	Gastric epithelial cells
GRP78	78-kDa glucose-regulated protein
H. pylori	*Helicobacter pylori*
HECT	Homologous to E6AP C-terminus
HEPES	4-(2-Hydroxyethyl) piperazine-1-ethanesulfonic acid
Hop	*H. pylori* outer membrane protein
HRP	Horse-radish peroxidase
Hsp	Heat shock proteins
LC-MS/MS	Liquid chromatography-mass spectrometry
LPS	Lipopolysaccharide
Lys	Lysine
MG132	Z-Leu-Leu-Leu-al
MOI	Multiplicity of infection
MRCKβ	Myotonic dystrophy kinase-related Cdc42-binding kinase β

MS	Mass spectrometry
NAC	N-acetylcysteine
NFDM	Non-fat-dried milk
Nrf2	Nuclear erythroid-related factor 2
OD	Optical density
OipA	Outer inflammatory protein A
OMPs	Outer membrane proteins
OMVs	Outer membrane vesicles
PBS	Phosphate buffered saline
PD	Population doubling
PFA	Paraformaldehyde
PHPI	Post *H. pylori* infection
P-Ser^6-Siah2	Phosphorylated-serine^6-Siah2
P-Siah2	Phosphorylated-Siah2
P-Thr^{279}-Siah2	Phosphorylated-threonine^{279}-Siah2
PTMs	Posttranslational modifications
PVDF	Polyvinylidene fluoride
RBR	RING-between-RING
RING	Really interesting new gene
ROS	Reactive oxygen species

RPMI	Roswell park memorial institute
RT	Room temperature
SabA	Sialic acid-binding adhesin A
SBD	Substrate-binding domain
SDS-PAGE	Sodium dodecyl sulphate–polyacrylamide gel electrophoresis
SEM	Standard error of mean
Ser	Serine
SFM	Serum free media
Siah	Seven in absentia homolog
sina	Seven in absentia
T4SS	Type IV secretion system
TCGA	The Cancer Genome Atlas
TEMED	N,N,N',N'-tetramethylethylenediamine
Thr	Threonine
UPS	Ubiquitin-proteasome system
UTMB BRF	University of Texas Medical Branch, Biomolecular Resource Facility
VacA	Vacuolating cytotoxin A
WHO	World Health Organization
WT	Wild type

LIST OF FIGURES

LIST OF TABLES

Chapter 1

Introduction

Section A

1.A.1. Gastric cancer overview

Gastric cancer (GC) is one of the common malignancies in the developing world. Approximately, one million new cases of gastric cancer (GC) have been reported in the year 2018 while the mortality recorded in the same year was approximately eight million [1]. Reportedly, the incidence of GC is the highest in the Eastern Asia and the lowest in the Northern and Eastern Africa (GLOBOCAN 2018). In India, Mizoram has the highest incidence of GC as per a published report from the year 2020 [2]. GC has become one of the most common cancers for males in India and has been projected as the fifth most incident cancer amongst males. As observed globally, the incidence of this disease is twice more in males than in females [2, 3].

1.A. 2. Historical perspective

The ancient Egyptian texts, papyri, dating back to more than 1600 BC described possible cases, methods of diagnosis and treatment of GC. Hippocrates (4th BC), who first used the Greek words "καρκίνος" (karkìnos = cancer) and "καρκίνωμα" (karkìnoma = carcinoma) because of the digit-like extensions that come out of the tumor resembling the shape of the crab's appendages, also reported about a possible case of GC [4].

Ancient Indian texts describe diagnosis and treatment of many gastrointestinal diseases including cancer. The most correlative terms used for cancer were *arbuda*, *granthi*, and *gulma* [5]. The term *gulma* has been widely associated with GC and has been classified into many subtypes [6].

In the modern era, cases of benign and malignant gastric ulcers were first described by J. Cruveilhier, in 1835. The first successful surgical removal of cancer-affected part of the stomach was performed by Theodor Billroth in Vienna on 22nd January 1881 [7].

1.A. 3. Etiology

Various factors are involved in the progression of GC. The major factors involved are represented as Figure 1.
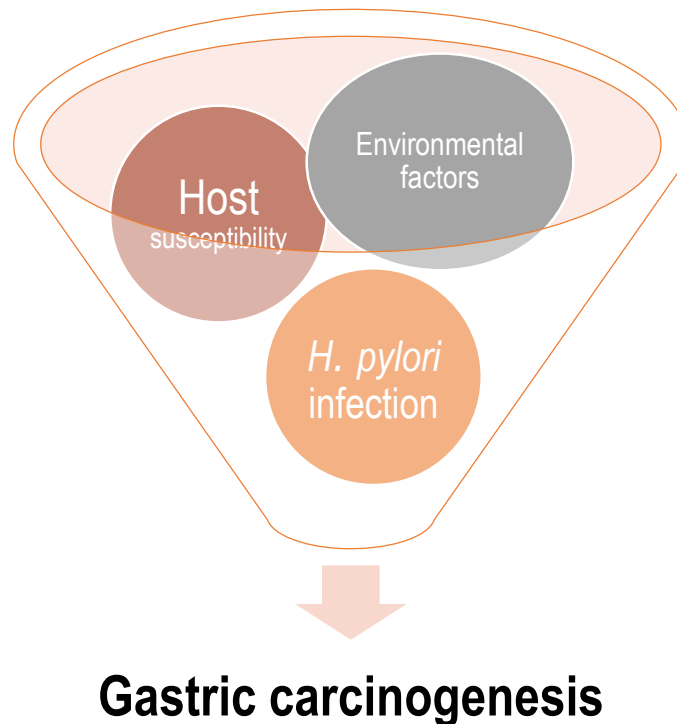
Figure 1. Factors involved in GC. Host susceptibility, environmental factors and *Helicobacter pylori* infection determine the outcome of the disease.

Host susceptibility: Host genetics plays an important role in determining the disease-risk. Genetic variation and polymorphisms increase the risk of GC [8-10]. Persons with certain hereditary conditions like Lynch syndrome, Li-Fraumeni syndrome, familial adenomatous polyposis and Peutz-Jeghers syndrome have increased risk of GC [11]. The degree of relatedness with the GC patient also increases the risk of the disease [12]. Risk of GC also increases with the modulation of gastric acid secretion either by *H. pylori* infection or use of drugs [13, 14]. Persons belonging to certain blood groups or with certain haematological

disorders and geriatric population are more prone to GC [14-16]. These factors either independently or in combinations increase the risk of GC.

Environmental factors: Heavy metal-contamination and salty food are associated with the development of GC [17-19]. The chances of developing GC increase with certain mining activities, exposure to radiation and high temperature [20, 21]. The higher the altitudes and latitudes, the higher is the prevalence of GC. Intake of alcohol and smoking increase the chances of GC [18]. Poor hygiene practices also increase the risk of GC [22].

*H. pylori***:**

Taxonomy

Dr. Barry J. Marshal and Dr. John Robin Warren successfully isolated and cultured *Campylobacter pyloridis* in 1983 [23]. They isolated this bacterium from the pylorus part of the human stomach and hence, named it "*pyloridis*". This Gram negative, spiral, lophotrichous bacterium was believed by them to be responsible for gastritis and peptic ulcer disease. Due to the unacceptance of their hypothesis and the lack of suitable animal models, Dr. Marshal inoculated himself with *C. pyloridis* culture. The results published in 1985 established *C. pyloridis* as the causative agent of gastritis [24]. Similar results were also reported by A. Morris and G. Nicholson in 1987 [25]. In 1987, Marshal and Goodwin revised the name of the bacterium to *C. pylori* [26]. Goodwin *et al.* created a new genus *Helicobacter* and suggested *C. pylori* to be transferred to the newly-created genus [27]. Thus, based on the evidences, *C. pylori* came to be known as *H. pylori* in 1989. The International Agency for Research on Cancer assigned *H. pylori* as a Group 1 (definite) carcinogen in 1994 [28]. "For their discovery of the bacterium *H. pylori* and its role in gastritis and peptic ulcer disease" Dr. Barry J. Marshal and Dr. Robin Warren were awarded the Nobel prize in Physiology and Medicine in the year 2005 (www.nobelprize.org).

Epidemiology/ prevalence

Humans are the principal reservoir of *H. pylori*. This bacterium infects nearly 50% of the humanity. The prevalence of *H. pylori* infection varies globally [29]. India has 63.5% prevalence of this bacterium [30]. Poor sanitation practises are the main causes behind *H. pylori* prevalence [29]. Improvement in the hygienic practises decreases the prevalence of *H. pylori* infection [31, 32].

Transmission of infection

The *H. pylori* infection is usually acquired during childhood mainly via interpersonal transmission routes [33]. These routes include gastro-oral, oral-oral and faecal-oral transmission. Family members of an *H. pylori*-infected individual are at a greater risk of getting the infection due to these interpersonal transmission routes. In addition, the transmission of *H. pylori* through contaminated water and food is also reported [34].

Pathogenicity of *H. pylori*

H. pylori infects the gastric mucosa and dominates the human stomach microbiome [35, 36]. The distribution of *H. pylori* is generally concentrated within the gastric glands close to the epithelial cells [37-39]. Albeit *H. pylori* is a classical extracellular pathogen, some evidences support its intracellular localization as well [40, 41]. Intracellular invasion, mechanisms of which are still being elucidated, might play a role in the maintenance of infection and disease induction [42, 43]. To survive the acidic environment of human stomach and to establish infection, *H. pylori* has developed a number of adaptations. These adaptations are the result of its longstanding association with the human host. The crucial steps required for *H. pylori* colonization and successful pathogenesis are discussed below:

1. **Acid acclimatization:** The human stomach, with the pH varying from 1.0 to 3.5 and a diurnal median of ~1.4, acts as an ecological filter against a variety of pathogens [44]. *H.*

pylori is a neutralophile, surviving within the pH range of 4.0 to 8.2 [45-48]. Survival or acclimatization in the acidic environment is made possible by the nickel metalloenzyme urease. *H. pylori* urease gene cluster is an array of seven genes, expressing accessory assembly proteins (*ureE-H*), a proton-gated ion channel (*ureI*) and catalytic subunits (*ureA/B*) [49]. Nickel is essential for the urease activity and its availability is regulated in a pH-dependent manner [50, 51]. Low pH stimulates urea channel UreI which allows urea entry into the cell [52]. Urease catalyses the hydrolysis of urea to ammonia and carbamate [53, 54]. Carbamate spontaneously decomposes to yield another molecule of ammonia and carbonic acid. The net effect is neutralization of pH in the cytoplasm of *H. pylori*. Additionally, *H. pylori* surface urease (10%-30% of the total bacterial urease content) also contributes towards the survival of the bacteria [55-57]. The surface urease is acquired by a process of "altruistic autolysis". Though the relative contributions in the neutralization of pH by the surface and the cytoplasmic ureases are debatable [54, 58-61], the net result is the survival of bacteria in the acidic medium. The urease activity is not only essential for the survival and establishment of *H. pylori* infection but is also required for the maintenance of infection [62]. *H. pylori* urease activity, regulated by two-component systems [63], also determines the infection site in varied acidic environment of human stomach [46, 63].

2. **Mucus invasion and chemotaxis:** Human gastric epithelium is covered with a protective layer of mucus which is in a continuum of secretion and degradation. The mucus of the stomach is bilayer- an inner layer is attached to the epithelium while the outer layer is unattached [64]. Mucins are the main component of mucus and several mucin genes are found in humans [65]. Gastric epithelial cells (GECs) secrete bicarbonate which diffuses into the surrounding mucus layer and forms an acid gradient which is acidic towards the lumen and neutral towards the GECs [66]. Similarly, a urea gradient generated by the action of bacterial urease also exists [37]. *H. pylori* is repelled by the hydrochloric acid present in

the gastric lumen and attracted towards metabolites originating from GECs. Various acid sensors control these chemotactic responses of *H. pylori* [67, 68]. Flagella provide the kinetic ability to *H. pylori.* Four to eight flagella are arranged in a lophotrichous manner and act in harmony to propel the bacterium [69]. As *H. pylori* moves toward the epithelium in response to various chemical cues, it encounters the mucus layer. The mucus barrier is breached with the help of *H. pylori* urease which changes the pH in the vicinity of the bacterium [70]. This change in pH converts mucus from the gel state to a sol one. Chemotactic responses and flagella help *H. pylori* orient towards epithelia [71]. The flagellar force aided by the alteration in the viscoelastic property of mucus helps *H. pylori* cross the mucosal barrier. Various flagellar mutants of *H. pylori* are either unable or less efficient in colonizing the host stomach [69]. Hypermotility of *H. pylori* worsens the pathogenicity [72]. The characteristic helical shape of *H. pylori* is also essential for the colonization of the stomach [73, 74]. Thus, propelled by the flagella in a characteristic cork-screw motion, *H. pylori* reaches the gastric epithelium.

3. **Attachment to GECs:** *H. pylori* persistence is required for a successful infection. As *H. pylori* approaches the gastric epithelium, it needs to firmly attach itself to the GEC. This is essential in order to avoid being washed out or dislocated due to continuous shedding of the mucosal layer. *H. pylori* has an armoury of outer membrane proteins [75] which help it remain firmly attached to the GECs. Approximately 4% of the *H. pylori* genome codes for these adhesion proteins [76]. The adhesion proteins along with their host targets are mentioned in Table 1. These factors play crucial roles in *H. pylori* adherence, initiation and maintenance of infection.

Table 1. Various *H. pylori* adhesion molecules and their cellular receptors.

Sl. No.	*H. pylori* adhesion proteins	Host receptor proteins	References
1.	Adherence associated lipoprotein (Alp) A/B (HopC/B)	Laminin, Collagen IV	[77, 78]
2.	Blood group antigen-binding adhesin A (BabA)/ *H. pylori* OMP S (HopS)/ OMP28	Lewis b (Le[b]) blood group antigen, MUC5AC and MUC1	[79, 80]
3.	CagL	$\alpha_5\beta_1$ integrin	[81]
4.	HopQ/ OMP27	Carcinoembryonic antigen-related cell adhesion molecules (CEACAMs) 1, 3, 5 and 6	[82, 83]
5.	HopZ	Unknown	[78, 84]
6.	Lipopolysaccharide (LPS)	Laminin, LewisX	[85, 86]
7.	Outer inflammatory protein A (OipA)/ HopH	Unknown	[84, 87]
8.	Sialic acid-binding adhesin (SabA)/ OMP17/ HopP	Sialylated glycans- sialyl-LewisX, sialyl-LewisA and LewisX	[88, 89]

4. **Establishment of infection:** *H. pylori* virulence factors affect the host in a number of ways after the pathogen attach to GECs. Various molecular alterations in the infected host cells are initiated which lead to the pathogenesis of several diseases. Out of the several players in *H. pylori* disease-pathogenesis a few are discussed below.

A. **Cytotoxin-associated gene pathogenicity island (*cag* PAI):** Comprised of a 40 kb stretch of DNA, these gene elements encode ~32 genes in *H. pylori* [90, 91]. The type IV secretion system (T4SS) of *H. pylori* is a product of the *cag* PAI. T4SS forms a needle-like bridge that is inserted to the host epithelial cell to transfer effector molecules. These T4SS bridges have evolved from conjugation apparatus of bacteria [92-94]. β1 integrins expressed on the surface of GECs act as receptors for T4SS [81, 95]. The injection of *H. pylori* T4SS is not haphazard but is rather a very tightly controlled process [96, 97]. CagE forms the structural component of T4SS and is essential for the injection of effector molecules [90]. *cag* PAI-encoded CagY and CagL also play important roles in T4SS injection and translocation of CagA [90, 95]. CagL has also been reported to mimic the host cell fibronectin and affect the cellular morphology [81, 98]. On the basis of the presence or absence of *cag* PAI, *H. pylori* are classified into two categories: *cag* PAI (+) and *cag* PAI (-). The niche of *H. pylori* colonization is influenced by the *cag* PAI status [99]. The *cag* PAI (-) strains have mucosal predominance while *cag* PAI (+) ones are found near or adhered to the GECs. *H. pylori cag* PAI (+) strains are more pathogenic than the negative ones in causing GC [100-102].

The 3' terminal end of *cag* PAI encodes CagA [103]. CagA is the first identified *cag* PAI-encoded virulence factor of *H. pylori*. It is the only known oncogenic protein to be injected into the host cells by *H. pylori* [104]. In spite of being a very abundant protein in *H. pylori*, surprisingly, very small amount is translocated to host cells [105, 106]. The carboxy-terminal of CagA protein contains the variable tyrosine phosphorylation motifs (glutamate-

proline-isoleucine-tyrosine-alanine, EPIYA) [107, 108]. The four different (A-, B-, C-, and D-) EPIYA motifs are recognised based on the differences in the flanking amino acid sequences. This motif helps CagA protein attachment to the cytoplasmic side of the plasma membrane of GECs [109]. Once inside the host cell, CagA is quickly phosphorylated by the Src kinase which is then rapidly inactivated [110]. Later, the Abl kinase phosphorylates CagA and remains active continuously. The downregulation of Src kinase activity can be attributed to the activation of C-terminal Src kinase (Csk)-initiated negative feedback loop [111, 112]. This regulation of the primary CagA kinase, Src, controls availability of the phosphorylated CagA in the host cell [90]. Thus, these kinases act successively to phosphorylate and regulate CagA abundance and function [113-115]. The phosphorylated CagA initiates signalling cascades which lead to alteration of the cytoskeleton and formation of the characteristic "hummingbird phenotype" as a result of "scattering" [108, 116-118]. Additionally, phosphorylation-independent role of CagA in altering the cellular morphology has also been elucidated [90, 119, 120]. The pathways manipulated by CagA in the development of GC is summarized in Figure 2.
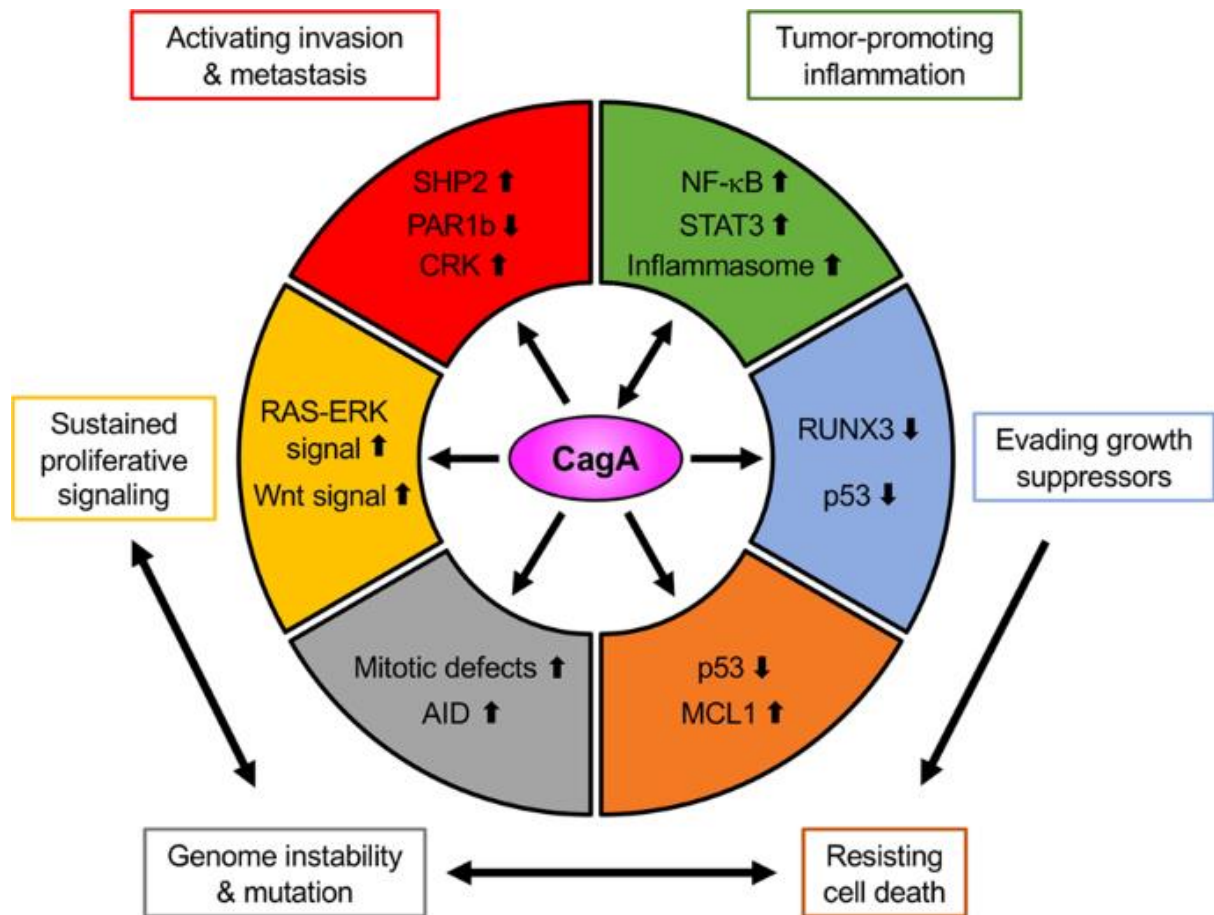
Figure 2. CagA-influenced pathways in the development of GC. Figure courtesy [108].

H. pylori outer membrane vesicles (OMVs) contain CagA along with other virulence factors [121, 122]. These are also delivered to the host cells and induce pathological changes. People infected with the *cag* PAI (+) *H. pylori* strains release exosomes containing CagA protein [123]. These exosomes are transported via the blood stream and might influence the development of the extra-gastric pathologies.

B. Vacuolating cytotoxin A (VacA): This is the proteinaceous "vacuolating cytotoxin" identified from the culture broth of *H. pylori* [124, 125]. Although present in most *H. pylori* strains, the virulence factor VacA exhibits polymorphism and is transcriptionally regulated [126-129]. Translated as a protein of 140 kDa, it is processed further to yield the active 88 kDa toxin [75, 125, 130, 131]. VacA remains anchored to the bacterial membrane or is secreted [125, 132]. The secreted VacA oligomerizes at neutral pH. Exposure to the acidic

or alkaline pH disrupts oligomerized VacA and enhances its vacuole forming potential [133-136]. This "acid or alkaline activation" of VacA is essential for its internalization. Multiple receptors have been elucidated in VacA internalization [119, 137, 138]. The internalized monomeric VacA oligomerizes again inside the host cell forming anion selective channels [129, 134, 139]. The efflux of metabolites required by *H. pylori* is enhanced by these ion channels [140-142]. These ion channels are also taken up by endosomes and lead to the formation of large cytoplasmic vacuoles [143-145]. Additionally, VacA disrupts the endosomal trafficking, membrane and mitochondrial permeability. Alterations in autophagy, cellular signalling and cytoskeletal organization have also been observed [131, 146-148]. VacA also plays immuno-modulatory roles for the persistent and successful *H. pylori* infection [119, 129].

A variant of VacA regulates CagA availability in the infected cells [149]. Synergistic as well as antagonistic interactions of CagA and VacA have been elucidated [119, 120, 150, 151]. These interactions create an optimal niche for *H. pylori* and improve its pathogenesis [120, 150]. Other than these, following *H. pylori* virulence factors are also significant- *H. pylori* neutrophil-activating protein, high temperature requirement A, heat shock proteins (Hsp 60, 10, 70), γ-glutamyl-transpeptidase, cholesteryl α-glucosyltransferase, LPS and arginase, to name a few [152].

Several signalling events are initiated by *H. pylori* which ultimately lead to GC pathogenesis (Figure 3). The severity of GC is determined by the interaction among host genetics, environmental factors and/or *H. pylori* infection.
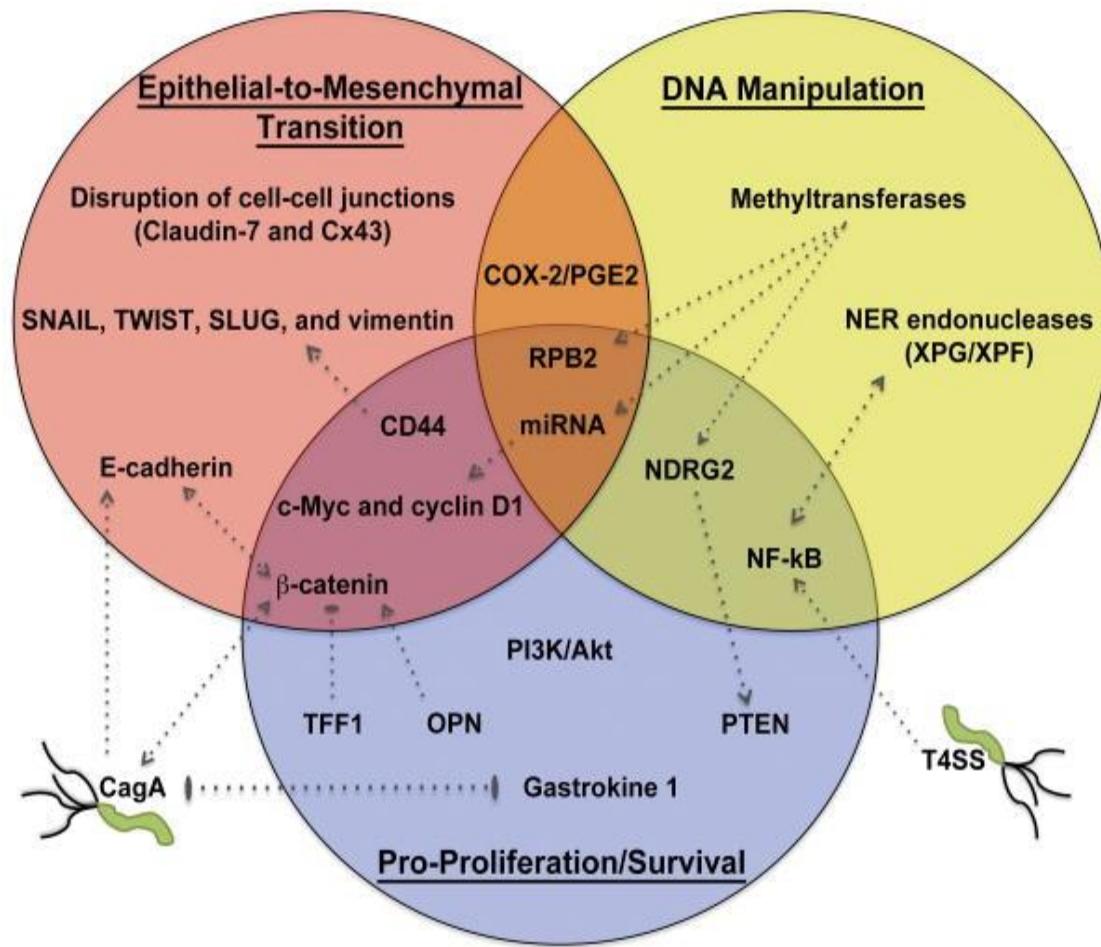
Figure 3. Summary of various *H. pylori*-induced signalling pathways. Figure courtesy [153].

1.A.4. Pathogenesis of GC

H. pylori is a "definite carcinogen" and initiates restricted host immune responses thereby initiating a series of events leading to GC [154, 155]. The cascade of *H. pylori*-driven GC events, as described by P. Correa, is initiated by gastritis or inflammation of the infected mucosa. Further sequences in the cascade may take several years to develop depending on the strain of *H. pylori*, the host and the environmental factors (Figure 4).
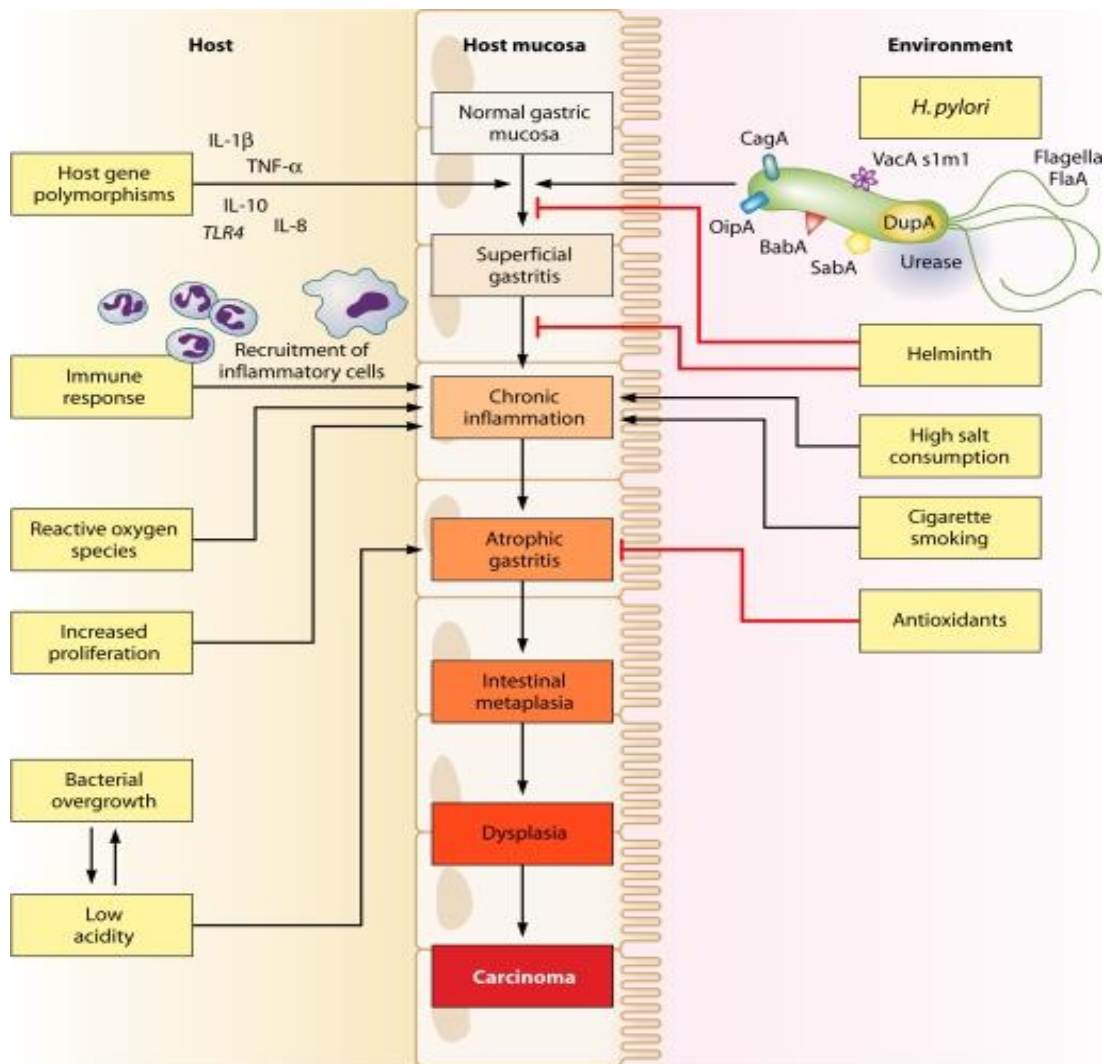
Figure 4. Sequence of events leading to *H. pylori*-initiated GC and the role of various factors. Figure courtesy [156].

The later stages of the cascade shown in Figure 4 are reached in a small proportion of the infected individuals. Of the multiple gastric pathologies initiated by *H. pylori*, GC occurs in 2-3% of the infected individuals [157]. *H. felis*-infected C57BL/6 mice also exhibit the classical "Correa's cascade" [158]. This makes the bacterium an ideal choice for infecting C57BL/6 mice in order to mimic the human *H. pylori* infection. First isolated from the stomach of cats, *H. felis* is found rarely in the human stomach [159]. Histologically, GC has been classified into various types, of which adenocarcinoma forms 90-95% of the cases [155, 160]. P. Lauren, in

1965, identified two distinct forms of adenocarcinomatous GC: intestinal and diffuse [161]. Later a third type, indeterminate, was added to address the inconsistent histology. On the basis of their incidence, the three types can be arranged as: intestinal type> diffuse type> indeterminate type [162]. Of these, only the intestinal type exhibits a true Correa's cascade. Eventually, the World Health Organization (WHO) provided a detailed histological classification of all types of GC [163]. Classification based on the gene expression profiles of various GC types was undertaken by "The Cancer Genome Atlas (TCGA)" research network [164, 165]. Different GC types are comparable and correlated but may show diverse histological, immunological and molecular characteristics [164, 166-168]. They also vary in proportion to their incidence.

1.A.5. *H. pylori* and GC metastasis

H. pylori-induced "humming bird phenotype" due to "cell scattering" *in vitro* is due to the initiation of various signalling pathways. Majorly, cell-cell adhesion aberrations are induced which lead to epithelial-mesenchymal transition (EMT) [169, 170]. EMT is crucial for GC progression and metastasis, key events of which are summarized in Figure 5. GC malignancies spread in the human body at various sites and routes (Figure 5).
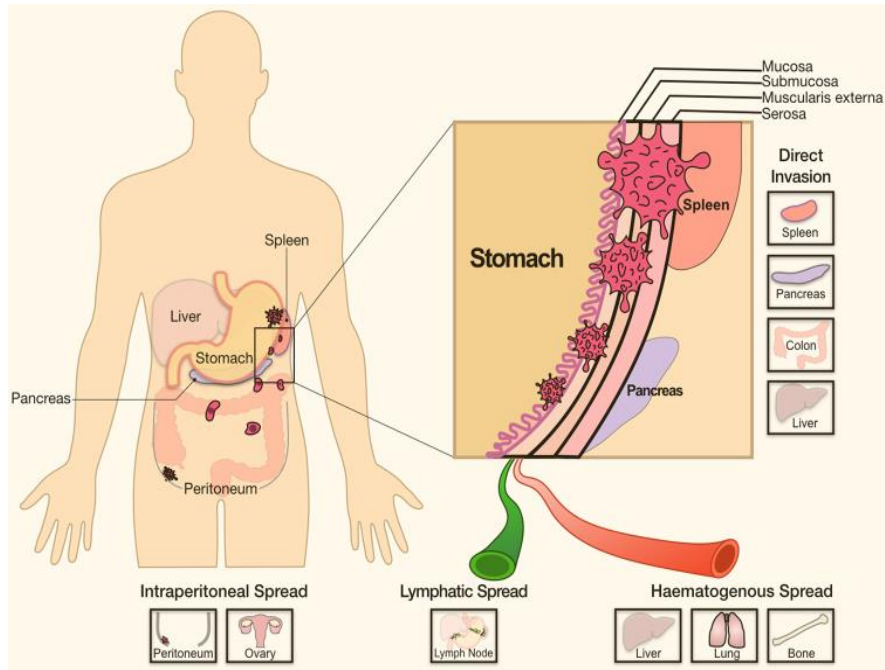
Figure 5. Various sites and routes of GC metastasis. Figure courtesy [171].

The progress and dissemination of GC is also aided by gastric tumor-derived exosomes [172-174].

Section B

1.B.1 *H. pylori* and the host ubiquitin-proteasome system (UPS)

One of the major regulatory machinery controlling cancer initiation to metastasis is the UPS [175-177]. It regulates the presence/ abundance of proteins involved in various pathologies. The UPS regulates these processes by the addition of a small regulatory protein ubiquitin to the target protein. The 76 amino acids long ubiquitin gets attached covalently to the substrate protein [178]. Ubiquitin attachment involves multiple enzymes which regulate the processes from "ubiquitin activation" to "ubiquitin ligation" (Figure 6).
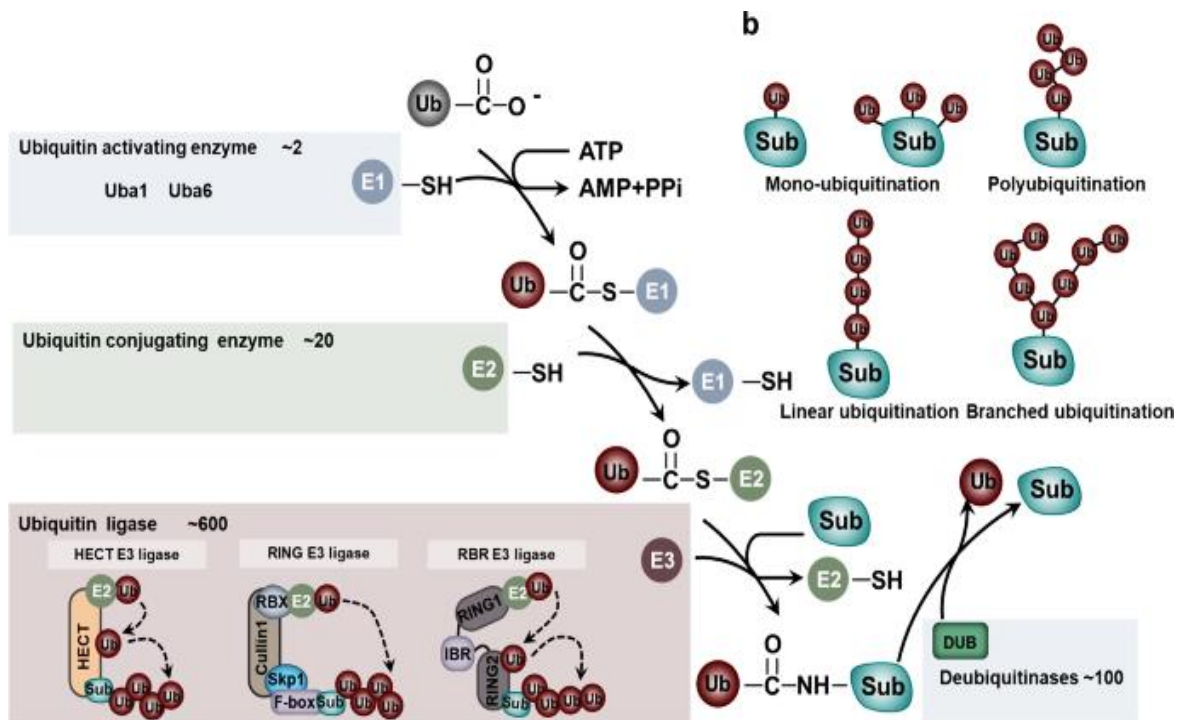
Figure 6. The components and outcomes of the UPS. Figure courtesy [179].

The attached ubiquitin can serve as a site for further addition of ubiquitin residues, thus, leading to the poly-ubiquitination of the substrate protein [179]. The residue of ubiquitin at which poly-ubiquitination is initiated helps develop a unique "ubiquitin code". The most common "code" is Lys 48-polyubiquitination which leads to the degradation of the targeted protein by the 26S proteasome [180, 181]. This degrading executioner of the UPS is composed of a 20S core catalytic barrel and a 19S regulatory cap. The entry of substrate protein to the catalytic core is "gated" and regulated by many proteins (Figure 7). "For the discovery of ubiquitin-mediated protein degradation", Aaron Ciechanover, Avram Hershko and Irwin Rose were jointly awarded "The Nobel Prize in Chemistry 2004" (www.nobelprize.org).
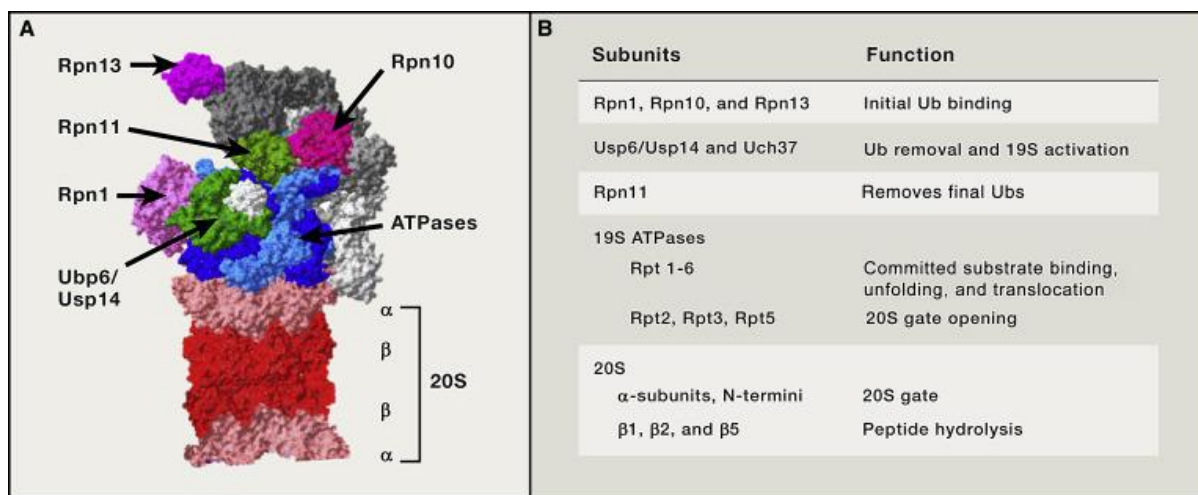
Figure 7. The 26S proteasome (A) and functions of its various components (B). Figure courtesy [182].

Tsvetkov *et al.* reported that viability of cancer cells is dependent on the 26S proteasome levels and proposed of "addiction of cancer cells to high 26S proteasome" [183]. *H. pylori* infection modulates the host cell UPS which regulates bacterial adherence [184] and inflammation [185]. Various pathways essential for the initiation, proliferation and dissemination of *H. pylori-*mediated GC are also altered by UPS [186-188].

1.B.2. E3-ubiquitin ligases

Specificity to the ubiquitination process is provided by the E3-ubiquitin ligase enzymes [189, 190]. Various E3-ubiquitin ligase enzymes, based on their structure and mechanism of action, have been classified into three classes: homologous to E6AP C-terminus (HECT), RING-between-RING [147] and really interesting new gene (RING) [191]. E3-ubiquitin ligases have been implicated in the development of cancers, including GC, by alterations of various cellular pathways [192, 193] (Figure 8). Seven in absentia homolog (Siah) proteins, belonging to the family of RING E3-ubiquitin ligases, are implicated in GC.
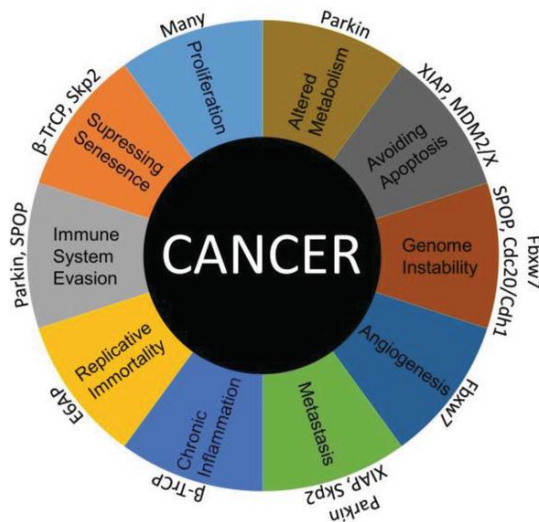
Figure 8. E3-ubiquitin ligases regulate various cellular processes which lead to cancer. Figure courtesy [194].

1.B.3. Siah2

Overview

Siah2 is involved in the regulation of various cellular processes [195]. This 324 amino acids long protein, encoded by the human *siah2* gene on chromosome 3q25, is a homologue of the *Drosophila* seven in absentia gene. The RING domain is present at the N-terminal followed by zinc finger motifs and the substrate-binding domain (SBD) at the C-terminal. The N- terminal RING domain serves as a site for binding of E2 enzymes. The SBD interacts with a variety of proteins and helps Siah2 regulate various cellular processes. Gopalsamy *et al*. have identified substrate specificity of Siah2 SBD to be regulated by various crucial residues [196]. Based on the consensus among various substrate proteins of Siah, "degron motifs" have been suggested [197, 198]. The presence of these motifs in the substrate protein enhances the likelihood of its Siah2-mediated degradation.

Multifaceted Siah2

Siah2 controls many aspects of cellular physiology and are implicated in the development of various cancers (Figure 9). Metabolism, oxidative stress [199-201] and hypoxia response [200, 202, 203] are regulated by Siah2. Additionally, various immunological processes [204-206], cellular polarity and cell-cell adhesion are also regulated by Siah2 [207].
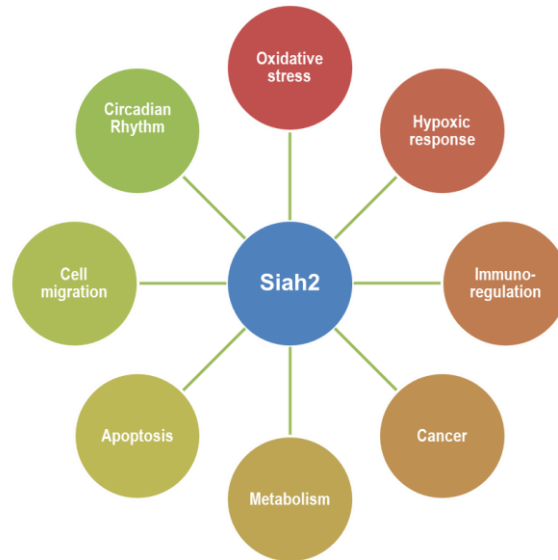
Figure 9. Siah2 regulates multiple cellular processes.

Siah2 and *H. pylori*

Aerobic respiration and a variety of cellular stress (such as *H. pylori* infection) generate reactive oxygen species [208-210]. Although low levels of ROS are essential for the normal cellular functions, their high levels impair cellular processes. Thus, a homeostasis is achieved by employing various antioxidant proteins [211]. One of the major regulators of ROS is nuclear erythroid–related factor 2 (Nrf2) [212]. The abundance of Nrf2 is controlled by Siah2 under hypoxia and hypoglycaemia [201, 213]. *H. pylori* infection-generated ROS enhance the invasiveness of GECs [214]. However, the role of Siah2 in regulating the redox homeostasis of *H. pylori*-infected GECs remains unknown.

H. pylori also modulates various transcription factors such as Twist1 and E26 transformation-specific sequence 2 (ETS2) and enhance Siah2 protein level in gastric epithelial cells (GECs) [215]. Increased Siah2 promotes cellular proliferation, migration and invasion in *H. pylori*-infected GECs. Siah2 controls the invasiveness and migration of GECs by adjusting the availability of various cytoskeletal proteins [216]. Posttranslational modifications (PTMs) of Siah2 regulate its availability in the cell, sub-cellular localization and function [199, 217, 218].

PTMs of Siah2

The abundance and activity of the RING family of E3-ubiquitin ligases are maintained by auto-ubiquitination and proteasomal degradation [219, 220]. Siah2 abundance and activity are also controlled by its auto-ubiquitination [199, 221]. The RING domain of Siah2 is crucial for this auto-regulation [222]. However, the extent of Siah2 auto-ubiquitination is determined by its PTMs [217]. p300-mediated acetylation of Siah2 at Lys^{139} residue increases its stability in GECs infected with *H. pylori* [223]. Acetylated Siah2 in turn regulates the availability of cytoskeletal proteins and increases GC invasiveness [218]. One of the most prominent PTMs is phosphorylation. A multitude of kinases phosphorylate Siah2 at various residues [224]. Phosphorylation of Siah2 regulates its functioning and subcellular localization (Figure 10 and Table 2).
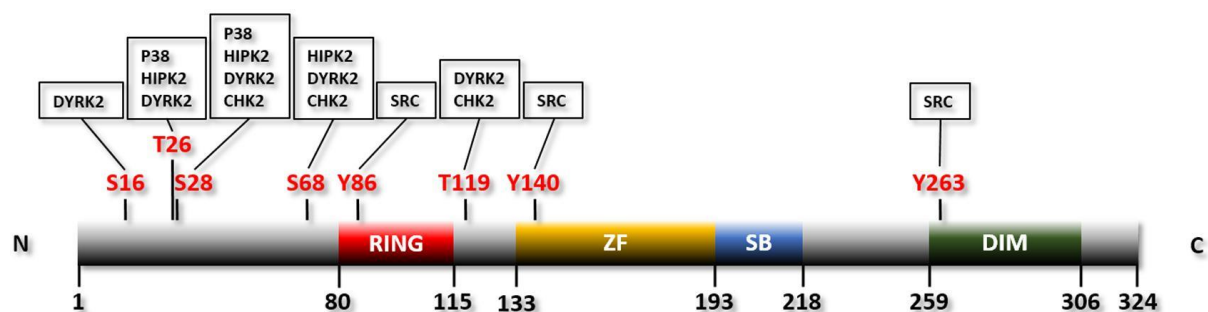
Figure 10. Multi-domain structure of Siah2 indicating phosphorylation sites and the kinases involved. Figure courtesy [224].

Table 2. Cellular responses modulated by Siah2 phosphorylation.

Siah2: residues phosphorylated	Function	Report
T^{26}, S^{28}, T^{119}	Cell cycle progression	[225]
T^{26}, S^{28}, S^{68}, T^{119}	DNA damage response	[226]
S^{16}, T^{26}, S^{28}, S^{68}, T^{119}	PHD3 degradation	[227]
T^{24}, S^{29}	PHD3 degradation	[228]
Y^{86}, Y^{140}, Y^{263}	Invasion and migration	[229]

However, the status and mechanism of Siah2 phosphorylation in *H. pylori*-mediated GC remains unknown. Hence, this thesis aimed to explore the role of phosphorylation in functioning and subcellular localization of Siah2 in GECs infected with *H. pylori*.

Chapter 2

Siah2 is phosphorylated at Ser^6 and Thr^{279} by MRCKβ

2.1 Mass spectrometry of GECs infected with *H. pylori* uncovered the kinase involved in Siah2 phosphorylation

H. pylori-enhanced Siah2 promotes tumorigenicity of GC [223, 230]. Several kinases phosphorylate Siah2 [224]. However, the status and mechanism of Siah2 phosphorylation in GECs infected with *H. pylori* remained unexplored. To determine the kinase(s) responsible for Siah2 phosphorylation, empty vector (pcDNA3.1+) and *siah2* overexpression plasmids were expressed in MKN45 cells. This was necessary in order to enrich the levels of Siah2 and its interactions. 200 multiplicity of infection at 12 h post *H. pylori* infection (PHPI) optimally induced Siah2 in GECs [223, 230]. 36 h post transfection, the above cells were infected for 12 h with 200 MOI of *H. pylori*. This was followed by immunoprecipitation of the whole cell lysates with Siah2 antibody. SDS-PAGE was used to separate the immuno-complexes collected above. The differentially-expressed bands after Coomassie brilliant blue R-250 (CBB) staining of the gel were cut and mass spectrometric (MS) analysis was performed (UTMB, Texas, USA). The kinases identified are presented as Table 3.

Table 3. Kinases detected by MS.

Kinases	Protein accession No.s	Scores	Siah degron motif (amino acid residues)
6-phosphofructokinase, platelet type	Q01813	67.68	Partial/ Core: VLP (482-484)

Ser/Thr-protein kinase MRCKβ	Q9Y5S2	61.32	Partial/ Core: VCP (1074-1076), VAP (1371-1373), VNP (1409-1411), VDP (1448-1450) Full: PLSAVPP (1608-1614)
6-phosphofructokinase, liver type	P17858	36.33	Partial/ Core: VIP (523-525)

To find the most probable Siah2 kinase out of the three identified, the presence of Siah "degron motifs" was analysed. Both isoforms of 6-phosphofructokinase had only a partial Siah "degron motif" each, whereas, the Ser/Thr kinase MRCKβ (myotonic dystrophy kinase-related Cdc42-binding kinase β) had four partial and one full Siah "degron motif". As several partial and full Siah "degron motifs" were present in MRCKβ, it indicated to the likelihood of MRCKβ-Siah2 interaction. Additionally, the probability of MRCKβ-Siah2 interaction was analysed using the LR_PPI protein-protein interaction prediction tool [231]. The high probability of interaction also pointed towards MRCKβ-Siah2 interaction (Figure 11). Thus, MRCKβ seemed to be the probable kinase interacting with Siah2.

```
>SIAH2
MSRPSSTGPSANKPCSKQPPPQPQHTPSPAAPPAAAATISAAGPGSSAVPAAAAVISGPG
GGGGAGPVSPQHHELTSLFECPVCFDYVLPPILQCQAGHLVCNQCRQKLSCCPTCRGA
LTPSIRNLAMEKVASAVLFPCKYATTGCSLTLHHTEKPEHEDICEYRPYSCPCPGASCKW
QGSLEAVMSHLMHAHKSITTLQGEDIVFLATDINLPGAVDWVMMQSCFGHHFMLVLEKQ
EKYEGHQQFFAIVLLIGTRKQAENFAYRLELNGNRRRLTWEATPRSIHDGVAAAIMNSDC
LVFDTAIAHLFADNGNLGINVTISTCCP
>MRCKβ
MSAKVRLKKLEQLLLDGPWRNESALSVETLLDVLVCLYTECSHSALRRDKYVAEFLEWA
KPFTQLVKEMQLHREDFEIIKVIGRGAFGEVAVVKMKNTERIYAMKILNKWEMLKRAETA
CFREERDVLVNGDCQWITALHYAFQDENHLYLVMDYYVGGDLLTLLSKFEDKLPEDMAR
FYIGEMVLAIDSIHQLHYVHRDIKPDNVLLDVNGHIRLADFGSCLKMNDDGTVQSSVAVG
TPDYISPEILQAMEDGMGKYGPECDWWSLGVCMYEMLYGETPFYAESLVETYGKIMNH
EERFQFPSHVTDVSEEAKDLIQRLICSRERRLGQNGIEDFKKHAFFEGLNWENIRNLEAP
YIPDVSSPSDTSNFDVDDDVLRNTEILPPGSHTGFSGLHLPFIGFTFTTESCFSDRGSLK
SIMQSNTLTKDEDVQRDLEHSLQMEAYERRIRRLEQEKLELSRKLQESTQTVQSLHGSS
RALSNSNRDKEIKKLNEEIERLKNKIADSNRLERQLEDTVALRQEREDSTQRLRGLEKQH
RVVRQEKEEELHKQLVEASERLKSQAKELKDAHQQRKLALQEFSELNERMAELRAQKQK
VSRQLRDKEEEMEVATQKVDAMRQEMRRAEKLRKELEAQLDDAVAEASKERKLREHSE
NFCKQMESELEALKVKQGGRGAGATLEHQQEISKIKSELEKKVLFYEEELVRREASHVL
EVKNVKKEVHDSESHQLALQKEILMLKDKLEKSKRERHNEMEEAVGTIKDKYERERAML
FDENKKLTAENEKLCSFVDKLTAQNRQLEDELQDLAAKKESVAHWEAQIAEIIQWVSDEK
DARGYLQALASKMTEELEALRSSSLGSRTLDPLWKVRRSQKLDMSARLELQSALEAEIR
AKQLVQEELRKVKDANLTLESKLKDSEAKNRELLEEMEILKKKMEEKFRADTGLKLPDFQ
DSIFEYFNTAPLAHDLTFRTSSASEQETQAPKPEASPSMSVAASEQQEDMARPPQRPSA
VPLPTTQALALAGPKPKAHQFSIKSFSSPTQCSHCTSLMVGLIRQGYACEVCSFACHVS
CKDGAPQVCPIPPEQSKRPLGVDVQRGIGTAYKGHVKVPKPTGVKKGWQRAYAVVCDC
KLFLYDLPEGKSTQPGVIASQVLDLRDDEFSVSSVLASDVIHATRRDIPCIFRVTASLLGA
PSKTSSLLILTENENEKRKWVGILEGLQSILHKNRLRNQVVHVPLEAYDSSLPLIKAILTAAI
VDADRIAVGLEEGLYVIEVTRDVIVRAADCKKVHQIELAPREKIVILLCGRNHHVHLYPWS
SLDGAEGSFDIKLPETKGCQLMATATLKRNSGTCLFVAVKRLILCYEIQRTKPFHRKFNEI
VAPGSVQCLAVLRDRLCVGYPSGFCLLSIQGDGQPLNLVNPNDPSLAFLSQQSFDALCA
VELESEEYLLCFSHMGLYVDPQGRRARAQELMWPAAPVACSCSPTHVTVYSEYGVDVF
DVRTMWVVQTIGLRRIRPLNSEGTLNLLNCEPPRLIYFKSKFSGAVLNVPDTSDNSKKQML
RTRSKRRFVFKVPEEERLQQRREMLRDPELRSKMISNPTNFNHVAHMGPGDGMQVLM
DLPLSAVPPSQEERPGPAPTNLARQPPSRNKPYISWPSSGGSEPSVTVPLRSMSDPDQ
DFDKEPDSDSTKHSTPSNSSNPSGPPSPNSPHRSQLPLEGLEQPACDT


-------Predicted interaction result of the 1st two proteins:-------------------
-------------------------------------------------------------------------------------------------
The probability for interacting of the 1st two proteins:  0.9943
The probability for non-interacting of the 1st two proteins:  0.0057
Decision:  SIAH2 and MRCKB can interact
-------------------------------------------------------------------------------------------------
```

Figure 11. The probability of MRCKβ-Siah2 interaction as predicted using the LR_PPI tool.

2.2 Siah2 phosphorylation is enhanced in GECs infected with *H. pylori*

To determine the optimal cell to bacteria ratio of infection, MKN45 cells were infected with 100, 200 and 300 multiplicity of *H. pylori* for 12 h. Western blot of whole cell lysates showed that 200 MOI of *H. pylori* at 12 h optimally enhanced P-Thr-Siah2, P-Ser-Siah2 and Siah2 levels (Figure 12A). In order to elucidate the status of Siah2 phosphorylation after *H. pylori* infection, MKN45 cells were infected with 200 MOI of *cag* PAI (+) *H. pylori* strain 26695 for

12 h. Whole cell lysates were collected and western blotting was performed. An optimal increase in Siah2 was observed at 12 h PHPI (Figure 12B). Similarly, optimal levels of P-Thr-Siah2 and P-Ser-Siah2 were also detected at 12 h PHPI (Figure 12B). Siah2 induction in GECs infected with *H. pylori* is *cag* PAI status-independent [223, 230]. To evaluate the *cag* PAI-dependence of Siah2 phosphorylation, MKN45 cells were infected with 200 MOI of *cag* PAI (+) *H. pylori* strain 26695 and *cag* PAI (-) *H. pylori* strain 8-1 for 12 h. Both the strains enhanced P-Thr-Siah2, P-Ser-Siah2 and Siah2 levels, as showed by the western blot of the whole cell lysates from control and infected MKN45 cells (Figure 12C). Collectively, these results suggested that Siah2 phosphorylation was enhanced in GECs infected with *H. pylori* when compared with uninfected cells and this increase was optimal at 200 MOI, 12 h PHPI. Hereafter, "*H. pylori* infection" will mean infection with *H. pylori* strain 26695 at 200 MOI for 12 h, unless mentioned otherwise.
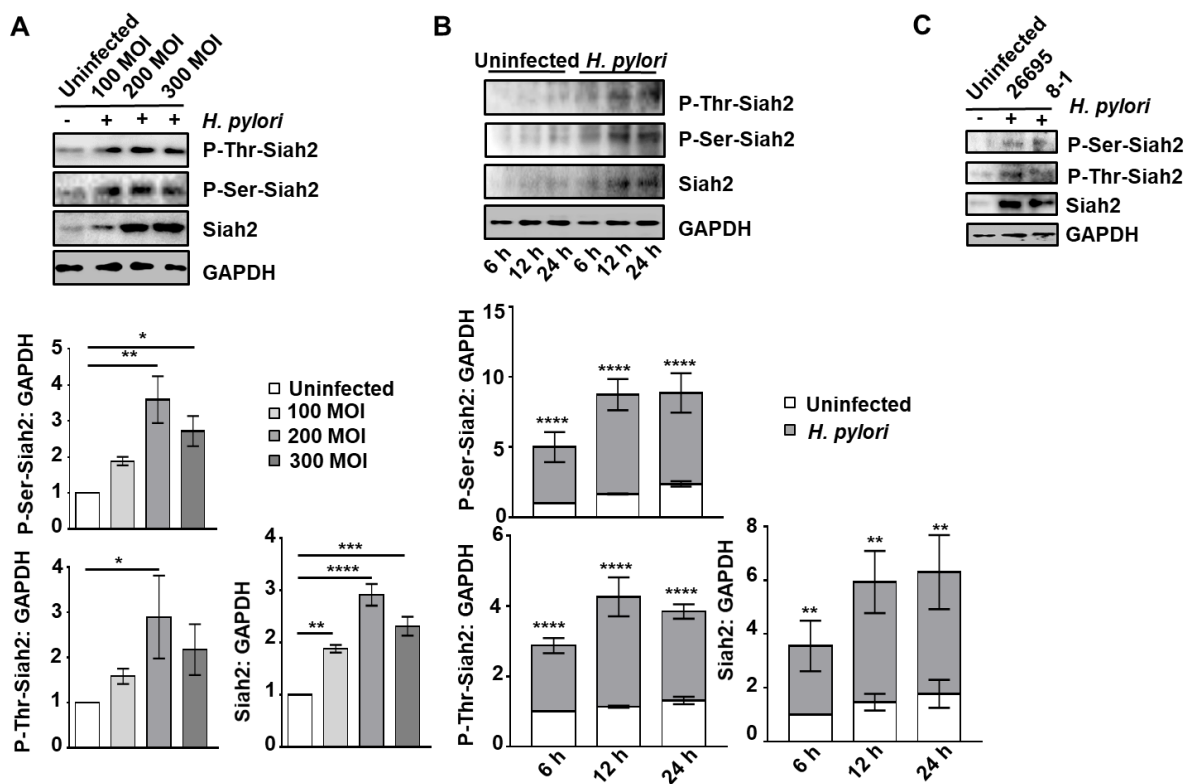
Figure 12. GEC infected with *H. pylori* show enhanced Siah2 phosphorylation. (A) When compared with uninfected cells, an upsurge in Siah2 and its phosphorylation was detected by western blot from infected (with various MOIs of *H. pylori* for 12 h) MKN45 cell lysates. P-Thr-Siah2, P-Ser-Siah2 and Siah2 were significantly enhanced at 200 MOI as shown by the bar graphs. Statistical significance was determined by one-way ANOVA. **(B)** Western blot of whole cell lysates from MKN45 cells infected with 200 MOI *H. pylori* for 6, 12 and 24 h exhibiting increased P-Thr-Siah2, P-Ser-Siah2 and Siah2. Bar graphs indicate a significant increase of P-Thr-Siah2, P-Ser-Siah2 and Siah2 at each time point PHPI. Two-way ANOVA accompanied by Tukey's post hoc analysis was used to determine the statistical significance. **(C)** Western blot of whole cell lysates from uninfected and infected (with *H. pylori* 26695 strain [*cag* PAI +] or 8–1 strain [*cag* PAI −]) MKN45 cells enhanced P-Ser-Siah2, P-Thr-Siah2 and Siah2 post infection (12 h, 200 MOI). GAPDH = loading control. Graphs are mean ± sem. n = 3. *$P < 0.05$, **$P < 0.01$, ***$P < 0.001$, ****$P < 0.0001$.

2.3 *H. pylori*-mediated GC shows decreased MRCKβ protein

Phosphorylation-induced enhanced Siah2 activity leads to proteasomal degradation of its kinases [225-227]. As the identified kinase MRCKβ has Siah "degron motifs", this necessitated elucidation of *H. pylori* infection-driven regulation of MRCKβ. In order to elucidate the status of MRCKβ PHPI, MKN45 cells were infected for varied durations. Western blot of the total cellular lysates showed a decrease in MRCKβ protein levels PHPI. The decrease was optimal at 12 h of infection (Figure 13A). MKN45 cells were either left uninfected or were infected with 100, 200 or 300 MOI *H. pylori* for 12 h. Western blot from the whole cell lysates confirmed an optimal decrease of MRCKβ at 200 MOI (Figure 13B). Western blot of uninfected and *H. pylori* 26695 or 8-1 strain-infected (200 MOI, 12 h) MKN45 cells determined MRCKβ decrease to be independent of the *H. pylori cag* PAI status (Figure 13C). Further, MRCKβ protein levels were evaluated in human GC biopsy tissues. Biopsies were

obtained from consenting GC patients' gastric antrum who were urea breath-test positive. Immunostaining of the tissues showed a reduction in MRCKβ protein level in metastatic tissues as compared to their paired-normal (Figure 13D).
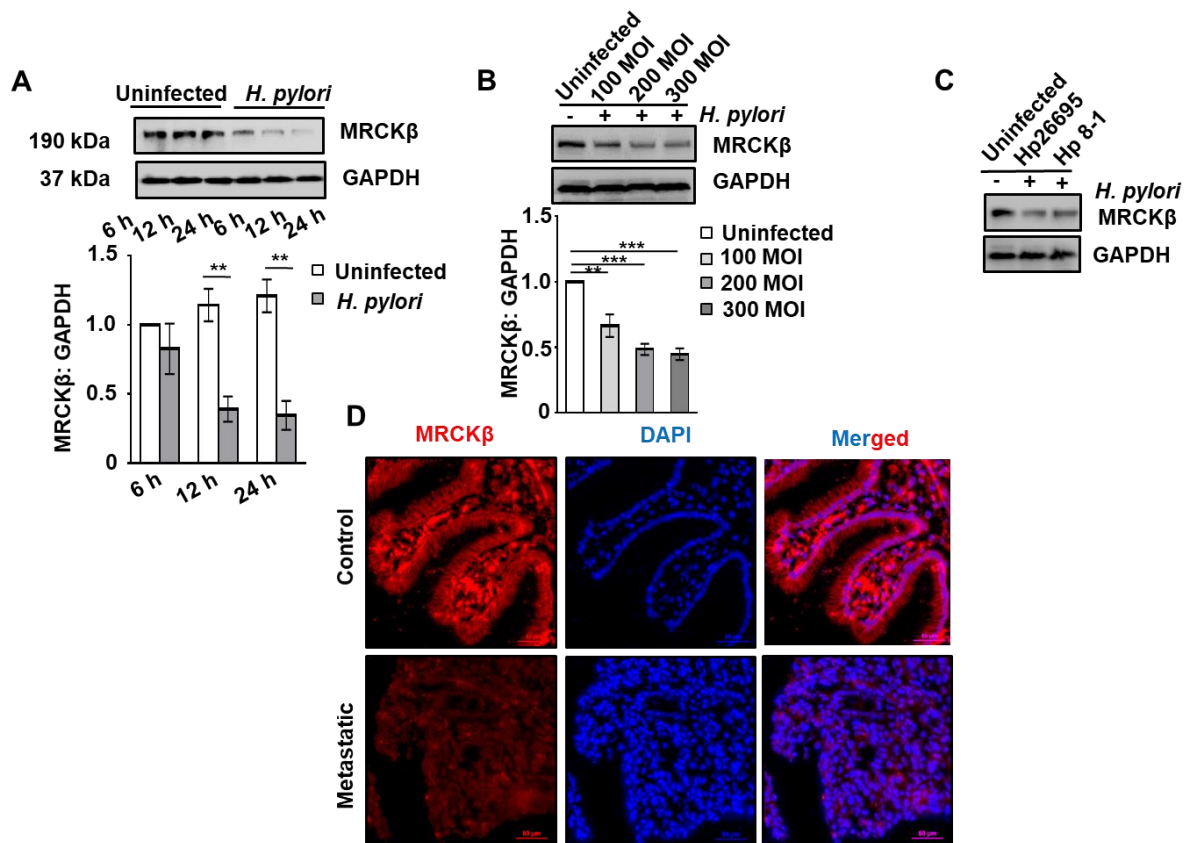
Figure 13. *H. pylori* decreases MRCKβ in the gastric epithelium. (A) Western blot of whole cell lysates from uninfected and infected MKN45 cells showed decreased MRCKβ level with infection. Graphs show significant decrease in MRCKβ at 12 h and 24 h PHPI. Statistical significance was determined by two-way ANOVA followed by Tukey's post hoc analysis. GAPDH was used as loading control. Graphs are mean ± sem. n = 3. $**P < 0.01$. **(B)** Total cellular lysates from uninfected and infected MKN45 cells showed an optimal decrease at 200 MOI as assessed by western blot. Bar graphs depict MRCKβ protein level. Statistical significance was determined by one-way ANOVA. GAPDH = loading control. Graphs are mean ± sem. n = 3. $**P < 0.01$, $***P < 0.001$. **(C)** Western blot of whole cell lysates from the

2.4 MRCKβ colocalizes and interacts with Siah2

To elucidate colocalization of MRCKβ with Siah2, AGS cells were used. AGS cells were seeded on coverslips and were either left uninfected or were *H. pylori*-infected. These cells were then immuno-probed using Siah2 and MRCKβ antibodies. Confocal microscopy exhibited that MRCKβ decrease was accompanied with increased Siah2 levels PHPI. Analysis of the Pearson's coefficient and the Mander's overlap coefficient indicated colocalization between Siah2 and MRCKβ in both uninfected as well as *H. pylori*-infected GEC (Figure 14A). The high degree of colocalization also pointed towards Siah2-MRCKβ interaction. The interaction between Siah2 and MRCKβ was confirmed by infecting MKN45 cells. The whole cell lysates were subjected to co-immunoprecipitation using Siah2 antibody. The obtained immuno-complexes confirmed of the Siah2-MRCKβ interaction as assessed by western blot (Figure 14B). Western blots also pointed to the decreased MRCKβ interaction in *H. pylori*-infected cell lanes. As Siah2 is an E3 ubiquitin ligase, it ubiquitinates its interacting partners and marks them for proteasomal degradation [199, 232]. Hence, it became imperative to assess the ubiquitination status of MRCKβ in *H. pylori*-infected GECs. For this, MKN45 cells were either uninfected or were infected with *H. pylori* along with treatment of 50 μM proteasomal inhibitor Z-Leu-Leu-Leu-al (MG132) for 12 h. The formed ubiquitin aggregates were detected by probing the western blot membranes with anti-ubiquitin antibody. Detection of western blots showed rescue of the ubiquitinated proteins in the *H. pylori*-infected and MG132-treated lanes (Figure 14C). Confirmation of MRCKβ rescue post MG132 treatment was done by reprobing the blots with MRCKβ antibody. Further, the change in Siah2-MRCKβ interaction post MG132

treatment was assessed. For this, MKN45 cells were either left uninfected or were infected with *H. pylori* along with 50 µM MG132 treatment for 12 h. Co-immunoprecipitation of the whole cell lysates using Siah2 antibody followed by western blotting showed that MG132 rescued Siah2-MRCKβ interaction (Figure 14D).
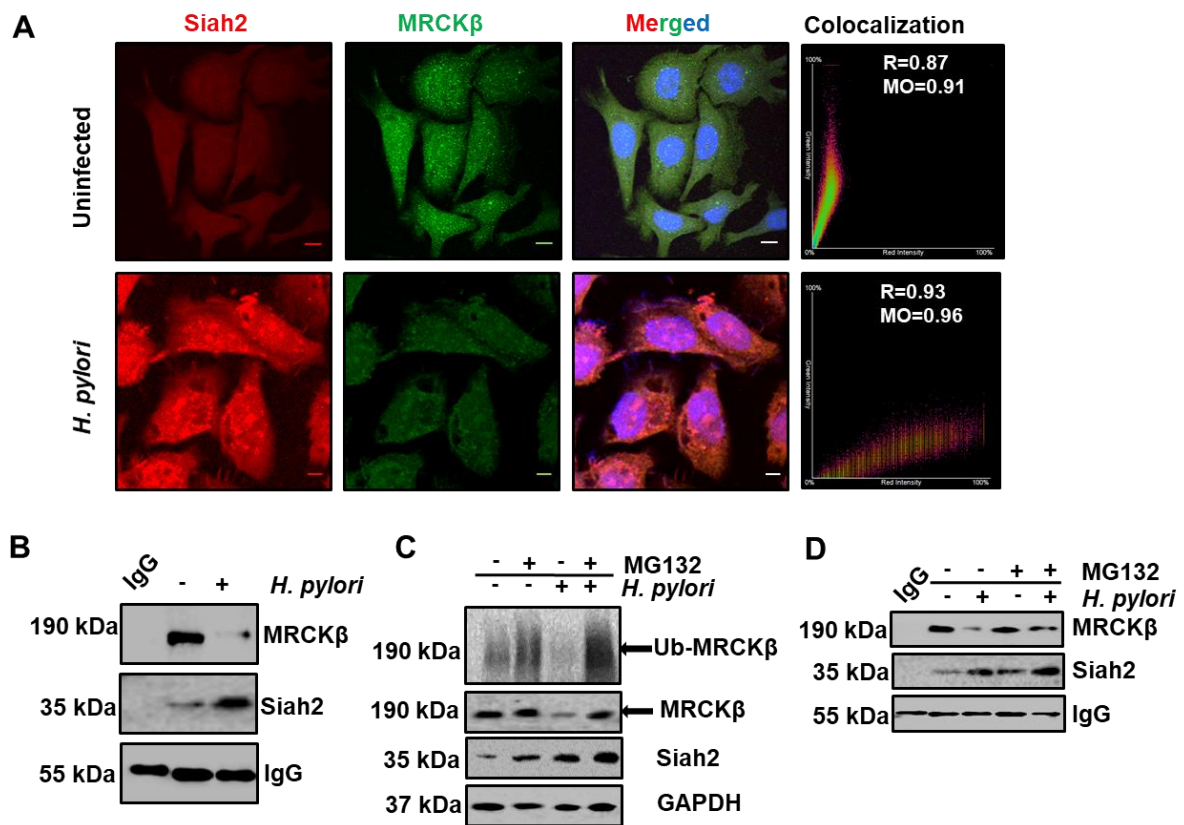
Figure 14. MRCKβ-Siah2 colocalization and interaction in *H. pylori*-infected GECs. (A) Confocal microscopy images of uninfected and *H. pylori*-infected AGS cells exhibiting subcellular localization of Siah2 and MRCKβ. Scale bars = 5 µm. The scatter plots exhibiting the degree of colocalization was generated using Nikon advance research software. **(B)** Western blot of the immuno-complexes obtained from co-immunoprecipitation of the uninfected and *H. pylori*-infected total cell lysates. IgG band = loading control. **(C)** Western blot of the whole cell lysates from 50 µM MG132-treated uninfected and *H. pylori*-infected MKN45 cells exhibited MRCKβ ubiquitination status. MRCKβ, Siah2 and the loading control GAPDH has been obtained by reprobing. Arrows indicate the position of MRCKβ band. **(D)**

Western blot indicating MRCKβ and Siah2 protein status in immunocomplexes obtained from 50 μM MG132-treated uninfected or *H. pylori*-infected MKN45 cells using Siah2 antibody. IgG band = loading control.

2.5 MRCKβ degradation in *H. pylori*-infected GEC is Siah2-mediated

These results so far confirmed of Siah2-MRCKβ interaction and colocalization. Also, as Siah2 increases there is a concomitant decrease of MRCKβ. In order to elucidate whether this MRCKβ decrease is due to Siah2 upregulation, pcDNA3.1+ and *siah2* WT-overexpressing MKN45 stable cells were infected with *H. pylori*. These cells were then processed for immunofluorescence microscopy and probed using Siah2 and MRCKβ antibodies. Fluorescence microscopy images and the bar graphs showed that as the levels of Siah2 increase, there was a concomitant decrease of MRCKβ (Figure 15A). Siah2-dependent MRCKβ regulation was further confirmed by transfecting MKN45 cells with either human control siRNA or human *siah2* siRNA for 36 h followed by *H. pylori* infection. Western blot of whole cell lysates showed that MRCKβ protein was salvaged after *siah2* suppression (Figure 15B). Thus, these results confirmed that Siah2 mediated the *H. pylori*-driven decrease in MRCKβ.
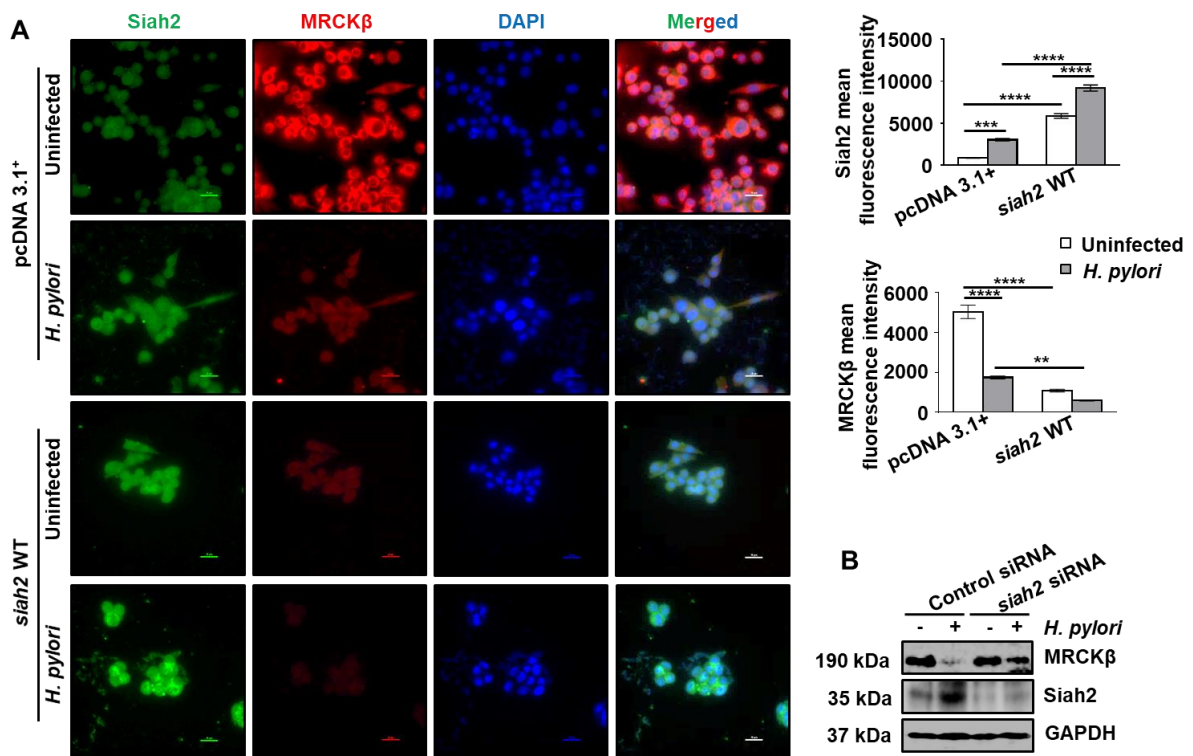
Figure 15. Siah2 reduces MRCKβ. (A) Immunofluorescence microscopy images of pcDNA3.1+ and *siah2* WT overexpressing MKN45 stable cells exhibiting Siah2 and MRCKβ protein status. Objective used = 60X. Scale bars = 20 μm. Graphs represent mean fluorescent intensities of Siah2 and MRCKβ protein. Statistical significance was determined by two-way ANOVA. n = 3. Graphs = mean ± sem. $**P < 0.01$, $***P < 0.001$, $****P < 0.0001$. **(B)** Western blot of whole cell lysates from control and *siah2* siRNA transfected MKN45 cells (either uninfected or *H. pylori*-infected). GAPDH = loading control.

2.6 Siah2 phosphorylation and stability are mediated by MRCKβ in GECs infected with *H. pylori*

To elucidate the role of MRCKβ on Siah2 phosphorylation, MKN45 cells were transfected with either pEGFP-N1 (empty vector) or *mrckβ* overexpression plasmids for 36 h followed by 6 h or 12 h of *H. pylori* infection (200 MOI). Whole cell lysates were western blotted which depicted that Siah2 and its phosphorylation were increased post *mrckβ* overexpression and *H. pylori* infection (Figure 16). These increases were found to be significant at 12 h PHPI.
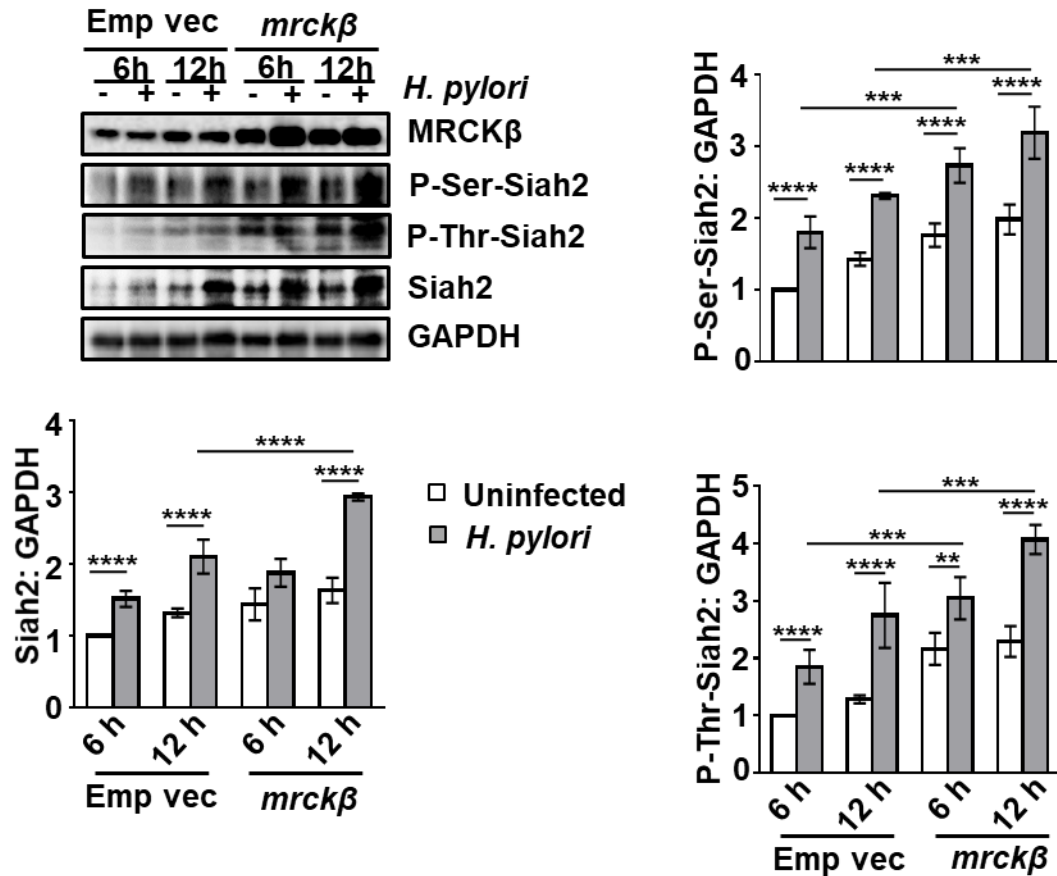
Figure 16. Enhanced Siah2 phosphorylation upon *H. pylori* infection in *mrckβ*-overexpressed MKN45 cells. Western blot of the whole cell lysate from uninfected and *H. pylori*-infected empty vector or *mrckβ* overexpressing MKN45 cells. GAPDH = loading control. Graphs represent the protein levels of Siah2, P-Ser-Siah2 and P-Thr-Siah2. Statistical significance determined by two-way ANOVA. n = 3. Graphs = mean ± sem. **$P < 0.01$, ***$P < 0.001$, ****$P < 0.0001$.

Further, NetPhos3.0 software [233] was used to elucidate the possible residues of Siah2 phosphorylation. Among the identified Siah2 residues, the ones with high possibility of phosphorylation are represented in Table 4.

Table 4. Phosphorylation prediction of Siah2 determined by the NetPhos 3.0 software.

Siah2 sites	Predicted score
Ser^6	0.996
Thr^{275}	0.986
Thr^{279}	0.931
Ser^{282}	0.992

The above identified residues are represented in the sequence and multi-domain structure of Siah2 (Figure 17).

Figure 17. The sequence and multi-domain structure of Siah2 with probable phosphorylatable residues.

In order to assess the importance of Siah2 phosphorylation at the above-mentioned residues, we substituted the Ser/Thr residues with that of Ala using site-directed mutagenesis. Empty vector, *siah2* WT and the generated *siah2* S6A, T275A, T279A and S282A plasmids were overexpressed in MKN45 cells. Stable-transfected cells were generated to avoid disparities due to transfections. As *mrckβ* overexpression led to enhanced Siah2 phosphorylation,

identification of the Siah2 residue(s) which could be phosphorylated by MRCKβ became imperative. Thus, empty vector, *siah2* WT and Siah2 phospho-null mutants-expressing MKN45 stable cells were transfected with *mrckβ* for 36 h succeeded by *H. pylori* infection. Western blots of the whole cell lysates revealed that P-Ser-Siah2 levels increased in all lanes except for *siah2* S6A. Similarly, P-Thr-Siah2 level was reduced in case of *siah2* T279A-expressing stable cells as compared to the *siah2* WT and *siah2* T275A phospho-null mutant-expressing stable cells (Figure 18A, B). Thus, Siah2 Ser[6] and Thr[279] were identified to be the prime residues of MRCKβ-mediated Siah2 phosphorylation and the phosphorylated residues also affected Siah2 stability. Taking into account the importance of Siah2 phosphorylation at Ser[6] and Thr[279] residues, antibodies detecting phosphorylated-Ser[6]-Siah2 (P-Ser[6]-Siah2) and phosphorylated-Thr[279]-Siah2 (P-Thr[279]-Siah2) were generated. In order to confirm MRCKβ-mediated Siah2 Ser[6] and Thr[279] phosphorylation, MKN45 cells were transfected with control and *mrckβ* siRNAs for 36 h succeeded by *H. pylori* infection. Western blot depicted that by suppressing *mrckβ*, Siah2 and its phosphorylation were abrogated as detected by using customized Siah2 phospho-specific antibodies (Figure 18C). The importance of MRCKβ on Siah2 Ser[6] and Thr[279] phosphorylation was further confirmed by challenging the empty vector and *mrckβ*-overexpressing AGS cells with *H. pylori*. Fluorescence microscopy reaffirmed the previous results that Siah2 phosphorylation is enhanced after *mrckβ* overexpression and *H. pylori* infection (Figure 18D). Taken together, these results established that MRCKβ facilitated Siah2 Ser[6] and Thr[279] phosphorylation and contributed to enhance the stability of the latter in GECs infected with *H. pylori*.
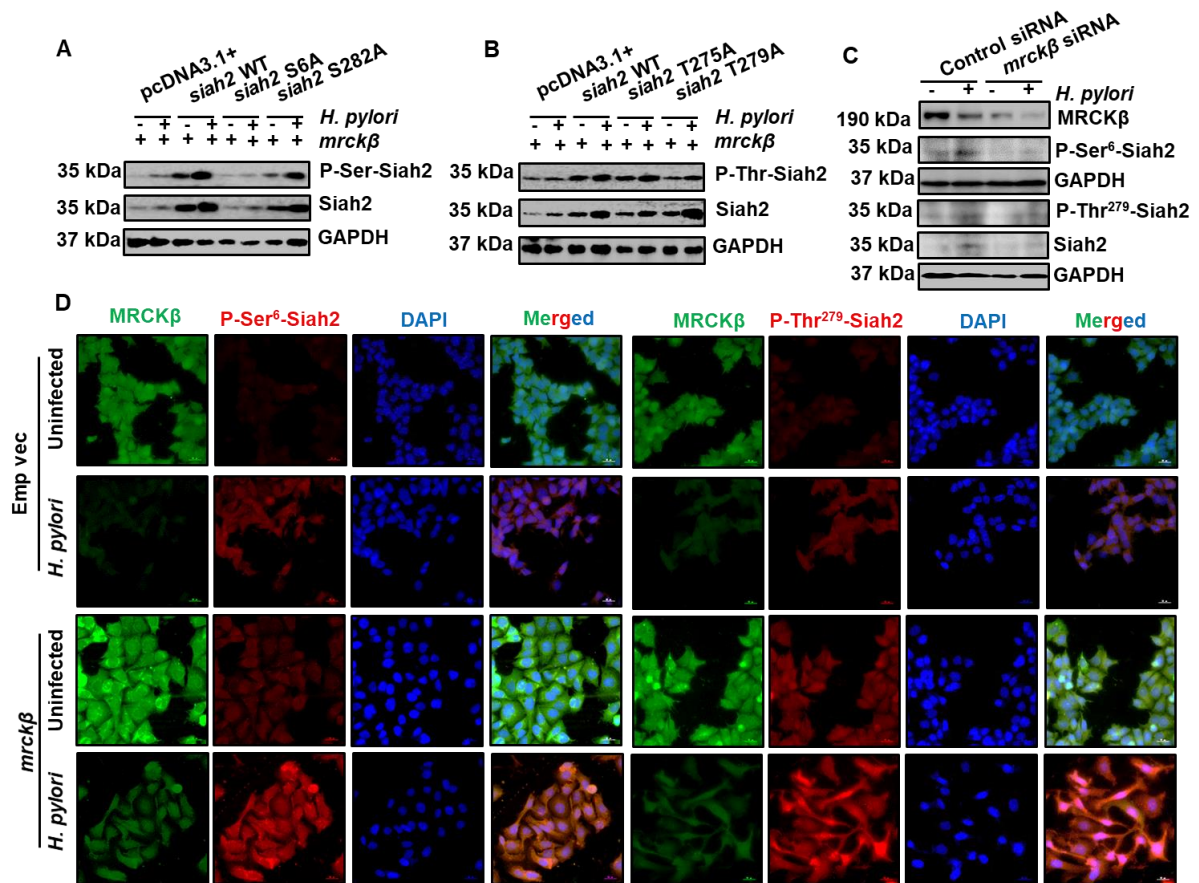
Figure 18. MRCKβ-mediated Siah2 phosphorylation in *H. pylori*-infected GECs. (A) Western blot representing the status of P-Ser-Siah2 and Siah2 in MKN45 pcDNA3.1+, *siah2* WT, *siah2* S6A and *siah2* S282A-overexpressing stable cells transfected with *mrckβ* and infected with *H. pylori*. GAPDH was used as the loading control. **(B)** Western blot representing the status of P-Thr-Siah2 and Siah2 in MKN45 pcDNA3.1+, *siah2* WT, *siah2* T275A and *siah2* T279A-overexpressing stable cells transfected with *mrckβ* and infected with *H. pylori*. GAPDH was used as the loading control. **(C)** Western blot of the whole cell lysates from MKN45 cells transfected with control and *mrckβ* siRNAs for 36 h followed by *H. pylori* infection showing the levels of MRCKβ, P-Ser^6-Siah2, P-Thr^{279}-Siah2 and Siah2. GAPDH = loading control. **(D)** Immunofluorescence micrographs showing enhanced P-Ser^6-Siah2 and P-Thr^{279}-Siah2 in *mrckβ*-overexpressed and *H. pylori*-infected AGS cells. Objective used = 60X. Scale bars = 20 μm.

To investigate whether the enhanced Siah2 phosphorylation was dependent on the stage of GC, AGS and MKN45 cells were infected with *H. pylori*. Western blot of the whole cell lysates revealed that protein levels of Siah2, P-Ser^6-Siah2 and P-Thr^{279}-Siah2 increased, however, MRCKβ decreased PHPI (Figure 19A). Similar findings were also observed in immortalized but non-neoplastic HFE145 cells (Figure 19B).
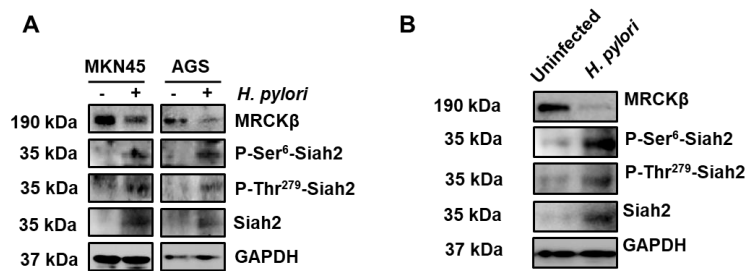
Figure 19. *H. pylori* **infection enhanced P-Siah2 in GECs. (A)** Western blot of whole cell lysates from AGS and MKN45 cells indicating the status of Siah2 and its phosphorylation as assessed by using the customized antibodies. GAPDH = loading control. **(B)** Western blot of the whole cell lysates from uninfected and *H. pylori*-infected HFE145 cells indicating enhanced P-Siah2 and Siah2 PHPI. GAPDH = loading control.

2.7 Discussion

Phosphorylation is the most prominent PTM [234]. Several cellular processes are regulated by phosphorylation. This study identifies for the first time the status and the mechanism of Siah2 phosphorylation *H. pylori*-infected GECs. The identified Ser/Thr kinase MRCKβ is a member of the Rho GTPases subfamily, a part of the AGC family of kinases (i.e., protein kinases A, G and C). This multi-domain protein is important for the modulation of actin-myosin cytoskeletal dynamics [235, 236]. MRCKβ-mediated cytoskeletal dynamics regulation justifies its role in the invasion and migration of various cancers.

The identified Siah2-MRCKβ interaction in *H. pylori*-infected GECs is a novel finding. Challenge with *H. pylori* decreases MRCKβ protein in GECs. MRCKβ is also decreased in metastatic human antral GC biopsy tissues. Since Siah2 is an E3-ubiquitin ligase and ubiquitinates its interacting partners, it is a "kiss of death signal" for MRCKβ. Siah2 ubiquitinates MRCKβ in GECs infected with *H. pylori*. Rose *et al*. have also identified MRCKβ ubiquitination using mass spectrometric approach in several cells and tissue samples [237]. Treatment with the proteasomal inhibitor MG132 rescues MRCKβ from degradation, thus, indicating Siah2-mediated regulation of MRCKβ abundance in GECs infected with *H. pylori*. This finding is in agreement with other reports which suggest Siah2 to regulate the abundance of its kinases [225, 238]. This study is the first report of Siah2 phosphorylation in *H. pylori*-infected GECs and this phosphorylation is MRCKβ-mediated. Phosphorylation at Ser^6 and Thr^{279} residues has also been confirmed by the use of custom-generated P-Ser^6-Siah2 and P-Thr^{279}-Siah2 antibodies. Mass spectrometric approach has identified Siah2 Ser^6-phosphorylation in myelogenous leukemia cell line K562 [239]. However, elucidation of the kinase involved and the functional implications are out of scope of their study. Having identified the kinase and the residues involved in Siah2 phosphorylation, this study has further explored the insinuations of Siah2 phosphorylation at Ser^6 and Thr^{279} residues.

Chapter 3

Phosphorylation of Siah2 at Ser^6 regulates ROS generation

3.1 Siah2 Ser^6-phosphorylation regulates ROS in *H. pylori*-infected GECs

H. pylori infection generates ROS [240-242]. The generated ROS enhance the invasiveness of *H. pylori*-infected GECs [214]. Siah2 protein, enhanced PHPI, has been implicated in the regulation of ROS generation under various conditions [201, 213]. However, the understanding of ROS regulation by Siah2 in *H. pylori*-infected GECs remained elusive. pcDNA3.1+, *siah2* WT, *siah2* phospho-null mutants S6A and T279A stably-expressed MKN45 cells were either left uninfected or were infected. After infection, these cells were treated with 1 μM ROS indicator 2,7-dichlorodihydrofluorescein diacetate (DCFDA) for 1 h. Fluorescence microscopy followed by measurement of mean fluorescence intensity indicative of ROS generation was performed. ROS were enhanced with *siah2* overexpression which further surged after the disruption of Siah2 phosphorylation at Ser^6 but not after the disruption of phosphorylation at Siah2 Thr^{279} (Figure 20A, B). This established the importance of Siah2 phosphorylation at Ser^6 in reducing the ROS burden of *H. pylori*-infected GECs. As Siah2 phospho-null mutant S6A generated maximum ROS PHPI, only these phospho-null mutants were considered for further experiments.
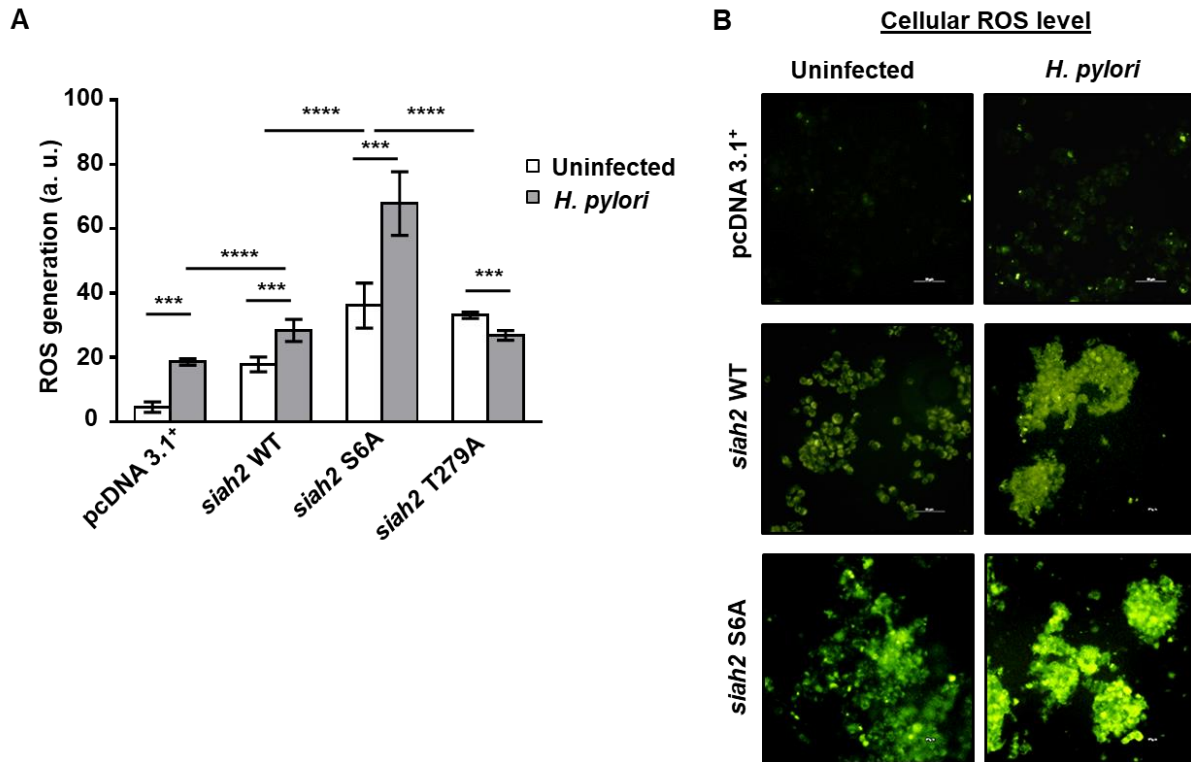
Figure 20. ROS modulation by Siah2 and its phospho-null mutants in *H. pylori*-infected GECs. (A) Graphical representation of ROS generation by pcDNA3.1+, *siah2* WT, *siah2* phospho-null mutants S6A and T279A stably-expressed MKN45 cells uninfected or infected with *H. pylori*. Graphs represent evaluations from at least 90 cells (10 cells from three different fields and repeated for three different experiments). Graphs = mean ± sem. Statistical significance determined by two-way ANOVA. ***$P < 0.001$, ****$P < 0.0001$. **(B)** Representative immunofluorescence images depicting ROS generation in uninfected or *H. pylori*-infected pcDNA3.1+, *siah2* WT and *siah2* phospho-null mutant S6A MKN45 stable cells. Objective used = 40X. Scale bars = 50 μm.

3.2 GRP78 modulates ROS generation in *H. pylori*-infected GECs

ROS homeostasis is maintained by an intricate balance between the ROS generation and the antioxidant proteins. As Siah2 modulates ROS generation, finding its role in the regulation of redox proteins became imperative. For this, MKN45 cells were transfected with either empty

vector or *siah2* overexpression plasmids for 36 h succeeded by *H. pylori* infection. Whole cell lysates were co-immunoprecipitated using Siah2 antibody and the obtained immuno-complexes were subjected to SDS-PAGE followed by staining with CBB. The differentially-expressed bands were excised and mass spectrometric analysis was done. Amongst the interacting partners, only one antioxidant protein, a 78-kDa glucose-regulated protein (GRP78) was identified (Table 5).

Table 5. MS results for GRP78 protein.

Protein	Score	Coverage	Unique peptides	Predicted MW
GRP78	1182.81	42.66	21	72.3 kDa

GRP78 mediates antioxidant response in various cancers [243, 244]. However, so far. its role in ROS modulation of *H. pylori*-infected GECs remained unknown. To elucidate the role played by GRP78 in ROS modulation, empty vector and *grp78*-expressing AGS stable cells were either left uninfected or were infected with *H. pylori*. These cells were then processed for detection of ROS. Fluorescence microscopy revealed that ROS levels decreased with *grp78* overexpression (Figure 21A). Further, ROS generation was assessed by suppressing *grp78* using siRNA. AGS cells transfected with *grp78* siRNA depicted enhanced ROS generation as compared to the cells transfected with control siRNA. ROS generation was further surged after *H. pylori* infection in *grp78*-suppressed AGS cells (Figure 21B). Thus by overexpression-suppression studies, this study established GRP78 to be at the centre stage of ROS regulation in *H. pylori*-infected GECs.
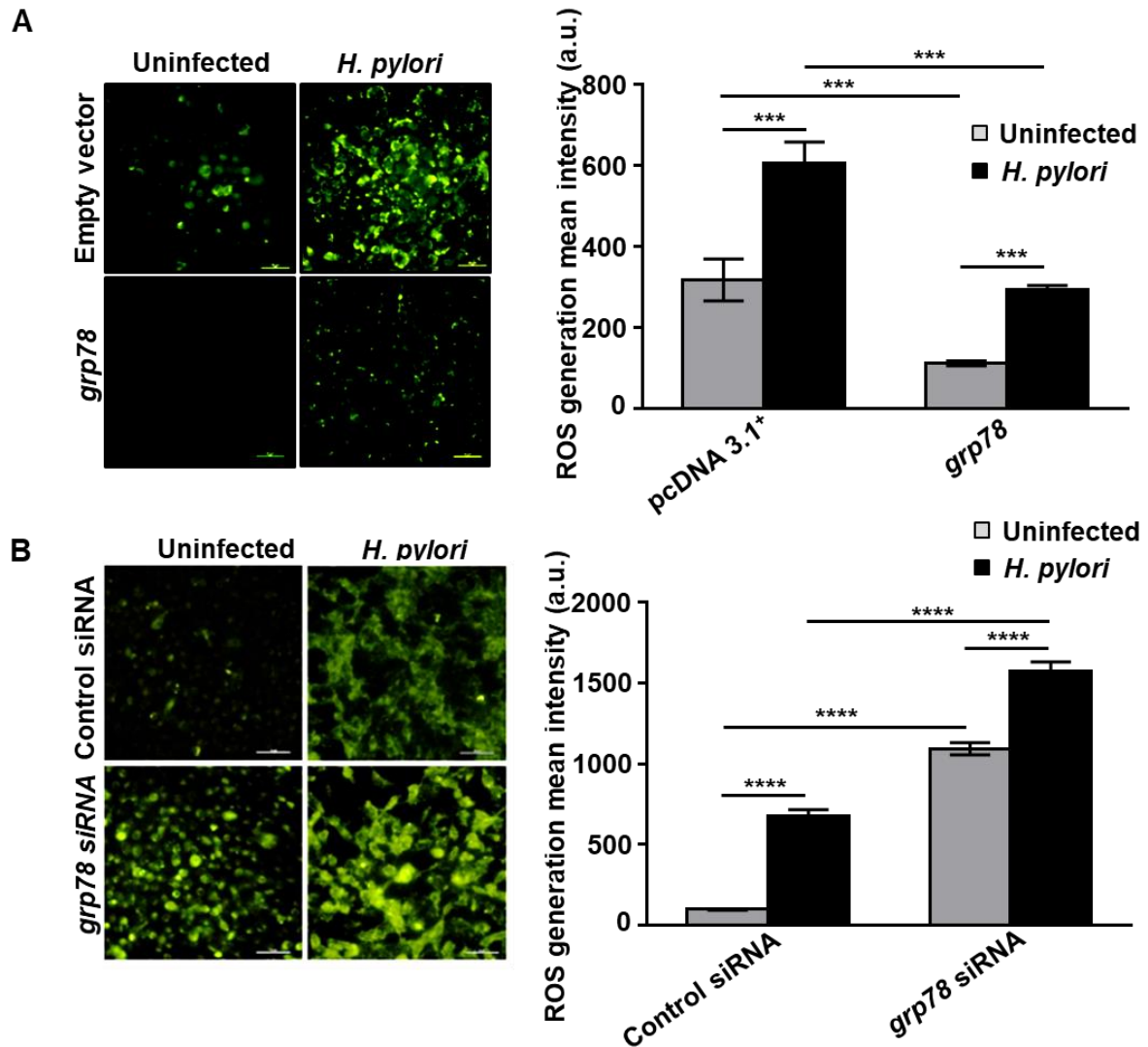
Figure 21. GRP78 modulates ROS generation in *H. pylori*-infected GECs. (A) Fluorescence microscopy images depicting ROS generation in uninfected or *H. pylori*-infected (200 MOI, 12 h) empty vector and *grp78* AGS stable cells. Graphs represent ROS generation mean intensity. **(B)** Images representing ROS generation in AGS cells transfected with control and *grp78* siRNA for 36 h succeeded by 12 h of *H. pylori* infection. Graphs represent ROS generation mean intensity. For all images, objective used = 40X; scale bars = 50 μm. Graphs = mean ± sem. Statistical significance determined by two-way ANOVA. n = 3. ***$P < 0.001$, ****$P < 0.0001$.

3.3 GRP78 interacts with Siah2 and is decreased in *H. pylori*-infected GEC

GRP78 amino acid sequence exhibited the presence of Siah "degron motifs", which were indicative of possible Siah2-GRP78 interaction (Figure 22).

```
>NP_005338.1 78 kDa glucose-regulated protein precursor [Homo sapiens]
MKLSLVAAMLLLLSAARAEEEDKKEDVGTVVGIDLGTTYSCVGVFKNGRVEIIANDQGNRITPS
YVAFTPEGERLIGDAAKNQLTSNPENTVFDAKRLIGRTWNDPSVQQDIKFLPFKVVEKKTKPYI
QVDIGGGQTKTFAPEEISAMVLTKMKETAEAYLGKKVTHAVVTVPAYFNDAQRQATKDAGTIAG
LNVMRIINEPTAAAIAYGLDKREGEKNILVFDLGGGTFDVSLLTIDNGVFEVVATNGDTHLGGED
FDQRVMEHFIKLYKKKTGKDVRKDNRAVQKLRREVEKAKRALSSQHQARIEIESFYEGEDFSE
TLTRAKFEELNMDLFRSTMKPVQKVLEDSDLKKSDIDEIVLVGGSTRIPKIQQLVKEFFNGKEPS
RGINPDEAVAYGAAVQAGVLSGDQDTGDLVLLD**VCP**LTLGIETVGGVMTKLI**PRNTVVP**TKKSQ
IFSTASDNQPTVTIKVYEGERPLTKDNHLLGTFDLTGIPPAPRGVPQIEVTFEIDVNGILRVTAED
KGTGNKNKITITNDQNRLTPEEIERMVNDAEKFAEEDKKLKERIDTRNELESYAYSLKNQIGDKE
KLGGKLSSEDKETMEKAVEEKIEWLESHQDADIEDFKAKKKELEEIVQPIISKLYGSAGPPPTG
EEDTAEKDEL
```

Figure 22. GRP78 protein sequence showing presence of Siah "degron motifs". The sequences present are underlined and highlighted.

The Siah2-GRP78 interaction was confirmed by western blot of immuno-complexes from uninfected and *H. pylori*-infected (200 MOI, 12 h) MKN45 cells co-immunoprecipitated using Siah2 antibody. *H. pylori* infection decreased Siah2-GRP78 interaction (Figure 23A). This necessitated elucidation of GRP78 status in GECs infected with *H. pylori*. For this, MKN45 cells were infected with 200 MOI *H. pylori* for various time durations (6 h, 12 h, and 24 h). Western blot analysis showed that GRP78 decreased optimally at 12 h PHPI (Figure 23B). The optimal ratio of infection for GRP78 decrease was determined by infecting MKN45 cells with various MOIs. Western blot analysis of the whole cell lysates confirmed that GRP78 was decreased optimally at 200 MOI, 12 h (Figure 23C). *cag* PAI-dependence of GRP78 protein expression was assessed further. For this, MKN45 cells were infected with *cag* PAI (+) *H. pylori* strain 26695 and *cag* PAI (-) strain 8-1 (200 MOI, 12 h). Western blot analysis showed that GRP78 was decreased independent of *H. pylori cag* PAI status (Figure 23D).
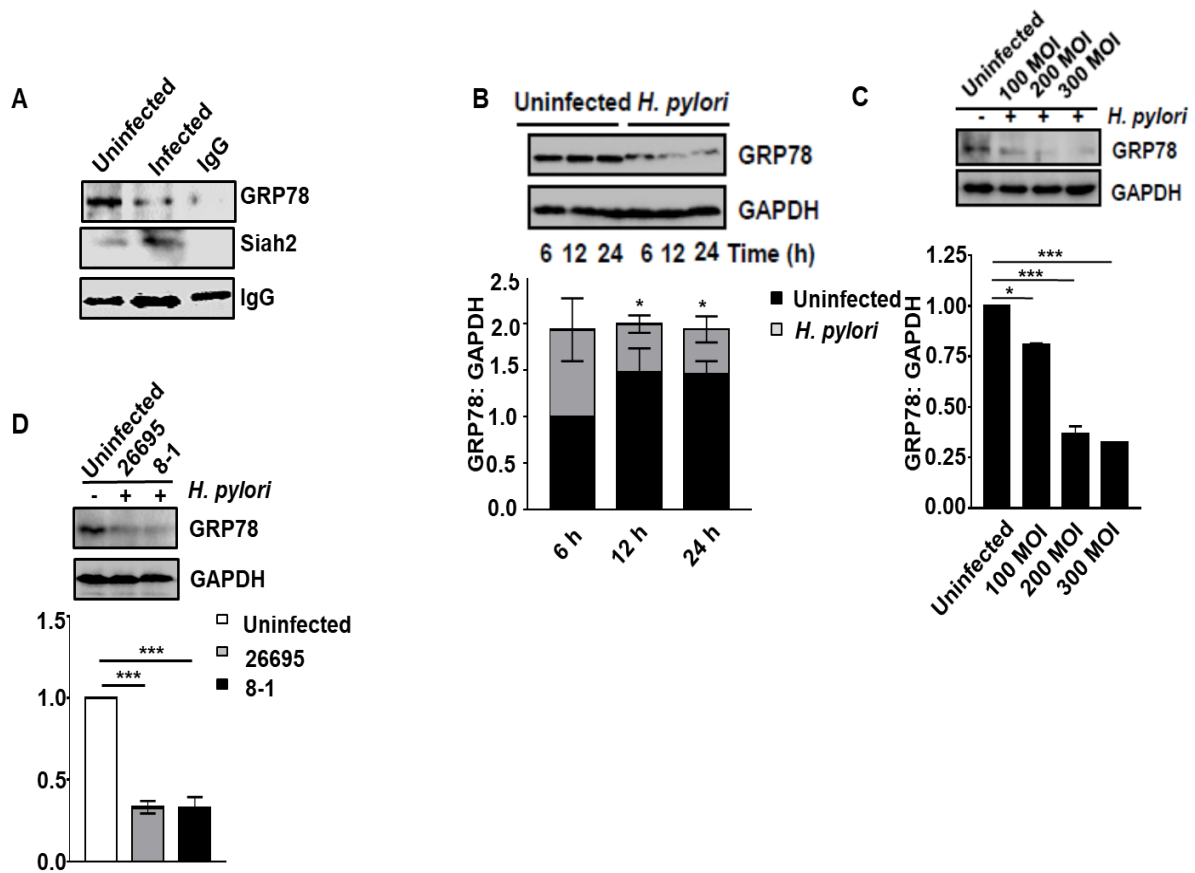
Figure 23. Siah2-GRP78 interaction and status of GRP78 in GECs infected with *H. pylori*.

(A) Western blot of the immuno-complexes obtained from co-immunoprecipitation of uninfected and *H. pylori*-infected MKN45 cells exhibiting Siah2-GRP78 interaction. IgG band was used as the loading control. **(B)** Western blot of the whole cell lysates from uninfected and *H. pylori*-infected MKN45 cells showing GRP78 decrease PHPI. GAPDH = loading control. Graphs show the densitometric analysis of the western blots. Two-way ANOVA was used to determine the statistical significance. **(C)** Decrease of GRP78 at various *H. pylori* MOIs as shown by the western blot analysis from whole cell lysates of uninfected and infected MKN45 cells. GAPDH = loading control. Bar graphs showing decrease of GRP78 at various *H. pylori* MOIs. Statistical significance was determined by one-way ANOVA. **(D)** Western blot of whole cell lysates from uninfected and infected (with *H. pylori* strain 26695 or 8-1) MKN45 cells depicting the *cag* PAI-independence of GRP78 decrease. Graphs depicting similar decrease of

Further, human antral GC biopsy tissues were probed with GRP78 antibody and processed for fluorescence microscopy. Micrographs depicted that the levels of GRP78 decreased in both adenocarcinoma as well as metastatic GC tissues as compared to their paired normal tissues (Figure 24).
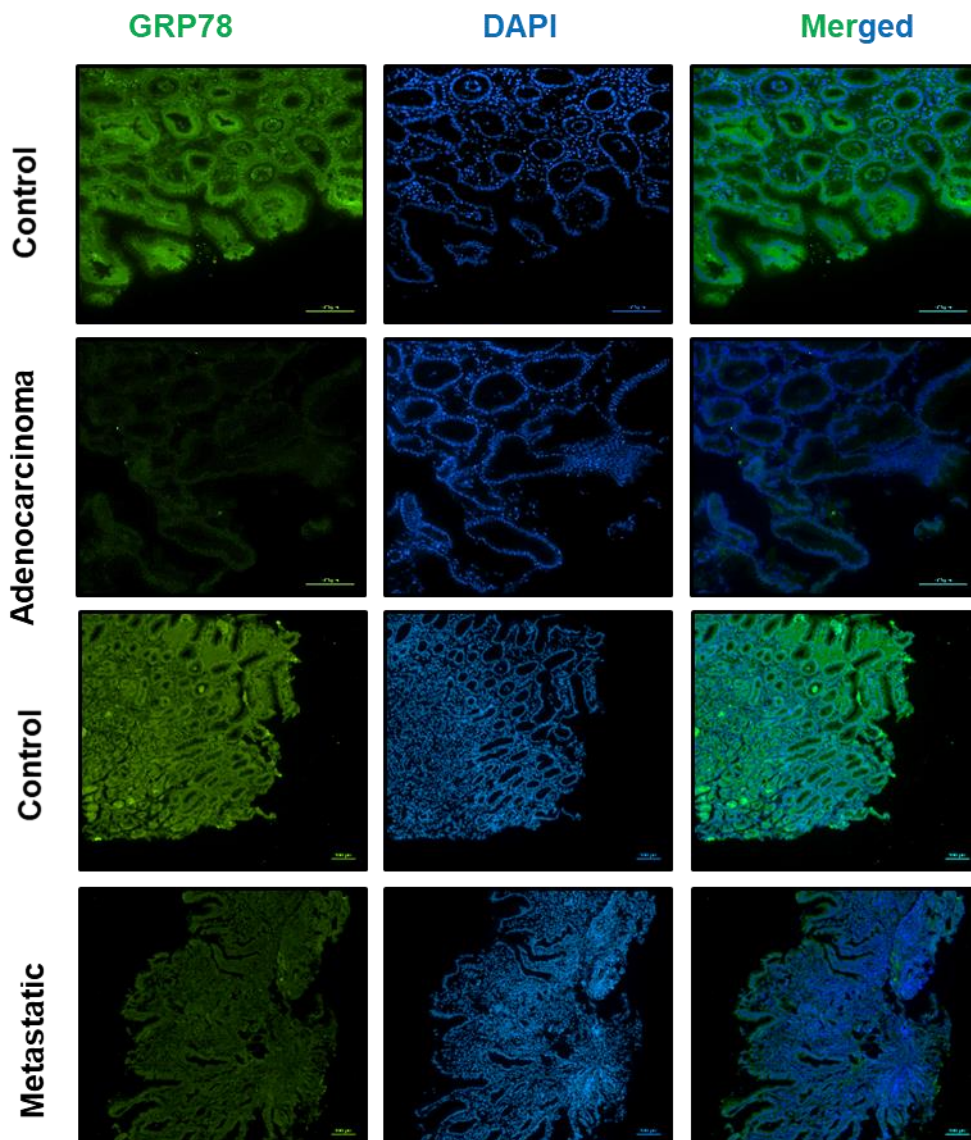
Figure 24. GRP78 is decreased in human gastric biopsy tissues. Human antral adenocarcinoma and metastatic GC biopsy tissues depicting the status of GRP78 protein. Objective used = 10X. Scale bars = 100 μm.

3.4 Siah2 causes proteasomal degradation of GRP78

From the results shown above it was evident that GRP78 decreased in *H. pylori*-mediated GC. Since GRP78 interacts with Siah2, it became crucial to elucidate whether GRP78 decrease is Siah2 mediated or not. For this, empty vector and *siah2* stably-expressed MKN45 cells were cultured on coverslips. These cells were either left uninfected or were infected with *H. pylori*. Confocal microscopy indicated that infection-mediated GRP78 decrease was further lowered after *siah2* overexpression (Figure 25A). To assess proteasome dependence of GRP78 decrease, pcDNA3.1+ and *siah2*-expressing MKN45 stable cells were treated with 50 μM MG132 or equivalent of medium control {dimethyl sulfoxide (DMSO)} along with *H. pylori* infection (200 MOI, 12 h). Confocal microscopy depicted that MG132 rescued GRP78 in infected cells (Figure 25B). These results established that GRP78 decrease was Siah2-dependent and proteasome-mediated.
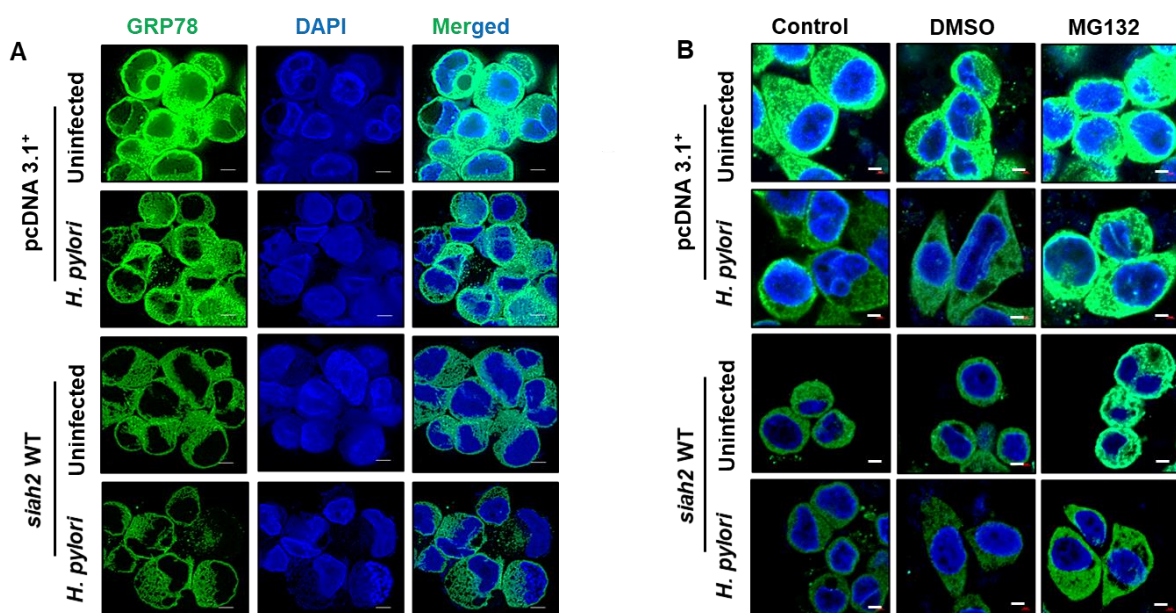
Figure 25. Siah2 mediates GRP78 decrease. (A) Confocal microscopy images depicting Siah2-dependent decrease of GRP78 in uninfected and infected pcDNA3.1+ and *siah2* stably-expressing MKN45 cells. Scale bars represent 5μm. **(B)** Confocal micrographs representing abatement of GRP78 decrease in MG132-treated uninfected and infected pcDNA3.1+ and *siah2* stable MKN45 cells as compared with the control and DMSO-control cells. Scale bars represent 5 μm.

Ubiquitination drives proteasomal degradation. Hence, we evaluated whether GRP78 decrease was ubiquitination-driven or not. For this, uninfected and *H. pylori*-infected (200 MOI, 12 h) MKN45 cells were co-treated with 50 μM MG132. Total cell lysates obtained were subjected to western blotting. Immunoblots probed with anti-ubiquitin antibody revealed ubiquitin accumulation in *H. pylori*-infected and MG132-treated cells (Figure 26A). These blots were reprobed for GRP78 to confirm its ubiquitination. Abated GRP78 decrease post MG132 treatment was found to be statistically significant (Figure 26B). To assess the effect of GRP78 decrease on Siah2-GRP78 interaction, uninfected and *H. pylori*-infected MKN45 cells were treated with 50 μM MG132. Co-immunoprecipitation of whole cell lysates using Siah2 antibody or IgG control antibody was performed. Western blot of the collected immuno-complexes revealed that Siah2-GRP78 interaction decreased PHPI but was rescued in *H. pylori*-infected and MG132-treated lanes (Figure 26C). Further, the effect of *siah2* suppression on GRP78 protein level was investigated by transfecting MKN45 cells with *siah2* siRNA for 36 h followed by 12 h of *H. pylori* infection. Western blot of the whole cell lysates revealed that GRP78 was rescued from degradation in *H. pylori*-infected *siah2*-suppressed MKN45 cells (Figure 26D). Collectively, results established that Siah2-mediated GRP78 proteasomal degradation in *H. pylori*-infected GECs.
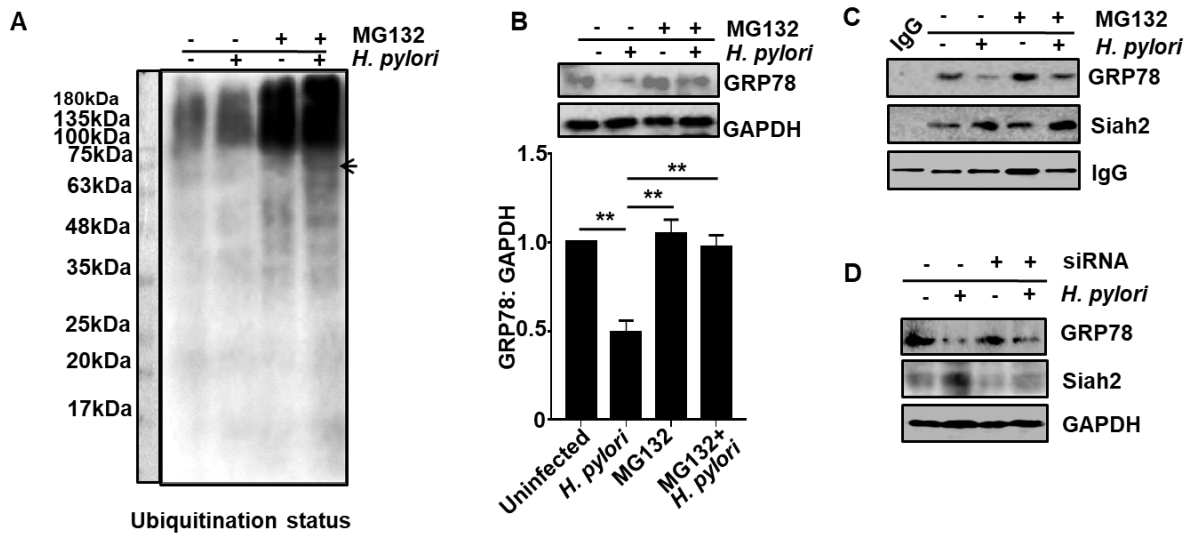
Figure 26. Proteasomal degradation of GRP78 is Siah2-mediated. (**A**) Western blot representing ubiquitin aggregates in *H. pylori*-infected and MG132-treated MKN45 cells. Arrow indicated the position of ubiquitinated-GRP78. (**B**) Immunoblot representing rescue of GRP78 in MKN45 cells after MG132 and *H. pylori* co-treatment. GAPDH = loading control. Graphical representation showing significant GRP78 protein rescue in MG132-treated and *H. pylori*-infected MKN45 cells. One-way ANOVA was used to determine statistical significance. Graphs = mean ± sem. n = 3. **$P < 0.01$. (**C**) Western blot of the immuno-complexes obtained from co-immunoprecipitation of uninfected and *H. pylori*-infected MG132-treated MKN45 cells depicting Siah2-GRP78 interaction. IgG band = loading control. (**D**) Whole cell lysate western blot showing the levels of GRP78 and Siah2 in control or *siah2* siRNA-transfected MKN45 cells with or without *H. pylori* infection. GAPDH = loading control.

3.5 Discussion

An imbalance between ROS generation and its detoxification results in oxidative stress [245]. Gastric carcinogenesis is enhanced due to *H. pylori*-mediated oxidative stress [246]. Oxidative stress induced in *H. pylori*-infected cells initiate several carcinogenic events in the infected host cells. ROS-oxidized mutagenic DNA accumulate in the infected cells as *H. pylori* disrupts

the DNA glycosylases (enzymes responsible for the recognition and initiation of DNA damage repair) (J Biol Chem. 2020, 295(32): 11082–11098). This results in accumulation of mutations. GRP78 is a molecular chaperone induced under various cellular stresses [247]. GRP78 modulates oxidative stress under different conditions by acting as an antioxidant protein [243, 248-251]. This is the first report showing GRP78 at the centre-stage of ROS regulation in GECs infected with *H. pylori*. Overexpression and suppression studies have shown GRP78 to reduce ROS burden in *H. pylori*-infected GECs.

Expression of GRP78 has been extensively characterized in various cancers including GC [252, 253]. The first account of GRP78 expression in *H. pylori*-challenged GECs was provided by Namba *et al*. [254]. My results concur with their findings, i.e., GRP78 decreases PHPI. Baird *et al*. have shown that *H. pylori* infection for a short duration does not affect GRP78 levels [255]. However, long durations of *H. pylori* infection decreases GRP78. Similar results have also been observed in this study where GRP78 decrease is not significant after 6 h of *H. pylori* infection but is significant at 12 h and 24 h PHPI. Further, this is the first report of Siah2 interaction with GRP78 which causes GRP78 proteasomal degradation by Siah2-mediated ubiquitination in GECs infected with *H. pylori*. This explains the mechanism of downregulation of GRP78 in *H. pylori*-infected GECs. GRP78 ubiquitination has been identified by multiplexed mass spectrometric approach [237] and experimentally proven to be proteasomally degraded [256, 257].

H. pylori infection also induces Siah2 which enhances GC invasiveness and tumorigenicity [230]. Siah2 promotes oxidative stress in hypoxia [213] and hypoglycaemia [258]. This study is the first report of ROS modulation by Siah2 in *H. pylori*-infected GECs. Oxidative stress is promoted by Siah2 in GECs infected with *H. pylori* which is in accordance with its role in hypoxia and hypoglycaemia. Since phosphorylation of Siah2 affects its stability and function, identification of role of phospho-Siah2 in ROS generation is a novelty of this study. Abrogation

of Siah2 phosphorylation at Ser^6 enhances ROS production which confirms its importance in Siah2-mediated ROS generation. Therefore, the next chapter deals with the role of phospho-Siah2 on ramifications of ROS regulation.

Chapter 4

P-Ser^6-Siah2 regulates mitochondrial morphology and aggresome formation

4.1 *H. pylori* infection enhances mitochondrial localization of Siah2

Mitochondria is closely associated with ROS generation [210, 259, 260]. Siah2 regulates mitochondrial homeostasis and function [199, 202, 261]. GRP78 localizes to mitochondria and regulates ROS generation [262-264]. This necessitated elucidation of GRP78 and Siah2 mitochondrial localization in *H. pylori*-infected GECs. In order to enable consistent visualization of mitochondria, pDsRed2-Mito plasmid was overexpressed in AGS cells and stable cells were generated. pDsRed2-Mito AGS stable cells were processed for microscopy after 12 h of infection. P-Ser^6-Siah2 as well as Siah2 increased in mitochondria whereas GRP78 decreased in GECs infected with *H. pylori* as determined by confocal microscopy (Figure 27A). Further, MKN45 cells were either left uninfected or were infected followed by mitochondrial and cytoplasmic fractionation of the cells. Western blot data reaffirmed the above findings (Figure 27B).
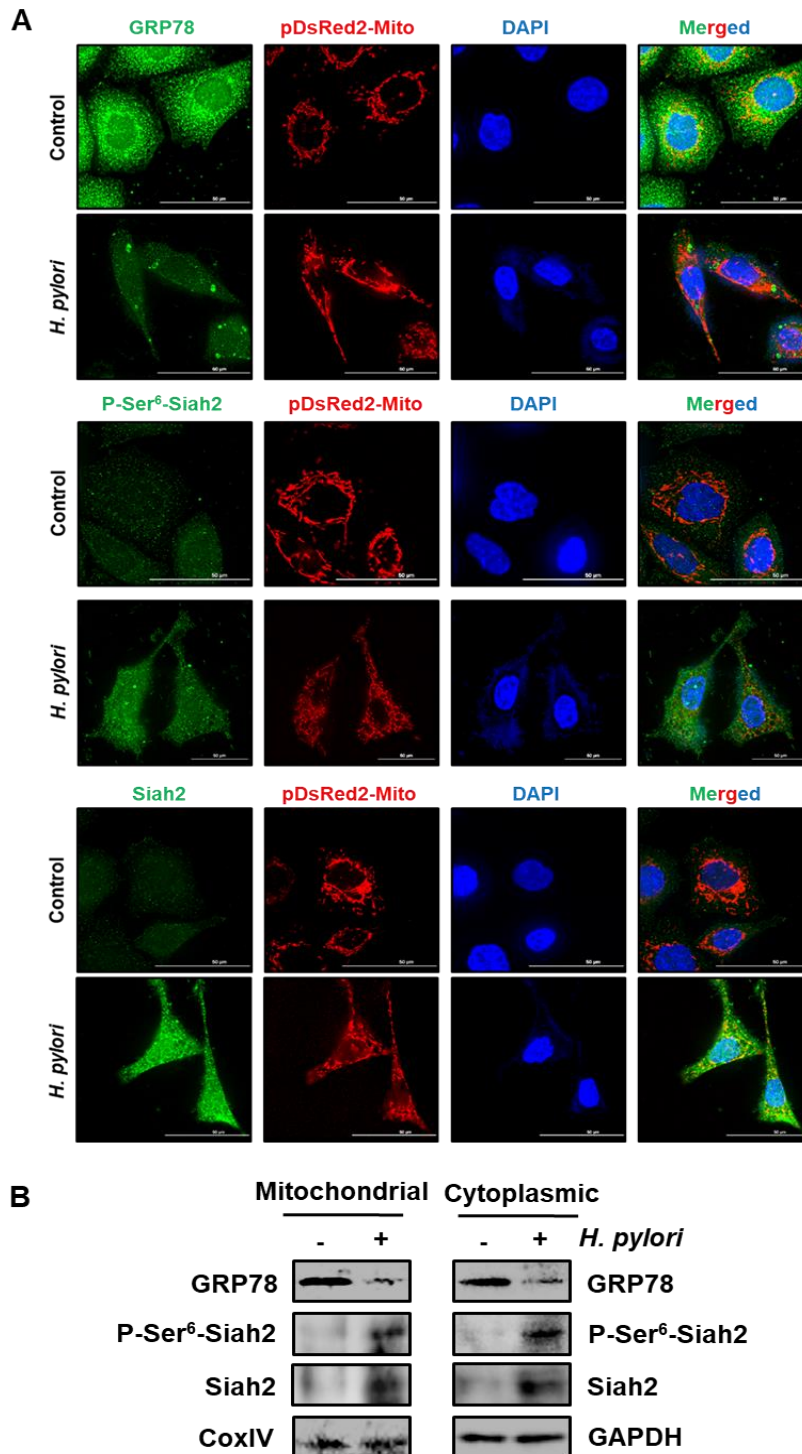
Figure 27. Siah2 and GRP78 are present in the mitochondria of *H. pylori*-infected GECs.
(**A**) Confocal microscopy images from uninfected or *H. pylori*-infected pDsRed2-Mito stably-expressed AGS cells depicting the levels of GRP78, P-Ser^6-Siah2 and Siah2. Scale bars = 50 μm. (**B**) Western blot from the mitochondrial and cytoplasmic fractions of uninfected or

4.2 Phosphorylation of Siah2 at Ser^6 is essential for mitochondrial morphology and aggresome formation in *H. pylori*-infected GECs

Abatement of Siah2 Ser^6-phosphorylation led to enhanced ROS production which made it imperative to study the involvement of Siah2 and its phosphorylation in the modulation of mitochondrial morphology. Mitochondrial morphology is affected by ROS generation [265-267]. For this, pDsRed2-Mito AGS stable cells were transfected with pcDNA3.1+, *siah2* WT and *siah2* phospho-null mutant S6A overexpression plasmids. 36 h after transfection, these cells were infected with *H. pylori* and processed for microscopy. Confocal microscopy depicted that mitochondrial morphology was altered PHPI. Mitochondrial length was shortened PHPI and was smallest in the *siah2* S6A-transfected cell. An enhanced alteration of mitochondrial shape, as examined by mitochondrial roundness and circularity, was found in *siah2* WT cells PHPI and was maximum in case of *siah2* S6A cells (Figure 28). Since *siah2* and its phospho-null mutant modulated ROS generation in a similar manner, these results establish that ROS alter mitochondrial morphology in GECs infected with *H. pylori*.
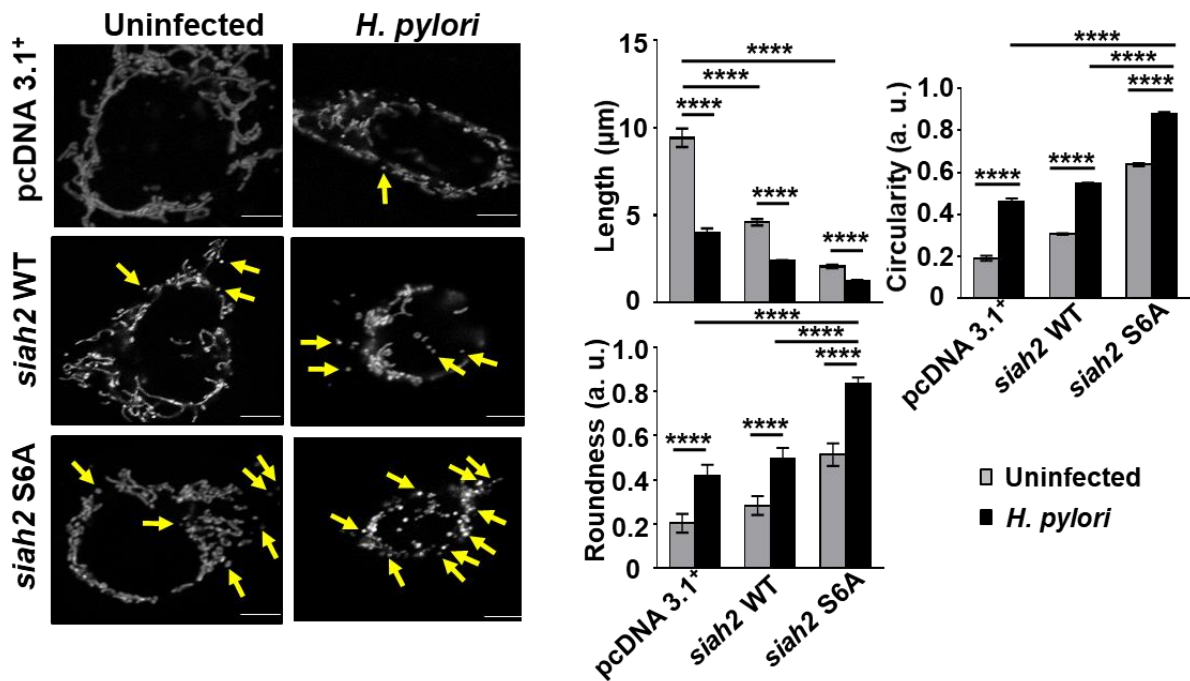
Figure 28. Siah2 Ser[6]-phosphorylation is essential for mitochondrial morphology. Confocal microscopy images depicting the alteration of tubulo-reticular mitochondrial morphology in pcDNA3.1+, *siah2* WT and *siah2* S6A overexpression plasmid-transfected pDsRed2-Mito AGS stable cells PHPI. Scale bars represent 5 μm. Bar graphs represent alterations of mitochondrial length, circularity and roundness calculated by using Fiji software from the above mentioned cells. Statistical significance was determined by two-way ANOVA followed by Tukey's post hoc analysis. Graphs represent mean ± sem. ***$P < 0.001$, ****$P < 0.0001$.

Further, ROS are known regulators of aggresome formation [268, 269]. In order to assess the status of aggresome formation, pcDNA3.1+, *siah2* WT and *siah2* S6A MKN45 stable cells were either left uninfected or were infected with *H. pylori*. After 12 h of infection these cells were stained for aggresomes. Confocal microscopy showed that aggresome formation was enhanced PHPI which surged in case of *siah2* WT cells. However, in case of Siah2 phospho-null mutant S6A, aggresome formation was disrupted. This established the importance of Siah2 phosphorylation at Ser[6] in aggresome formation of *H. pylori*-infected GECs (Figure 29).
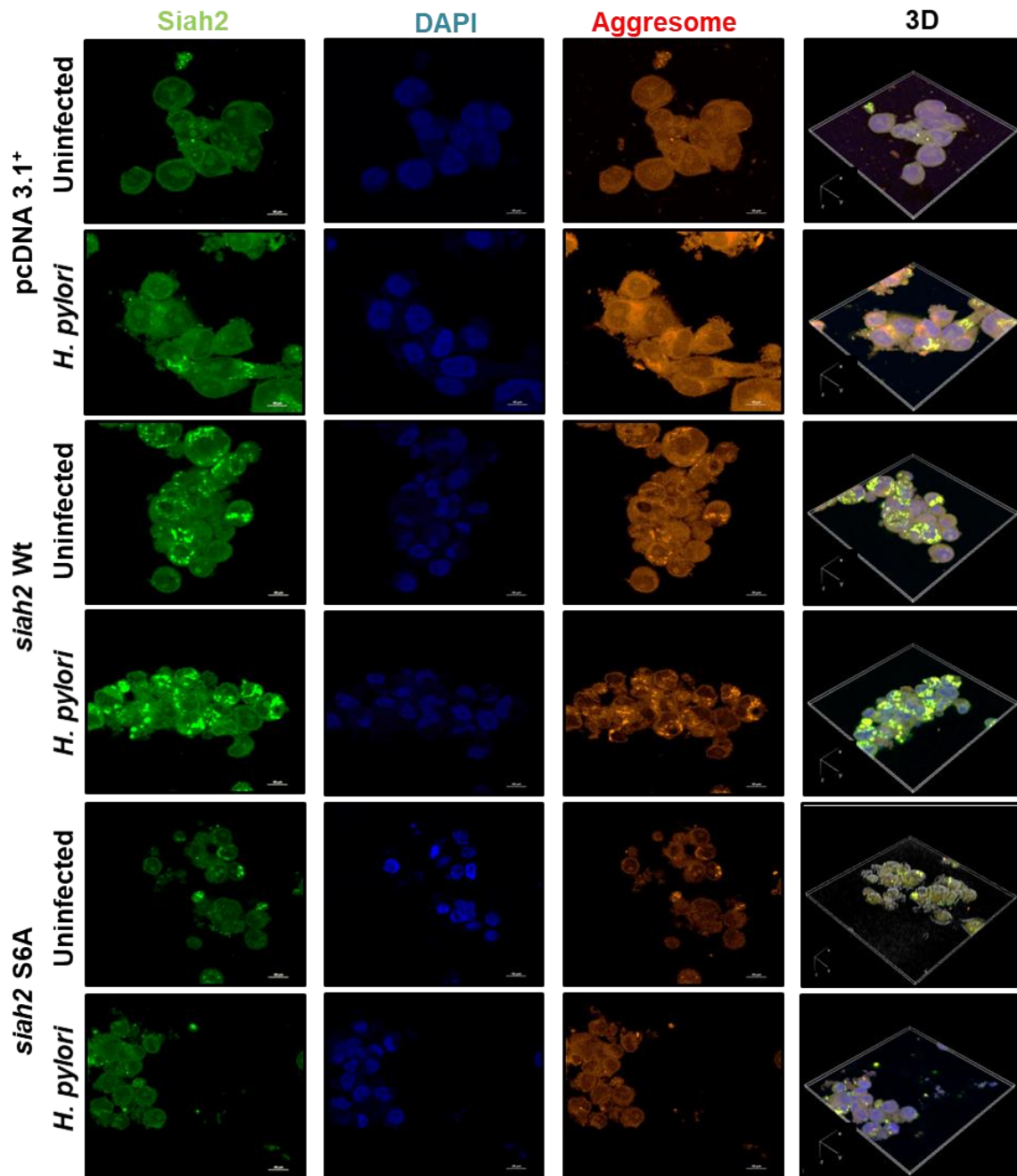
Figure 29. Siah2 phospho-null mutant S6A disrupts aggresome formation in GECs infected with *H. pylori*. Confocal microscopy images representing the status of aggresome formation in uninfected and *H. pylori*-infected pcDNA3.1+, *siah2* WT and *siah2* S6A MKN45 stable cells. 3D panel, generated using NIS AR software, showed that aggresome formation was disrupted in *siah2* S6A MKN45 stable cells. Scale bars = 10 μm.

In order to confirm the role of ROS on aggresome formation, pcDNA3.1+, *siah2* WT and *siah2* S6A stably-expressed MKN45 cells were treated with 10 mM n-acetylcysteine, an antioxidant, for 1 h followed by *H. pylori* infection. These cells were then stained for aggresomes and confocal microscopy was performed. Results showed that the enhanced aggresome formation in *H. pylori*-infected *siah2* WT cells was abrogated after NAC treatment. Similar results were also observed for all other cells (Figure 30). Overall, these results established that Siah2 Ser[6]-phosphorylation is essential for ROS-dependent aggresome formation.
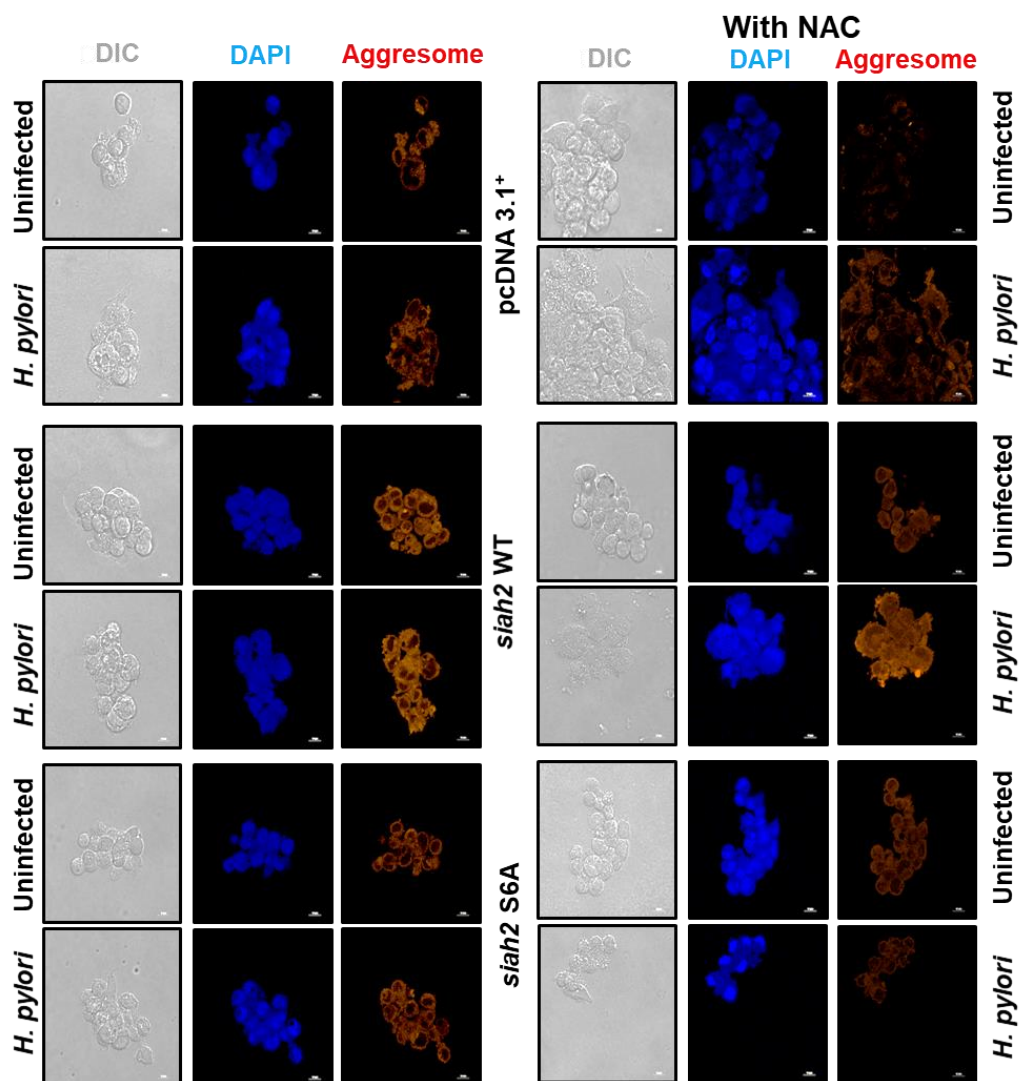
4.3 Discussion

Mitochondrial localization of GRP78 and Siah2 are reported in various path-physiological conditions [262, 263, 270-272]. This study is the first report of the mitochondrial localization of GRP78 and Siah2 in GECs infected with *H. pylori*. This study is also the first report of mitochondrial localization of Ser[6]-phosphorylated Siah2.

Mitochondria are not only "the power house" of cells but also modulate the redox homeostasis [273]. Altered ROS generation causes changes in the mitochondrial morphology [210, 265-267]. Since results from the previous chapter has established the importance of Siah2 and its phosphorylation on the regulation of ROS, this chapter elucidates its role on modulation of tubulo-reticular mitochondrial morphology. *H. pylori* infection disrupts the mitochondrial morphology which is enhanced by *siah2* overexpression. Results of this study are supported by reports which indicate that *H. pylori* mediates disruption of mitochondrial morphology of infected cells [274-276]. Recently, Sisalli *et al*. have also reported about *siah2*-mediated mitochondrial disruption [272] which is also in line with the findings of this study. *H. pylori*-infected GECs with abrogated Siah2 Ser[6]-phosphorylation show the most disrupted mitochondria and is the first report showing the importance of Siah2 phosphorylation on mitochondrial morphology modulation. Disruption of the mitochondrial morphology can be associated with the altered ROS generation by *H. pylori*-infected GECs.

Protein aggregates are formed in response to oxidative stress [268, 277-279]. These aggregates are collected and stored in microtubule-dependent perinuclear inclusion bodies- aggresomes [280, 281]. Formation of aggresomes by sequestration of cytotoxic protein aggregates is

cytoprotective [282-286]. Disruption of aggresome formation has been proposed to enhance the sensitivity of cells from various pathological conditions to drugs [287]. *H. pylori* infection enhances aggresome formation and is in agreement with the study by Yu *et al*. [288]. This study is the first to elucidate the importance of Siah2 and its phosphorylation on aggresome formation in GECs infected with *H. pylori*. *siah2* overexpression enhances aggresome formation which was increased further upon *H. pylori* infection. However, Siah2 phospho-null mutant S6A showed abrogated aggresome formation. These results establish the importance of Siah2 Ser^6-phosphorylation on aggresome formation. Carija *et al*. have reported that diffuse protein aggregates are the major elicitors of ROS [289]. This entails that enhanced ROS generation in Siah2 phospho-null mutant S6A cells is due to lack of aggresome formation. Thus, this chapter elucidates the importance of Siah2 Ser^6 phosphorylation on mitochondrial morphology and ROS-mediated aggresome formation. In the next chapter, the role of Siah2 phosphorylation on GC progression will be elucidated.

Chapter 5

Phosphorylated Siah2 promotes GC

5.1 Siah2 phosphorylation enhances carcinogenicity, invasiveness and proliferation of *H. pylori*-infected GECs

Invasion and metastasis of GC are promoted by Siah2 and its acetylation [218, 223, 230]. Siah2 is phosphorylated at Ser^6 and Thr^{279} residues, hence, the effect of phosphorylation abrogation at both of these residues were evaluated in the context of the carcinogenic potential of *H. pylori*-infected GECs. For this, pcDNA 3.1+, *siah2* WT, *siah2* phospho-null mutants S6A and T279A stably-expressed MKN45 cells were either infected or were left uninfected. Anchorage-independent growth of these cells was assessed by soft agar assay. Results showed that *siah2* WT MKN45 cells formed significantly high number of colonies PHPI as compared to the empty vector control or the phosho-null mutant-expressing cells (Figure 31A). A similar setup was used to assess the anchorage-dependent growth of these cells. Phospho-null mutants showed a significant reduction in the number of colonies formed when matched with *siah2* WT cells PHPI, which showed the significantly higher clonogenic potential (Figure 31B). Role of Siah2 phosphorylation on invasiveness was elucidated by using uninfected or *H. pylori*-infected pcDNA3.1+, *siah2* WT, *siah2* phospho-null mutants S6A and T279A AGS stable cells. AGS cells were used due to the semi-adherent nature of MKN45 cells, which makes it unsuitable for *in vitro* invasion assay [218, 230]. After 12 h of infection, these AGS stable cells were harvested and analysed for their invasive potential by *in vitro* invasion assay. Results showed that empty vector and Siah2 phospho-null mutant stable cells exhibited significantly lower invasiveness in comparison to *siah2* WT stable cells PHPI (Figure 31C). Further, MTT assay and cell population doubling assay were used to elucidate the importance of Siah2 phosphorylation on cellular proliferation. For this, pcDNA3.1+, *siah2* WT, *siah2* S6A and *siah2* T279A-expressing MKN45 stable cells were either left uninfected or were infected with *H. pylori*. Results from both the assays depicted that *siah2* WT cells have significantly higher proliferation when compared with pcDNA3.1+ or *siah2* phospho-null mutants PHPI (Figure

31D, E). Taken together, these results established the importance of Siah2 phosphorylation in

H. pylori-mediated GC tumorigenicity.
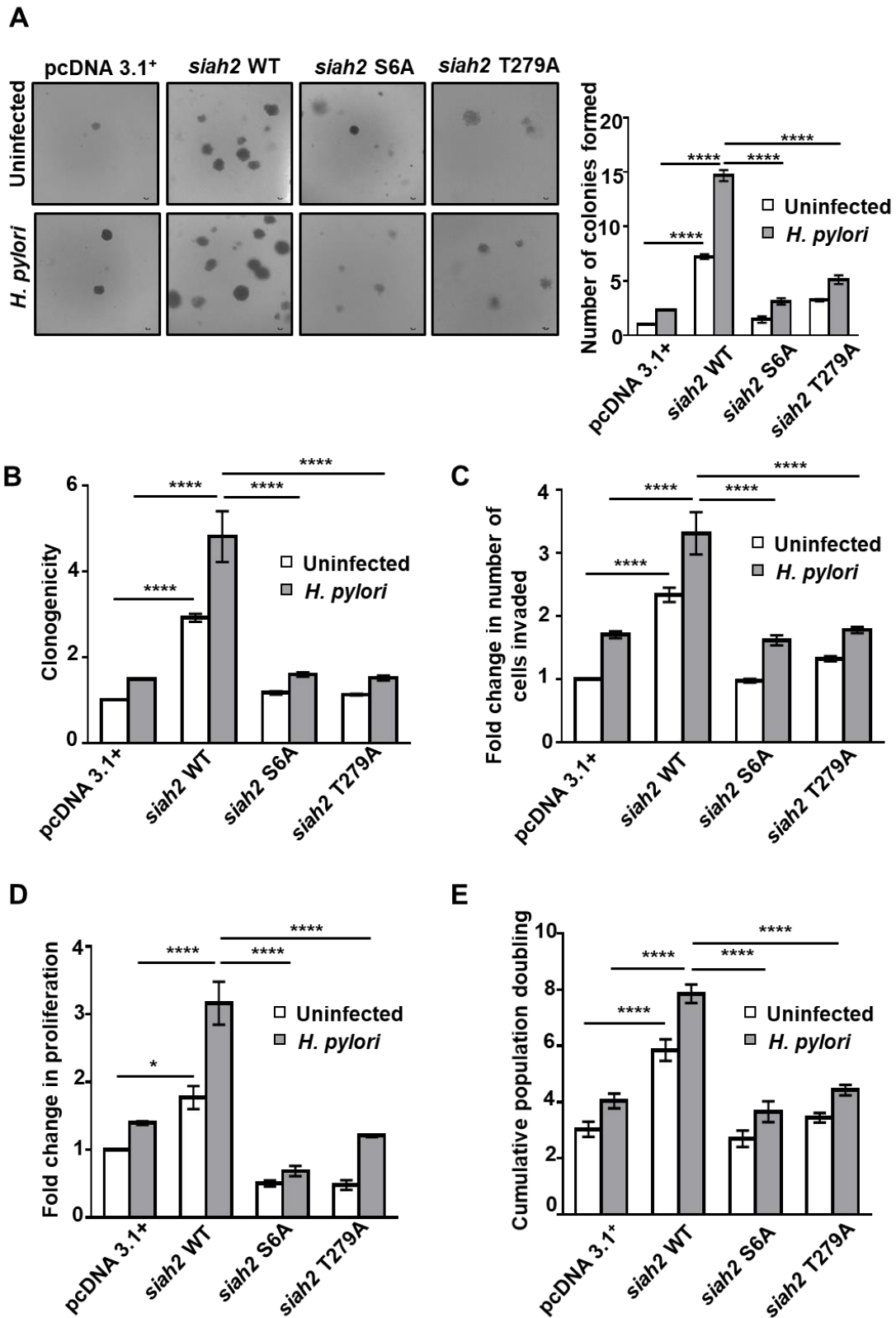
Figure 31. Phosphorylation of Siah2 is crucial for GC progression. (A) Micrographs of soft agar assay depicting colonies formed by uninfected and *H. pylori*-infected pcDNA3.1+, *siah2* WT, *siah2* S6A and *siah2* T279A stably-expressing MKN45 cells. Objective used = 4X. Scale bars = 100 μm. Bar graph representing quantification of the number of colonies formed (colony size > 50 μm). **(B)** Graphical representation of the clonogenic potential of uninfected and *H. pylori*-infected pcDNA3.1+, *siah2* WT and *siah2* phospho-null mutant MKN45 stable cells depicting enhanced clonogenicity of *siah2* WT cells PHPI. Values on Y-axis = normalized to empty vector control. **(C)** Bar chart representing the number of cells invaded in transwell invasion assay using pcDNA3.1+, *siah2* WT, *siah2* S6A and *siah2* T279A-expressed AGS stable cells PHPI. Values on Y-axis = normalized to empty vector control. **(D)** Graphical representation of the proliferative potential of uninfected and *H. pylori*-infected pcDNA3.1+, *siah2* WT and *siah2* phospho-null mutant stably-expressing MKN45 cells as assessed by MTT assay. Values on Y-axis = normalized to empty vector control. **(E)** Bar chart showing cumulative population doubling of uninfected and infected pcDNA3.1+, *siah2* WT, *siah2* S6A and *siah2* T279A-expressed MKN45 stable cells. For all the panels above, statistical significance was determined by two-way ANOVA followed by Tukey's post hoc analysis. All graphs represent mean ± sem. n = 3. *$P < 0.05$, ****$P < 0.0001$.

5.2 *H. felis*-infected C57BL/6 mice exhibit enhanced Siah2 phosphorylation

H. felis infection-mediated GC development in C57BL/6 mice events are similar to that of *H. pylori*-mediated human GC development [218, 290]. In order to assess the status of Siah2 phosphorylation in *H. felis*-infected mice, C57BL/6 mice were oral-gavaged with either phosphate buffered saline (PBS) or with PBS containing *H. felis*. Gastric antrum was collected and processed for immunofluorescence microscopy after 18 months of infection. Infected gastric tissue exhibited marked thickening of the mucosa and inflammatory mucus gland metaplasia (Figure 32A). Micrographs depicted that the levels of Siah2, P-Ser[6]-Siah2 and P-

Thr^{279}-Siah2 proteins were enhanced in infected mouse as compared to the uninfected ones. Also, protein levels of the kinase MRCKβ was found to be reduced in infected samples as compared to the uninfected ones (Figure 32B). These results reaffirmed the previous findings from *in vitro* experiments.
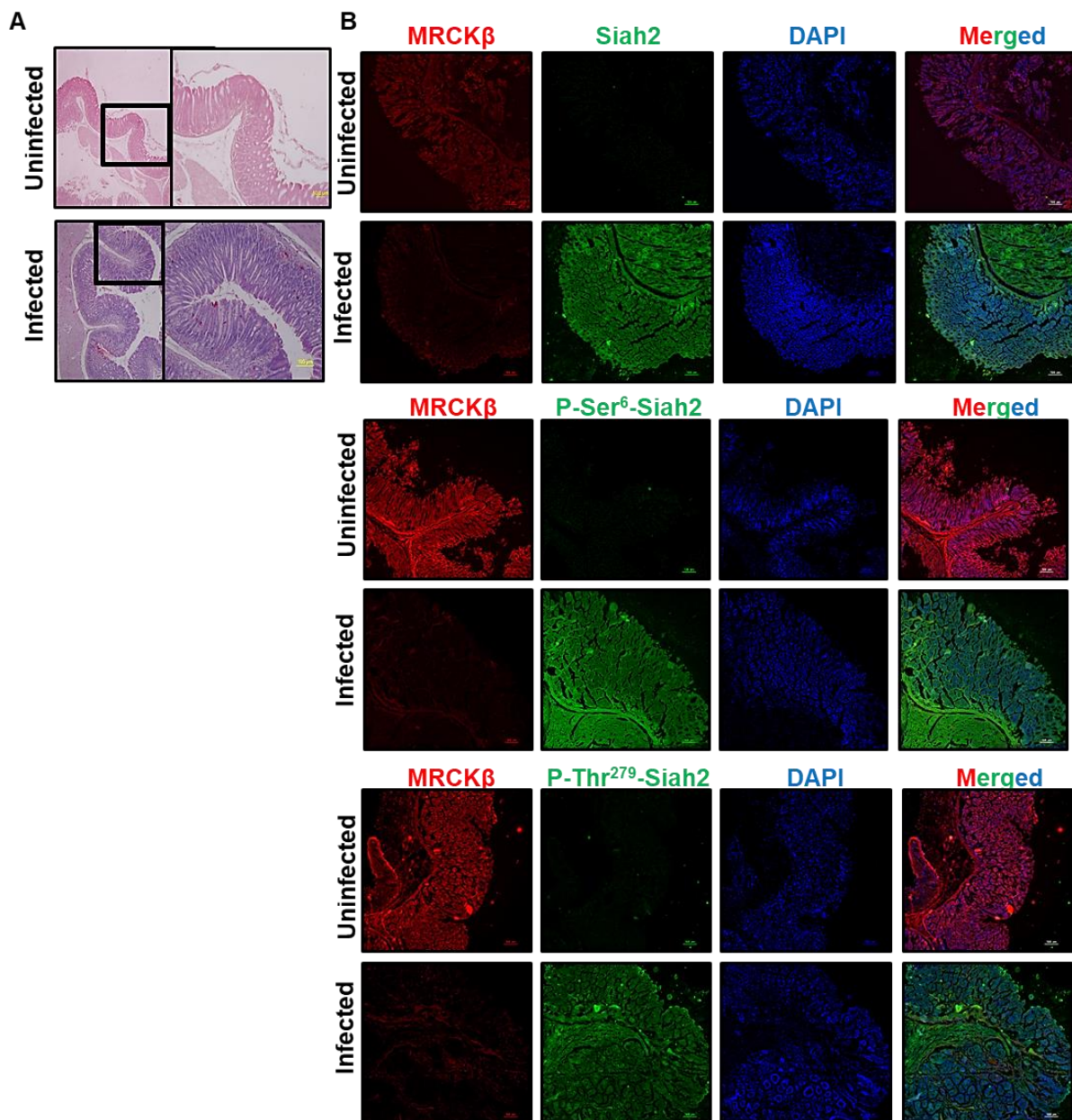
Figure 32. *H. felis* **infection augmented Siah2 phosphorylation in C57BL/6 mice. (A)** Brightfield images exhibiting thickening of the infected mucosa. Images on the left obtained using 4X objective. The square represents the area used for capturing images using 10X

objective shown on the right. **(B)** Widefield fluorescence microscopy images showing the levels of MRCKβ, Siah2 and phosphorylated-Siah2 (P-Siah2 = P-Ser^6-Siah2 and P-Thr^{279}-Siah2) in uninfected and *H. felis*-infected C57BL/6 murine gastric antral tissues. Tissue thickness = 5 μm. Objective used = 10X. Scale bars = 100 μm.

5.3 Enhanced P-Siah2 in human metastatic GC tissues

To elucidate the status of P-Siah2 and the kinase MRCKβ, human metastatic GC antral tissues were immuno-probed with P-Ser^6-Siah2, P-Thr^{279}-Siah2, Siah2 and MRCKβ antibodies. Immunofluorescence micrographs depicted that the levels of P-Siah2 and Siah2 were enhanced in metastatic GC tissues as compared to their paired controls but MRCKβ diminished (Figure 33).
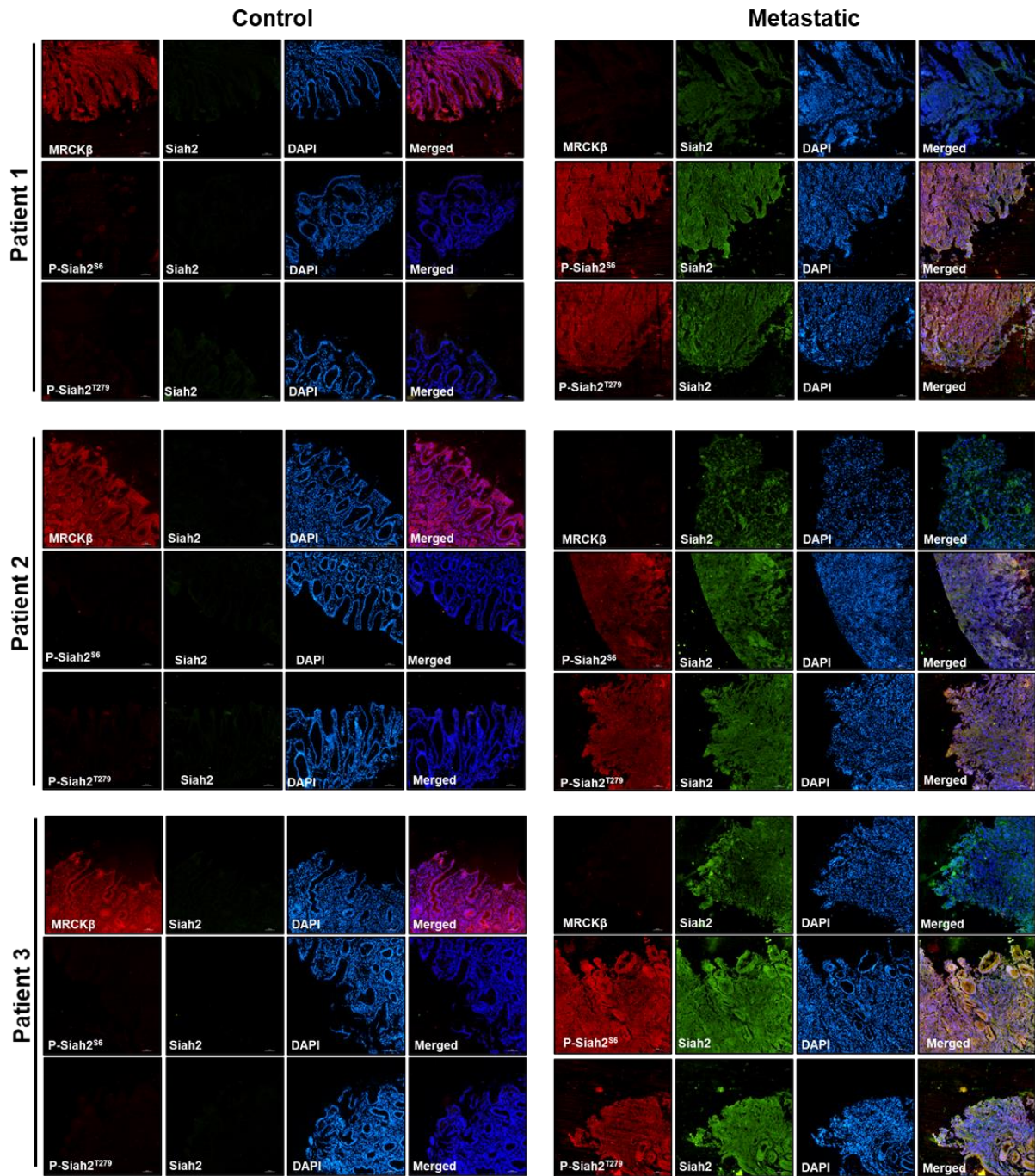
Figure 33. Augmented Siah2 phosphorylation in human metastatic GC biopsies. Micrographs representing protein expression of MRCKβ, Siah2, P-Ser^6-Siah2 (P-Siah2^{S6}) and P-Thr^{279}-Siah2 (P-Siah2^{T279}) in gastric antral biopsies of different patients. Tissue thickness = 5 μm. Objective used = 20X. Scale bars = 50 μm.

5.4 Discussion

This study elucidates the importance of Siah2 phosphorylation in the invasiveness and tumorigenic potential of *H. pylori*-infected GECs. Siah2 Ser^6 and Thr^{279} phosphorylation are found to be crucial for GC carcinogenicity, invasiveness and proliferation. *H. pylori* infection enhances Siah2 stability by its MRCKβ-orchestrated Ser^6 and Thr^{279} phosphorylation. P-Siah2 is more tumorigenic, invasive and enhances proliferation of GECs infected with *H. pylori*. These results concur with another study where Siah2 tyrosine phosphorylation by Src kinase has been reported to enhance breast cancer transformation [229].

Enhanced Siah2 has been previously reported in *H. felis*-infected C57BL/6 murine antral gastric tissues and human metastatic GC tissues [223]. However, this study is the first to report about increased P-Siah2 along with decreased MRCKβ in human metastatic GC antral biopsies and *H. felis*-infected C57BL/6 murine gastric antral tissues. These *in vivo* findings endorse this study's *in vitro* results. The results establish enhanced P-Siah2 and a concomitant decreased MRCKβ to be the prominent histological features of *Helicobacter*-mediated GC.

Chapter 6

Conclusions

6.1 MRCKβ-orchestrates Siah2 Ser^6 and Thr^{279} phosphorylation in *H. pylori*-mediated GC
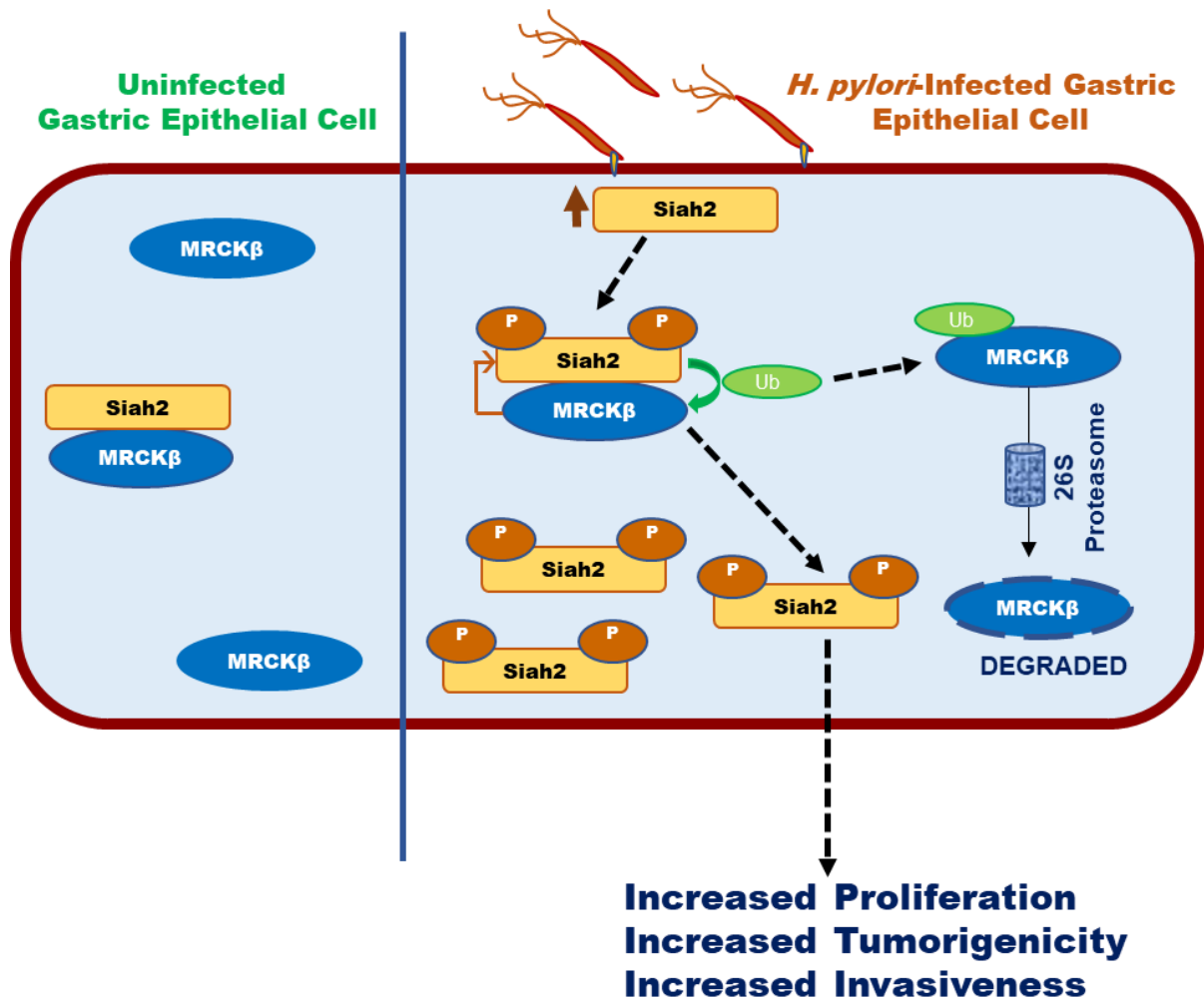
Concise of the above figure

❖ *H. pylori* infection increases the levels of Siah2 enhancing Siah2-MRCKβ interaction. MRCKβ phosphorylates Siah2 at Ser^6 and Thr^{279} residues in infected GECs and enhances Siah2 stability.

❖ P-Siah2 in turn ubiquitinates MRCKβ leading to its proteasomal degradation.

❖ Proliferation, tumorigenicity and invasiveness of *H. pylori*-infected GECs are enhanced by P-Siah2.

6.2 P-Siah2 regulates ROS generation in *H. pylori*-infected GECs
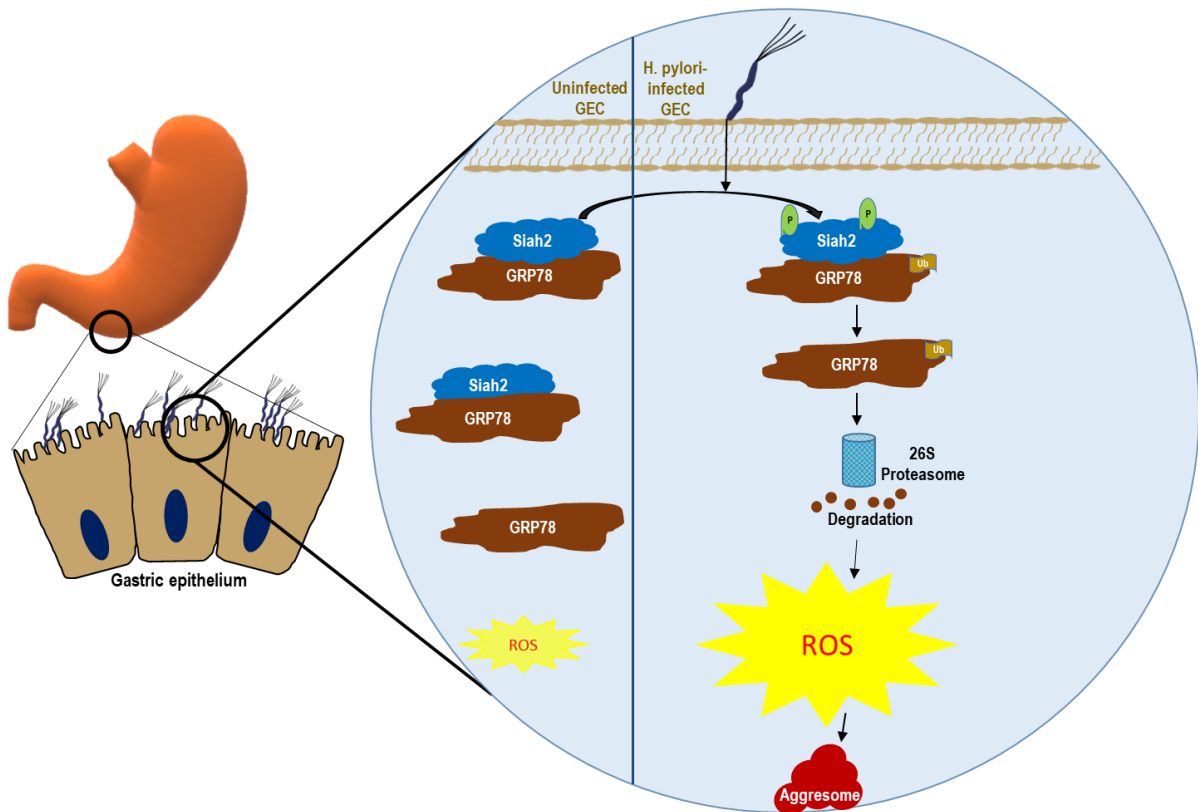
Concise of the above figure

- ❖ *H. pylori* infection enhances Siah2 phosphorylation and Siah2-GRP78 interaction.

- ❖ P-Siah2 ubiquitinates GRP78 leading to its proteasomal degradation.

- ❖ Degradation of antioxidant protein GRP78 leads to the upregulation of ROS generation by *H. pylori*-infected GECs.

- ❖ Increase in ROS generation is associated with altered mitochondrial morphology and aggresome formation.

To conclude, this thesis demonstrates MRCKβ-orchestrated Siah2 Ser^6 and Thr^{279} phosphorylation in *H. pylori*-infected GECs. Enhanced P-Siah2 stability leads to MRCKβ ubiquitination and proteasomal degradation. Siah2-MRCKβ interaction and the consequences thereof are elucidated for the first time. MRCKβ decrease along with the concomitant increase of P-Siah2 have been established to be the prominent hallmarks of *H. pylori*-mediated human

metastatic GC and *H. felis*-infected C57BL/6 murine gastric epithelia. Siah2 phosphorylation enhances proliferation, tumorigenicity and invasiveness of GECs infected with *H. pylori*. Elucidation of ROS modulation by Siah2 and its phosphorylation is a unique component of this thesis. Siah2-mediated regulation of the abundance of the antioxidant protein GRP78 in *H. pylori*-infected GECs is a novelty of this study. This study is unique to report about enhanced Siah2 phosphorylation in the mitochondria of *H. pylori*-infected GECs. The importance of Siah2 phosphorylation on cytoprotective aggresome formation has also been elucidated here. Taken together, this study unravels phosphorylation-mediated changes in the subcellular localization and functioning of Siah2 protein in *H. pylori*-mediated GC.

Chapter 7

Materials and methods

7.1 Materials used

7.1.1 GECs: GECs, MKN45 and AGS were procured from the American Type Culture Collection (ATCC), USA. Non-neoplastic GEC HFE145 was provided by Prof. Hassan Ashktorab (Department of Medicine, Howard University, Washington, DC, 20060, USA) and Prof. Duane T. Smoot (Department of Medicine, Meharry Medical Center, Nashville, TN, 37208, USA).

7.1.2 Bacteria used: For infection studies, various *H. pylori* {*cag* PAI (+) 26695 and *cag* PAI (-) 8-1} and *H. felis* (Cat. No. 49179, ATCC) variants were procured from the University of Virginia, USA. Except for cloning related to site-directed mutagenesis where XL10-Gold ultracompetent cells (Cat. No. 200514, Agilent, USA) were used, other clonings were performed using competent cells of *E. coli* DH5α (Cat. No. 18265-017, Invitrogen, USA).

7.1.3 Animals: With the help of NISER Animal house, C57BL/6 mice (4-5 weeks, both male and female) were purchased from the National Institute of Nutrition, Hyderabad, India.

7.1.4 Plasmids and siRNAs: Appendix I and II provide the list of plasmids and siRNAs used.

7.1.5 Antibodies: Appendix III and IV show the list of antibodies that were used in the study.

7.2 Methods

7.2.1 Maintenance and culture of GECs: GECs were perpetuated using Roswell park memorial institute (RPMI) media (Cat. No. AL028A; Himedia, India) completed with 10% heat-inactivated US origin fetal bovine serum (FBS; Cat. No. RM9970, Himedia). This combination of RPMI + FBS has been referred to as "media" unless otherwise stated. Cells were kept in humidified incubators (Model No. Galaxy 170R; New Brunswick, Eppendorf) set at 37ºC temperature and 5% CO_2.

Class II biosafety cabinet (Model No. 1300 Series A2; ThermoFisher Scientific, USA) was used to perform all the aseptic cell culture-related works. When cells reached 75-90% confluency, they were either used for experiment or passaged for maintenance. For passaging, the used media was discarded and 1 ml or 3 ml of trypsin (Cat No. TCL007, Himedia) was added to T25 (Cat. No. 430639; Corning, USA) or T75 (Cat. No. 430641, Corning) flasks, respectively. After 3-5 min of incubation in the incubator, the trypsinized cells were collected and added to new T25/75 cm^2 flasks with 10 ml/20 ml of media according to the suggested split ratio of the cells. For experiments, trypsinized cells were added to either 15 ml or 50 ml centrifuge tubes containing 5 ml or 15 ml of media. The media + trypsinzed cells in the centrifuge tubes were mixed properly and 10 µl of it added to Neubauer haemocytometer (Cat. No. 0640010; Paul Marienfeld GmbH & Co. KG, Germany) for enumerating cells. Visualization of the cells was achieved with the help of an inverted microscope (Model: CKX53, Olympus, Japan). Standard method of cell counting was employed followed by estimation of the cell number by the formula:

Number of cells

$$= \frac{\text{Total number of cells counted}}{4} \times 10^4 \times \text{Volume of the suspension}$$

The centrifuge tubes were then rotated at 500xg {for 8 min at room temperature (RT) using SL8R centrifuge from Thermo Scientific}. The supernatant was discarded and the pellet resuspended in the volume of media calculated according to the required concentration of cells. These cells were then seeded in cell culture plates of varied sizes according to experimental requirements.

7.2.2 Freezing and revival of GECs: For preservation of the cell stock in liquid nitrogen, GECs were trypsinized and collected in centrifuge tubes, as described above. The pellets obtained were resuspended in 1 ml of sterile filtered mixture of FBS + 10% dimethyl sulfoxide

(DMSO; Cat. No. TC185-100ML). These resuspended cells were then transferred to cryovials. Cryovials were kept at -80ºC for 14-16 h before being transferred to liquid nitrogen (-196ºC) for long term storage.

For revival, cryovials were thawed in water bath pre-set at 37°C. As soon as the content was thawed, vials were removed from the water bath and cleaned with 70% ethanol. The content of the vials was transferred to 15 ml centrifuge tube with 9 ml of complete media and centrifuged at 500xg for 8 min. The supernatant was discarded and the pellet was resuspended in 1 ml media. Resuspended cells were transferred to T25/T75 cm^2 flasks containing media. These flasks were then kept in the incubator.

7.2.3 *Helicobacter* strains culture and infection of cells: Various *Helicobacter* strains were maintained on 5% defibrillated sheep blood supplemented TSA plates (Cat. No. 221239; Becton, Dickinson and Company, USA). TSA plates were kept in the humidified incubator set at 37ºC and 10% CO_2. Bacteria were incubated on these plates for 72 h. After 72 h of incubation, the uniformly grown bacterial lawn was passaged to a fresh TSA plate using sterile cotton swab. For the purpose of infection, a small amount of bacterial growth was collected from the plate using sterile inoculation loop after 48 h of incubation. 1/3rd-loopful collected bacteria were dissolved in 10 ml of sterile filtered 10% FBS-supplemented Brucella broth (Cat. No. 211088, BD) and added in a T25 cm^2 flask. The flask was incubated for 14-16 h on a rotary shaker (150-180 rpm) inside the CO_2 incubator. After incubation, 1 ml of cultured bacterial suspension was assessed for growth by measuring the optical density at 600 nm by UV-visible spectrophotometer (Beckman Coulter, USA; Model No. DU-720). Bacterial culture with an OD between 0.6-1.1 was considered suitable for infection. Next, the cultured bacteria were centrifuged {400xg (Model No. 5810R; Eppendorf, Germany) for 8 min} at RT. The pellet was dissolved in media (RPMI+10%FBS) according to the formula below such that 10 µl of media contained 1 x 10^8 bacteria which is 100 MOI for 1 million of GECs.

Volume of media to be used for dissolving the bacterial pellet (µl)

$$= \frac{OD}{0.3} \times 2 \times 10^8 \times \text{Volume of bacterial culture used} \times 10$$

GECs were infected in accordance with the need of the experiment.

7.2.4 Freezing and revival of *Helicobacter* strains: Freezing mix for *Helicobacter* strains was prepared by sterile filtering Brucella broth + 10% FBS mixed with 10% glycerol (Cat. No. MB060-500ML, Himedia). After 48 h, bacterial growth from TSA plates were collected with the help of inoculation loop and resuspended in 15 ml centrifuge tube containing 1 ml of freezing mix. After mixing, the volume of freezing mix was adjusted according to the amount of bacterial growth collected. This mixture was then dispensed in cryovials and stored at -80ºC.

For revival, the cryovial was taken out from -80ºC and thawed on ice. The thawed mix was dispensed on pre-warmed TSA plates and spread with the help of L-shaped spreaders or inoculation loop. These plates were kept in incubators set at 10% CO_2 and 37ºC temperature. The handling of *Helicobacter* strains was carried out in biosafety cabinets as described for GECs.

7.2.5 Animal model: *H. felis*-infected C57BL/6 mice have been established as a successful animal model of *H. pylori*-mediated GC in human [223, 290, 291]. 4-5 weeks old C57BL/6 mice were kept at 23-25ºC temperature with 50-55% relative humidity under 12 h light and 12 h dark condition. 2-3 animals were housed in individual cages covered with filter cover lids. After they attained age of 7-8 weeks, they were separated as: uninfected and *H. felis*-infected. The uninfected group mice were restrained and fed 0.5 ml of 1X PBS orogastrically with the help of oral gavage needles. Similarly, animals of the other group were fed with 0.5 ml of *H. felis* resuspended in 1X PBS at a concentration of 10^{10} colony forming units. This was repeated twice after every two days interval. After 15-18 months of infection mice were euthanized and

gastric tissues were collected and preserved in 4% paraformaldehyde (PFA). This protocol (No. NISER/SBS/IAEC/AH-34) was approved by NISER Institutional Animal Ethics Committee (IAEC) in accordance with the "Committee for the Purpose of Control and Supervision of Experiments on Animals (CPCSEA) guidelines".

7.2.6 Human biopsies: Human antral gastric biopsy tissues were made available by Prof. S. P. Singh (Department of Gastroenterology, SCB Medical College, Odisha, India) and Prof. Niranjan Rout (Department of Pathology, Acharya Harihar Post Graduate Institute of Cancer, Odisha, India). Patients diagnosed with stage III/IV GC who were urea breath-test positive and did not have a prior history of *H. pylori* eradication were considered for the study. A small tumor biopsy was collected from the antral region of the stomach and the adjacent non-cancerous tissue was collected as paired control with the help of gastroduodenoscopy. A prior-informed written consent was obtained from the patients, their identity and personal data was protected. The obtained tissues were kept in 4% PFA till further use. This protocol (No. NISER/HEC/2012/AB-1) was permitted by the "Institutional Ethics Committee for Human Research, National Institute of Science Education and Research" in accordance with the "Helsinki Declaration (2013), World Medical Association" guidelines.

7.2.7 Processing and sectioning of tissues: The obtained mice/human tissues were transferred from 4% PFA to a solution of 15% sucrose and kept for 14-16 h or till the tissues settle down in the sucrose solution. These tissues were then transferred to 30% sucrose solution and kept overnight. Sucrose acts as a cryoprotectant and prevents the tissues from getting deformed or damaged. Next, the tissues were embedded in tissue freezing medium (Cat. No. 14020108926; Leica Biosystems, USA). They were kept in cryostat (Model No. CM3050S; Leica Biosystems, Germany) for at least 20-30 min before sectioning at 5 μm. The cut sections were carefully segregated from the blade towards the middle of the cutting stage with the help of fine brushes. The sections were then brought in contact with poly-l-lysine (Cat. No. P8920-100ML; Sigma,

USA) coated slides for adherence. Glass slides were coated with a uniform layer of poly-l-lysine and kept at 37ºC for 20-30 min before use. These sections were then processed for immunofluorescence microscopy or stored at -20ºC for future use.

7.2.8 Fluorescence/ confocal microscopy: For immunofluorescence microscopy of GECs, they were seeded on 12 mm diameter coverslips. These coverslips (Cat. No. 1254582; Fisher Scientific, USA) were washed with 70% ethanol and dried before exposure to UV for 30 min in the biosafety cabinets before plating. These coverslips were then kept in 24 well plates (Cat. No. 3526; Corning, USA) and seeded with 0.16×10^6 cells. After the desired treatment/infection and time duration, coverslips were washed with 1X PBS and fixed overnight with 4% PFA at 4ºC. Next, these were washed with 1X PBS and permeabilized with 0.1% Triton-X-100 in PBS for 10 min. This was followed by blocking for 1 h in 5% BSA in PBST (0.1% Tween 20 in 1X PBS) and overnight incubation with the desired primary antibody at 4ºC. Next day, coverslips were washed thrice with PBST for 5 min each and incubated with the desired fluorophore-tagged secondary antibody for 2 h at RT. Coverslips were washed again with PBST twice for 5 min each and then once with PBS for 5 min before counterstaining with 4', 6-diamidino-2-phenylindole (DAPI; Cat. No. D3571, ThermoFisher Scientific) for 20 min at RT. These were then washed twice with PBS for 5 min each and mounted on slide using Fluoromount-G (Cat. No. 0100-01; Southern Biotech, USA). Tissue samples were processed similarly except that they were permeabilized by using 0.5% Triton-X-100 in PBS for 20 min. This was followed by widefield fluorescence microscopy using Nikon Eclipse TiU microscope (Nikon, Japan). Images were captured using DS Qi2 camera (Nikon) with the help of NIS Advanced Research software (Nikon). Confocal micrographs were acquired by Leica DMi8 confocal microscope (Leica, Germany) using Leica Application Suite X software or by Carl Zeiss LSM-800 confocal microscope (Carl Zeiss, Germany) using LSM software (Carl Zeiss).

The captured images were processed and analysed using either NIS Advanced Research software or Fiji software [292].

7.2.9 Site-directed mutagenesis: This was performed using QuikChange Multi SDM kit (Cat. No. 200515; Agilent technologies, USA). Siah2 Ser[6], Thr[275], Thr[279] and Ser[282] residues were mutated to Ala to generate Siah2 phospho-null mutants.

Nucleotide sequence: Homo sapiens Siah2 mRNA (975 bp)

LOCUS: NM_005067; ACCESSION: NM 005067; REGION: 628.1602; VERSION: NM_005067.5; GI: 55925659.

    1 atgagccgcc cgtcctccac cggccccagc gctaataaac cctgcagcaa gcagccgccg

  61 ccgcagcccc agcacactcc gtccccggct gcgcccccgg ccgccgccac catctcggct

 121 gcgggccccg gctcgtccgc ggtgcccgcc gcggcggcgg tgatctcggg ccccggcggc

 181 ggcggcgggg ccggcccggt gtccccgcag caccacgagc tgacctcgct cttcgagtgt

 241 ccggtctgct ttgactatgt cctgcctcct attctgcagt gccaggccgg gcacctggtg

 301 tgtaaccaat gccgccagaa gttgagctgc tgcccgacgt gcaggggcgc cctgacgccc

 361 agcatcagga acctggctat ggagaaggtg gcctcggcag tcctgtttcc ctgtaagtat

 421 gccaccacgg ctgttccct gaccctgcac catacggaga aaccagaaca tgaagacata

 481 tgtgaatacc gtccctactc ctgcccatgt cctggtgctt cctgcaagtg gcaggggtcc

 541 ctggaagctg tgatgtccca tctcatgcac gcccacaaga gcattaccac ccttcaggga

 601 gaagacatcg tctttctagc tacagacatt aacttgccag gggctgtcga ctgggtgatg

 661 atgcagtcat gttttggcca tcacttcatg ctggtgctgg agaaacaaga gaagtacgaa

 721 ggccaccagc agttttttgc catcgtcctg ctcattgca cccgcaagca agccgagaac

781 tttgcctaca gactggagtt gaatgggaac cggcggagat tgacctggga ggccacgccc

841 cgttcgattc atgacggtgt ggctgcggcc atcatgaaca gcgactgcct tgttttcgac

901 acagccatag cacatctttt tgcagataat gggaaccttg gaatcaatgt tactatttct

961 acatgttgtc catga

The highlighted sequences indicate the position of Ser[6], Thr[275], Thr[279] and Ser[282] codons in Siah2 mRNA sequence. These were mutated to Ala by changing single nucleotide of the original codon (Table 6).

Table 6. Mutations required to replace Ser/Thr residues by Ala.

Amino acid	Original codon	Codon changed to Ala
Ser[6]	Tcc	gcc
Thr[275]	Acc	gcc
Thr[279]	acg	gcg
Ser[282]	Tcg	gcg

Primers were designed with the help of IDT online software incorporating these changes and in accordance with the kit's guidelines (Appendix V). Using these primers mutagenesis reaction was set up as follows:

Components	Volume
10X QuikChange multireaction buffer	2.5 µl
Quik solution	0.75 µl
dNTP mix	1 µl
10 µM mutagenic primer	1 µl

Template DNA plasmid (150 ng)	1 µl
Molecular grade water	17.75 µl
Total	**24 µl**

Lastly, 1 µl of Quick Change multi enzyme blend was added and tubes were tapped to mix the contents. Tubes were spun shortly before setting up in the thermocycler (Model No. Mastercycler Nexus, Eppendorf). Thermocycler settings were as follows:

Thermocycler Conditions:

Step	Temperature	Time	
Initial Denaturation	95ºC	1 min	
Final Denaturation	95ºC	1 min	
Annealing	55ºC	1 min	X 30
Extension	65ºC	12 min	
Final Extension	65ºC	12 min	
Hold	4ºC	∞	

To the amplified products, 1 µl Dpn I restriction enzyme (37ºC for 2 h) was added. Dpn I digested the methylated/ hemi-methylated parental DNA, leaving behind the intact mutated DNA. Next, the digested product was transformed in XL10-Gold ultracompetent cells provided with the kit.

Procedure for transformation: XL-10 Gold Ultra competent cell was gently thawed on ice. For transformation, 45 µl of competent cells was used. 2 µl of β-mercaptoethanol was added to the

competent cells and mixed by swirling the tube gently. The cells were incubated on ice for 10 min with gentle swirling every 2 min. 5 µl of Dpn I-treated DNA was added to the ultracompetent cells. The transformation reaction was mixed and then kept on ice for 30 min. Heat shock was given at 42ºC for 35 sec using water bath (Model No. CD-200F; Julabo, Germany). Then the tube was incubated for 2 min on ice followed by addition of 0.5 ml of preheated (42°C) SOC broth (Cat. No. 15544034, Invitrogen) and incubation at 37ºC for 1 h with shaking at 230 RPM (Model No. Innova 42R; New Brunswick, Eppendorf). The mixture was then plated on LB agar (Cat. No. M1151, Himedia) plates having 100 µg/ml of sodium salt of ampicillin (Cat. No. A022, Himedia) using L-shaped spreaders. The plate was then incubated overnight at 37ºC.

The observed colonies were picked and inoculated in 5 ml LB broth (Cat. No. M1245-500G, HiMedia) containing 100 µg/ml of sodium salt of ampicillin. These were then incubated at 37ºC for 12-16 h (with shaking at 230 RPM). Next, plasmids from these colonies was isolated using QIAprep Spin Miniprep Kit (Cat. No. 27106; Qiagen, USA). For plasmid isolation, company recommended protocol was followed except for elution of DNA by pre-warmed 30 µl EB buffer. The eluted plasmid's concentration and purity was assessed by its absorbance at 260/280 nm wavelength using spectrophotometer (Model No. NanoDrop 2000 Spectrophotometer, ThermoFisher). The mutation-positive clones were identified by sequencing. The mutation-positive plasmids were further transformed in *E. coli* DH5α ultracompetent cells using the transformation protocol described above (β-mercaptoethanol was not added, DNA and bacteria were mixed and kept for 30 min on ice with occasional tapping, rest of the procedure remained same). The colonies obtained were inoculated first in 5 ml LB broth with 100 µg/ml sodium salt of ampicillin. After 6-8 h, cultures were transferred to 95 ml of 100 µg/ml sodium salt of ampicillin containing LB broth and incubated overnight (37ºC, 230 RPM). The plasmids were isolated using Maxiprep kit (Cat. No. 43776, Qiagen)

following the manufacturer's protocol. The eluted plasmid's concentration and purity was assessed by its absorbance at 260/280 nm wavelength using spectrophotometer.

Preparation of glycerol stock: Glycerol was mixed with molecular grade water (1:1 ratio) and autoclaved to sterilize. 1 ml of this sterilized solution was added to 1 ml of the bacterial culture. The contents were mixed and dispensed in cryovials which were stored in -80ºC.

7.2.10 Transfection and stable cell lines generation: Transfection of the desired plasmid to the GECs was achieved by lipid-based transfection reagent {Lipofectamine 3000 reagent (Cat. No. L3000015, Invitrogen)}. GECs were seeded in the desired culture vessels and incubated at 37ºC with 5% CO_2 for 24 h. 1 h before transfection, media was changed. Transfection was carried out in accordance to the manufacturer recommended protocol. Briefly, Mix A {DNA of interest + P3000 reagent + Serum free media (SFM)} and Mix B (Lipofectamine 3000 + SFM) were prepared and incubated at RT for 5 min. The amount of DNA, P3000 reagent, Lipofectamine 3000 and SFM used was in accordance to the company's recommendations. The contents of Mix A and Mix B tubes were then blended together with gentle pipetting 4-5 times and incubated at RT for 15-20 min for formation of DNA-lipid complexes. After incubation, the contents of the mixture were added to GECs in a dropwise manner with constant and gentle shaking of the culture plates to ensure uniform distribution of the DNA-lipid complexes. These plates were then kept in incubator set at 37ºC and 5% CO_2. GECs were infected with *H. pylori* 36 h post transfection. For transfection of siRNAs to GECs, P3000 reagent was not used. Rest of the protocol remained the same as described above.

For generation of stable cells, 0.3×10^5 GECs were seeded in 96 well plates (Cat. No. CLS3596, Corning). 24 h after plating, transfection of the desired DNA was performed. 48 h post-transfection, cells were trypsinized and 10 µl of the trypsinized cells were transferred to 6 well plates containing 1.5 ml media supplemented with 200 µg/ml of selection antibiotic G418 (Cat.

No. G8168-10ML; Sigma-Aldrich, USA). Media was replenished every third day with fresh media containing 200 µg/ml G418. This was repeated thrice and then the concentration of G418 was enhanced to 300 µg/ml. Replenishing of the media was continued every third day till visible colonies were observed. The colonies were transferred to 12 well plates (containing 1 ml media with 300 µg G418) with the help of sterile cloning discs (Cat. No. F37847-0002, Sigma-Aldrich). After the cells settle, cloning discs were discarded. Few days later, confirmation of the stable cell line generation was performed either by fluorescent microscopy or by western blotting. Cells were then transferred to T25/T75 cm^2 flasks containing 7/17 ml media with 300 µg/ml G418. When the cells achieved a confluency of 70-90%, these were trypsinized and cryopreserved in liquid nitrogen.

7.2.11 Assessment of ROS generation: In order to investigate ROS formation, GECs were seeded on coverslips. After the desired infection period, the cells were treated with media containing 1 µM/ml of ROS indicator 2, 7-dichlorodihydrofluorescein diacetate {(DCFDA) Cat. No. D6883, Sigma} for 1 h. Next, the cells were fixed with 4% PFA for 10 min and washed with 1X PBS twice. These coverslips were then mounted on glass slides using FluoromountG and dried at RT in dark. Care was taken not to expose the cells to light during processing of the coverslips. These slides were then imaged using FITC filter of the fluorescence microscope. Images captured were analysed for their mean fluorescence intensity indicative of ROS generation using Nikon Advanced Research software.

7.2.12 Aggresome formation: To elucidate aggresome formation in *H. pylori*-infected GECs, Aggresome Detection Kit (Cat. No. ab139486; Abcam, USA) was used. Cells were seeded on coverslips and were either left uninfected or were infected with *H. pylori*. After 12 h of infection, the cells were fixed with 4% PFA (4ºC, overnight). The fixed cells were washed with 1X PBS thrice before permeabilization with 200 µl of permeabilizing solution {for 10 ml of permeabilizing solution (0.5% Triton X-100, 3 mM EDTA, pH 8): added 50 µl Triton X-100

and 60 μl of 0.5M EDTA, pH 8, to 9.89 ml of 1X Assay Buffer)} for 10 min. Next, washing with 1X PBS was repeated twice followed by blocking with 5% BSA for 1 h at RT. Cells were washed with PBST twice followed by addition of primary antibodies (4ºC, overnight). Next day, the coverslips were washed thrice with PBST followed by incubation with fluorophore-tagged secondary antibodies (2 h, RT). These were washed with 1X PBS twice and 200 μL of Dual Detection Reagent (preparation of Dual Detection Reagent: for every 2 ml of 1X Assay Buffer add 1 μl of Aggresome Detection Reagent and 2 μl of Hoechst 33342 Nuclear Stain or DAPI) was added on each coverslip for 30 min at RT in dark. The cells were finally washed with 1X PBS before mounting on glass slides using FluoromountG. Aggresome formation was visualized by using widefield fluorescent microscope or by confocal microscope using appropriate filters. When only aggresome formation was to be analysed, after permeabilization the cells were directly stained with Dual Detection reagent followed by washing with 1X PBS and counterstaining with DAPI.

Antioxidant N-Acetyl-L-cysteine (Cat. No. A7250-50G, Sigma) was used to elucidate the role of ROS on aggresome formation. GECs were pre-treated with 10 mM NAC for 1 h followed by infection with *H. pylori*. These were then processed for visualization of aggresome formation using the protocol described above.

7.2.13 Treatment of GECs with a proteasomal inhibitor: To study events involving the role of proteasome, proteasomal inhibitor MG132 (Cat. No. M7449-200UL, Sigma-Aldrich) was used. GECs were treated with 50 μM of MG132 along with *H. pylori* infection for 12 h.

7.2.14 Whole cell lysate preparation: After completion of the desired time period of *H. pylori* infection, cells were collected in a 1.5 ml tube either by physical dislocation (scraping) or by enzymatic dislocation (trypsin). Tubes were then centrifuged for 6 min at 250xg (4ºC). The supernatant was discarded with the help of a syringe and the obtained cell pellet was kept on

ice. To the pellet added the required amount of protease and phosphatase inhibitors {2X protease inhibitor cocktail (Cat. No. ML051-1ML, Himedia) + 80 mM sodium fluoride + phosphatase inhibitor (Cat. No. P0044-1ML, Sigma; added @ 4 µl for 1 ml of total cell lysate)} and vortexed twice for 15-20 sec. An equal volume of sample lysis buffer {2X Laemmli sample buffer (Cat. No. ML-021, HiMedia) + 5% β-mercaptoethanol (Cat. No. MB041-500ML, HiMedia)} was added to the tubes and vortexed for 10-15 sec. The tubes were then heated at 100ºC for 8 min followed by a short spin of 10 sec. Cleared whole cell lysate was used for SDS-PAGE or stored at -80ºC.

7.2.15 Cytoplasmic and mitochondrial lysate preparation: To study the cytoplasmic and mitochondrial abundance of proteins, 2.5×10^6 GECs were seeded in 60 mm^2 cell culture dishes (Cat. No. 430166, Corning). After the desired infection duration, cell were collected in a 1.5 ml tube by scraping. The tube was centrifuged at 250xg for 10 min at 4ºC. The supernatant was discarded and the pellet was resuspended in 150 µl of resuspension buffer {20 mM 4-(2-hydroxyethyl) piperazine-1-ethanesulfonic acid (HEPES), pH 7.5, 10 mM KCl, 1.5 mM MgCl$_2$, 1 mM ethylenediaminetetraacetic acid (EDTA), 1 mM ethylene glycol tetraacetic acid (EGTA) + Protease inhibitor cocktail (at 10 µl/ml of the total buffer volume) + 150 mM sucrose + 40 mM NaF + Phosphatase inhibitor cocktail (at 4 µl/ml of total buffer volume)}. Resuspended cells were lysed by passing it through 26 gauge syringe needle for 20 times. The lysate was then centrifuged at 750xg for 10 min (at 4ºC) to remove nuclei and unbroken cells. Supernatant from this step was transferred to another pre-chilled 1.5 ml tube and centrifuged at 10,000xg for 15 min at 4ºC. After centrifugation, the supernatant obtained was the cytoplasmic fraction and it was transferred to another labelled tube. The pellet obtained was mitochondria-enriched and was resuspended in mitochondrial lysis buffer {20 mM Tris-HCl pH 7.4 + 150 mM NaCl + 2X protease inhibitor cocktail + phosphatase inhibitor cocktail (concentration as described above)}. The resuspended mitochondrial fraction was mixed with

equal volume of sample lysis buffer and heated at 100ºC. The heated tubes were centrifuged for short duration and loaded on gel or stored at -80ºC.

7.2.16 Co-immunoprecipitation: To elucidate protein-protein interactions, co-immunoprecipitation was performed. GECs were seeded at a density of 2×10^6 in 60 mm^2 cell culture dishes. Desired treatment/infection was given for appropriate time duration. Cells were dislodged from the culture dishes either by scraping or by trypsinization. Tubes were then centrifuged for 6 min at 250xg (4ºC). Supernatant was discarded and 200 µl of TENT buffer {150 mM NaCl + 50 mM Tris, pH 7.5 + 1 mM EDTA + 1% Triton-X-100 + protease inhibitor cocktail + phosphatase inhibitor cocktail (concentration as described above)} was added to the pellet. The pellet was kept on ice for 30 min with intermittent vortexing (15-20 sec) after every 10 min. The tubes were centrifuged at 850xg (10 min, 4ºC) and the supernatant was transferred to another tube. 800 µl of TEN buffer {150 mM NaCl + 50 mM Tris, pH 7.5 + 1 mM EDTA + protease inhibitor cocktail + phosphatase inhibitor cocktail (concentration as described above)} was added to the tubes. To these tubes 10 µl 50% A/G-agarose (Cat. No. SC-2003, Santa Cruz Biotechnology, USA) was added and kept at 4ºC for 30 min with constant agitation. This was followed by centrifugation of tubes at 850xg (5 min, 4ºC) and the supernatant was transferred to another tube without disturbing the pellet formed. The desired primary antibody and an equivalent IgG control was added and incubated at 4ºC with constant agitation (for overnight). Next day, the tubes were centrifuged at 230xg (2 min, 4ºC) followed by addition of 50% A/G-agarose (15 µl) and incubation with constant agitation at 4ºC for 3 h. The agarose-protein immunocomplex was pulled-down by centrifugation at 230xg (5 min, 4ºC) and washed twice with 1X PBS. To the obtained agarose bead pellets, added 25 µl sample lysis buffer and heated at 100ºC for 8 min. The heated tubes were centrifuged shortly for 10 sec followed by loading of the supernatant to the gel.

7.2.17 SDS-PAGE: In order to segregate the obtained whole cell lysates, subcellular fractions or immuno-complexes by SDS-PAGE, the most commonly used discontinuous buffer method was employed (Laemmli's SDS-PAGE method, 1970). Mini-PROTEAN tetra-system gel assembly (Cat. No. 165-8003, Bio-Rad Laboratories) was used for polymerization and electrophoresis.

Materials required and the procedure for casting of the acrylamide gel:

Solution A: Stock solution of 30% acrylamide monomer and N,N'-methylene-bis-acrylamide crosslinker in a ratio of 29:1 (Cat. No. 1610156; Bio-Rad Laboratories, USA).

Solution B: 1.5 M Tris-HCl buffer (pH 8.8) containing resolving gel buffer (Cat. No. 161-0798, Bio-Rad Laboratories).

Solution C: 0.5 M Tris-HCl buffer (pH 6.8) containing stacking gel buffer (Cat. No. 161-0799, Bio-Rad Laboratories).

Glycerol: 50% solution of glycerol in molecular grade water (Cat. No. ML024-100ML, Himedia).

N, N, N', N'-Tetramethyl ethylenediamine (TEMED): For quick polymerization of gel, catalyst TEMED (Cat. No. 1610800, Bio-Rad Laboratories) was used.

Ammonium persulfate: Weighed 150 mg of APS (Cat. No. 1610700, Bio-Rad Laboratories) and dissolved it in 1.5 ml of water to make a solution of 10% APS. The tube containing 10% APS solution was covered with aluminium foil and kept in dark. APS was prepared fresh for its optimal activity.

Composition of the resolving gel: The table below describes the volume of individual components required for making two resolving gels of different percentages. The required volume of various components were adjusted accordingly for different number of gels.

Table 7. Components of the resolving gel.

Components	7.5%	9%	12.5%
Solution A	2.25 ml	2.7 ml	3.75 ml
Solution B	2.25 ml	2.25 ml	2.25 ml
50% glycerol	2.5 ml	2.5 ml	2.5 ml
Molecular grade water	2 ml	1.55 ml	1 ml
TEMED	5 µl	5 µl	5 µl
10% APS	70 µl	70 µl	70 µl

Composition of the stacking gel: Various components required to make two stacking gels are listed in the table below.

Table 8. Composition of the stacking gel.

Components	Volume
Solution A	0.9 ml
Solution C	1.5 ml
Molecular grade water	3.6 ml
TEMED	6 µl
10% APS	36 µl

The components of the resolving and the stacking gel were mixed together in two separate tubes or beakers. At last, TEMED was added and uniformly mixed before addition of 10% APS. The contents of the resolving gel mix were poured in a pair of glass separated by 1 mm spacer assembled on gel casting stand. Next, the stacking gel mix was poured without

disturbing the resolving gel. 1 mm thick 10/15 well comb was inserted in the glass assembly and the contents were left to polymerize for 20-30 min at RT.

After the gel was polymerized, they were assembled in the MINI-Protean electrodes. The electrodes were kept in gel running tank and the electrophoresis buffer (25 mM Tris-HCl, 190 mM glycine and 0.1% SDS) was added. The electrophoresis buffer was prepared by diluting 150 ml of 10X TGS buffer (Cat. No. 1610732, Bio-Rad Laboratories) in 1,350 ml of distilled water. The comb was removed from the gel and the wells were washed with electrophoresis buffer prior to sample loading. The samples were loaded along with the standard molecular weight protein marker (Cat. No. BM008-500; BR Biochem, India). The samples stored at -80ºC were thawed on ice and brought to RT before loading on gel. Appropriate volume of electrophoresis buffer was added to the gel running tank and electrodes were connected to the power pack {PowerPac™ Basic Power Supply (Cat. No. 1645050) Bio-Rad Laboratories}. Gel was run at a constant voltage (130 V) for 15 min and then at a constant voltage of 180 V till the dye front reached the end of the gel.

7.2.18 CBB staining of the gel: For staining a gel with CBB, the gel was carefully taken out of the glass assembly. An appropriate volume of CBB staining solution (Cat. No. 161-0436) was poured on the gel and heated in microwave oven for 10-15 sec. The gel in the staining solution was incubated overnight at RT. Next day, the gel was removed from the staining solution and put in destaining solution (Cat. No. 1610438). Destaining solution was changed till protein bands with clear background were observed.

7.2.19 Mass spectrometry (MS) analysis: For identifying the unique Siah2 interacting partners, MS analysis was performed. GECs were overexpressed with *siah2* and empty vector for 36 h followed by infection with *H. pylori* for 12 h. The whole cell lysates obtained were subjected to co-immunoprecipitation using Siah2 antibody. The obtained immuno-complexes

were subjected to SDS-PAGE followed by staining with CBB. Differentially expressed bands were excised with a clean scalpel blade and put in 1.5 ml tubes with 50 µl of molecular grade water. Care was taken to prevent keratin contamination at all stages. The tubes containing excised gel pieces were outsourced for Liquid Chromatography-Mass Spectrometry (LC-MS/MS) analysis at Mass Spectrometry Core Lab, University of Texas Medical Branch, Biomolecular Resource Facility (UTMB BRF). Obtained results were screened and negated for the presence of contaminants. Proteins were arranged on the basis of their score and sorted according to their function.

7.2.20 Western blot: In order to detect specific proteins, western blotting was performed using the modified form of method developed by Harry Towbin and group in 1979 [293]. Composition of the required buffers and procedures used were as follows.

Transfer buffer: To obtain 1.5 l of transfer buffer, 4.56 g of Tris-HCl and 21.63 g of glycine was added in 800 ml of distilled water. The contents were mixed thoroughly and 300 ml of methanol was added. 0.561 g of SDS was added to the above solution and the pH was adjusted to 8.3 followed by making the volume to 1.5 l.

10X TBS: A solution of 20 mM Tris-HCl and 500 mM NaCl was made with distilled water. pH of the solution was adjusted to 7.4. The solution was diluted to 1X concentration before use.

1X TBST: 1X TBS was mixed with 0.1% Tween-20 (Cat. No. RM156-500G, Himedia) to prepare 1X TBST.

Blocking buffers: For blocking the western blots and dilution of primary as well as secondary antibodies, 5% non-fat-dried milk (NFDM; Cat. No. RM1254, Himedia) or 5% BSA (Cat. No. RM3151, Himedia) was prepared in 1X TBST buffer.

<u>Procedure for wet transfer</u>: Polyvinylidene fluoride {(PVDF) Cat. No. VH00010; Millipore, USA} membrane was cut to the size according to the requirement and activated by keeping in pre-chilled methanol for 5 min. The membrane was washed in water for 2 min and then kept it in pre-chilled transfer buffer for 10 min. In a glass casserole added transfer buffer and with the black side of the gel holding cassette down kept a pre-wet sponge and a thin filter sheet (Cat. No. 1703933, Bio-Rad Laboratories). Gel was kept on the filter sheet and the activated PVDF membrane was placed above it. The assembly was ensured to be bubble-free with the help of a roller. This was followed by completing the assembly by keeping a filter sheet and a sponge above it. The gel holding cassette was closed and assembled in mini trans-blot cell wet transfer apparatus (Cat. No. 170-3940, Bio-Rad Laboratories). Polarity of the transfer was ensured by following the colour coding indicated on the transfer apparatus. A cooling pack and a magnetic bead was added to the tank. The tank was placed on a magnetic bead stirrer and transfer buffer was added. The electrodes of the assembly were connected to a power pack set at 40 V and timed to run for 240 min.

Method of semi-dry transfer: For transfer of low molecular weight proteins, semi-dry method of transfer was employed. This was performed using mini trans-blot semi-dry blot apparatus (Cat. No. 170-3940, Bio-Rad Laboratories) kept on horizontal surface. The apparatus was adjusted to be at even level with the help of a bubble-level tool. A thick filter sheet was cut and placed on the surface of the anode. Activated PVDF membrane followed by the gel was kept on it. Bubbles trapped in the assembly were removed with the help of a roller. The assembly was completed by placing a thick filter sheet on top of it. Cathode was placed on the top and the lid was closed. The electrodes were connected to the power pack set at 25 V and timed for 35 min. The polarity of the assembly was ensured by following the colour coding of the apparatus while connecting it to the power pack.

After the transfer of proteins, the PVDF membrane was washed with 1X TBS for 5 min. To prevent non-specific binding of antibodies, the membrane was blocked with the blocking buffer. Membranes which were to be probed with phosphorylated antibodies were blocked in 5% BSA and the rest in 5% NFDM. After blocking, blots were incubated with the desired primary antibody in a humidified chamber (4ºC, overnight). Next day, blots were washed with 1X TBST thrice for 10 min each followed by incubation with horse-radish peroxidase (HRP)-tagged secondary antibody at RT for 1 h with constant shaking. The membranes were then washed thrice with 1X TBST for 5 min each. Finally, membranes were then washed with 1X TBS for 5 min. Detection of the developed immunoblot was performed using SuperSignal West Femto Chemiluminescent Maximum Sensitivity Substrate kit (Cat. No. 34094, ThermoFisher Scientific) or Immobilon Western Chemiluminescent HRP Substrate kit (Cat. No. WBKLS-0050, Merck Millipore). Equal volumes of the provided reagents were mixed and the membranes were incubated in it. Chemiluminescence signals were detected using ChemiDoc XRS plus (Cat. No. 170-8265, Bio-Rad Laboratories) and analyzed with Quantity 1-D analysis software (version 4.6.9, Bio-Rad Laboratories).

Procedure for reprobing of the immunoblot: To detect different proteins from the same immunoblot, reprobing of the blot was performed using Western BLoT Stripping buffer (Cat. No. T7135A; TaKaRa, USA). Blot was incubated with the reprobing buffer for 20 min with constant shaking at RT to remove the bound primary and secondary antibodies from the membrane. Then, the blot was washed thrice with 1X TBST for 15 min each followed by incubation with the blocking buffer for 1 h at RT with constant shaking. The blot was incubated with the desired primary antibody. Washing, incubation with the secondary antibody and detection of the reprobed immunoblot were performed as described above.

7.2.21 Anchorage-independent growth assay: This assay (also known as the soft agar assay) was used to elucidate the anchorage-independent growth of various uninfected and *H. pylori-*

infected MKN45 stable cells. After infection, cells were treated with 150 μg/ml of gentamicin (Cat. No. A005, Himedia) for 3 h to kill extracellular bacteria. Cells were washed twice with media and trypsinized to collect them for seeding in soft agar assay. Simultaneously, 1.2% bacto agar (Cat. No. 199835, MP Biomedicals) solution (prepared by dissolving 1.2 g of bacto agar powder in 100 ml of distilled water followed by autoclaving for sterilization) was mixed with equal volume of 2X Ham's media (Cat. No. AT140A, HiMedia; prepared according to the manufacturer's instructions). This mixture (bottom agar) was poured in 6 well plate and kept in incubator for half an hour.

The top agar (0.3% bacto agar) was prepared by adding 1 ml Ham's media and 0.5 ml molecular grade water to 0.5 ml of 1.2% bacto agar. 10, 000 cells were added to the top agar mix and poured slowly on the solidified bottom agar. This setup was kept in incubator set at 37ºC and 5% CO_2. After 24 h, 1 ml of media was added slowly on the top agar. Media was changed regularly without disturbing the agar. After three weeks of incubation, the colonies formed in wells were imaged using inverted brightfield microscope. Colonies greater than 50 μm were counted and analysed from different fields of each well.

7.2.22 Clonogenic survival assay: Various MKN45 Siah2 stable cells were compared for their clonogenic potential by this assay. After infection, extracellular bacteria were killed by treating the cells with 150 μg/ml of gentamicin for 3 h (in the incubator set at 37ºC and 5% CO_2). Cells were washed twice with media before collecting them by trypsinization. 1×10^3 of these trypsinized cells were seeded in 60 mm^2 cell culture dishes with 2.5 ml media. The dishes were incubated for 3 weeks with intermittent addition of media. Once the colonies were observed, they were fixed with 4% PFA at RT for 30 min or at 4ºC for overnight. Colonies were washed thrice with 1X PBS and stained with 0.5% solution of Gram's Crystal Violet stain (Cat. No. S012, HiMedia) for 15 min. Finally, the colonies were washed once with 1X PBS and dried at

RT for 2 h. Images of the dishes with colonies formed were captured by using BioRad Chemidoc using Colorimetric protocol and analyzed using Fiji software.

7.2.23 Transwell invasion assay: To elucidate the invasiveness of the empty vector, WT and mutant Siah2-expressing stable AGS cells, cells were left uninfected or *H. pylori*-infected. 100 µl of matrigel matrix (Cat. No. 356230, Corning) was coated on top of 0.3 cm^2 polyethylene terephthalate transwell membrane with 8 µm pore size (Cat. No. 353097, Corning) and kept in the biosafety cabinet for 10 min. To the 24 well plate, 800 µl of 20% FBS-containing media was added to the desired wells. Transwell membranes with the solidified matrigel matrix were kept slowly on these wells. Care was taken to avoid formation of bubbles between the transwell and the cell culture media. 2 x 10^5 cells resuspended in 200 µl of 0.5% FBS-containing media were added on the top of the matrigel-coated transwell followed by *H. pylori* infection to the desired wells. The assembly was kept in the incubator (37ºC, 5% CO$_2$) for 12 h. After incubation, the matrigel on the transwell insert was removed with the help of a sterile cotton swab and inserts were fixed with 4% PFA for 30 min at RT. Inserts were washed twice with 1X PBS followed by permeabilization with 0.5% Triton-X-100-containing 1X PBS. Next, the inserts were washed with 1X PBST and stained with hematoxylin (Cat. No. S034; Hematoxylin, HiMedia) for 30 min at RT. Staining was followed by a final wash with 1X PBS and the insert membranes were dried. These membranes were then cut out from the inserts and mounted on a glass slide. These were then imaged with the help of a brightfield microscope and the captured images were analysed.

7.2.24 MTT assay: Proliferative potential of GECs was assessed by MTT assay. Cells were seeded in 96 well plates and were left uninfected or infected with *H. pylori*. 12 h PHPI, manufacturer-recommended protocol was followed for treatment of cells with MTT reagent [EZcount MTT Assay kit (Cat. No. CCK003-1000) HiMedia]. Following the protocol, solubilisation buffer was added and absorbance of the resulting solution in each well was taken

using a plate spectrophotometer (Varioskan flash multimode reader, Thermo Scientific) at 570 nm and 670 nm. The results obtained was analysed according to the manufacturer's recommendations.

7.2.25 Cell population doubling assay: Proliferative potential of GECs was also assessed using this assay. GECs were treated with150 μg/ml of gentamicin for 3 h (in the incubator set at 37ºC and 5% CO_2) PHPI. Cells were washed twice with media before collecting them by trypsinization. 1×10^4 of these trypsinized cells from individual experimental conditions were seeded in a labelled 24 well plate containing 0.5 ml media. These were kept in incubator set at 37ºC and 5% CO_2. These cells were trypsinized and the number of cells present was estimated on day 2, 3 and 4. Cellular proliferation as assessed by population doubling (PD) was calculated by the formula below [294, 295].

$$PD = [\log Nh - \log Ns]/\log 2$$

where, Ns was the number of seeded cells (i.e. 1×10^4) and Nh was the number of cells estimated on day 2, 3 and 4.

PD of each day was added to give cumulative PD (cPD) which was plotted on Y-axis along with experimental conditions on X-axis [296].

7.2.26 Statistical analysis: Statistical analysis and graphs were generated with GraphPad Prism software (Version 7.0; GraphPad, USA). Graphs represent mean ± sem values from three independent experiments. Statistical significance was determined at $P < 0.05$ using one-way ANOVA or two-way ANOVA followed by Tukey's post hoc analysis whichever was applicable.

Bibliography

1. Arnold, M., et al., *Global Burden of 5 Major Types of Gastrointestinal Cancer.* Gastroenterology, 2020. **159**(1): p. 335-349 e15.
2. Mathur, P., et al., *Cancer Statistics, 2020: Report From National Cancer Registry Programme, India.* JCO Glob Oncol, 2020. **6**: p. 1063-1075.
3. Etemadi, A., et al., *The global, regional, and national burden of stomach cancer in 195 countries, 1990–2017: a systematic analysis for the Global Burden of Disease study 2017.* The Lancet Gastroenterology & Hepatology, 2020. **5**(1): p. 42-54.
4. Topi, S., et al., *Gastric Cancer in History: A Perspective Interdisciplinary Study.* Cancers (Basel), 2020. **12**(2).
5. Smith, R.D. and M.K. Mallath, *History of the Growing Burden of Cancer in India: From Antiquity to the 21st Century.* J Glob Oncol, 2019. **5**: p. 1-15.
6. Vyas, K., et al., *www. ijrap. net.*
7. Santoro, E., *The history of gastric cancer: legends and chronicles.* Gastric Cancer, 2005. **8**(2): p. 71-4.
8. El-Omar, E.M., et al., *Interleukin-1 polymorphisms associated with increased risk of gastric cancer.* Nature, 2000. **404**(6776): p. 398-402.
9. El-Omar, E.M., *Role of host genetic susceptibility in the pathogenesis of gastric cancer*, in *The Biology of Gastric Cancers*2009, Springer. p. 235-250.
10. García-González, M.A. and A. Lanas, *Genetic susceptibility and gastric cancer risk: the importance of meta-analyses as a statistical tool.* Gastroenterologia y hepatologia, 2014. **37**(7): p. 421-426.
11. Kaurah, P. and D.G. Huntsman, *Hereditary diffuse gastric cancer.* GeneReviews®[Internet], 2018.
12. Dhillon, P.K., et al., *Family history of cancer and risk of esophageal and gastric cancers in the United States.* International journal of cancer, 2001. **93**(1): p. 148-152.
13. Wroblewski, L.E., R.M. Peek, Jr., and K.T. Wilson, *Helicobacter pylori and gastric cancer: factors that modulate disease risk.* Clin Microbiol Rev, 2010. **23**(4): p. 713-39.
14. Yu, H., et al., *Association of ABO Blood Groups and Risk of Gastric Cancer.* Scand J Surg, 2020. **109**(4): p. 309-313.
15. Mao, Y., et al., *Blood groups A and AB are associated with increased gastric cancer risk: evidence from a large genetic study and systematic review.* BMC Cancer, 2019. **19**(1): p. 164.
16. Murphy, G., et al., *Cancer Risk After Pernicious Anemia in the US Elderly Population.* Clin Gastroenterol Hepatol, 2015. **13**(13): p. 2282-9 e1-4.
17. Tsugane, S., *Salt, salted food intake, and risk of gastric cancer: epidemiologic evidence.* Cancer Sci, 2005. **96**(1): p. 1-6.
18. Peleteiro, B., et al., *Salt intake and gastric cancer risk according to Helicobacter pylori infection, smoking, tumour site and histological type.* Br J Cancer, 2011. **104**(1): p. 198-207.
19. Yuan, W., N. Yang, and X. Li, *Advances in Understanding How Heavy Metal Pollution Triggers Gastric Cancer.* Biomed Res Int, 2016. **2016**: p. 7825432.
20. Yin, J., et al., *Impact of environmental factors on gastric cancer: A review of the scientific evidence, human prevention and adaptation.* J Environ Sci (China), 2020. **89**: p. 65-79.
21. Raj, A., J.F. Mayberry, and T. Podas, *Occupation and gastric cancer.* Postgrad Med J, 2003. **79**(931): p. 252-8.

22.   Piazuelo, M.B., M. Epplein, and P. Correa, *Gastric cancer: an infectious disease.* Infect Dis Clin North Am, 2010. **24**(4): p. 853-69, vii.

23.   Warren, J.R. and B. Marshall, *Unidentified curved bacilli on gastric epithelium in active chronic gastritis.* The lancet, 1983. **321**(8336): p. 1273-1275.

24.   Marshall, B.J., et al., *Attempt to fulfil Koch's postulates for pyloric Campylobacter.* Med J Aust, 1985. **142**(8): p. 436-9.

25.   Morris, A. and G. Nicholson, *Ingestion of Campylobacter pyloridis causes gastritis and raised fasting gastric pH.* Am J Gastroenterol, 1987. **82**(3): p. 192-9.

26.   Marshall, B. and C. Goodwin, *Revised nomenclature of Campylobacter pyloridis.* International Journal of Systematic and Evolutionary Microbiology, 1987. **37**(1): p. 68-68.

27.   Goodwin, C.S., et al., *Transfer of Campylobacter pylori and Campylobacter mustelae to Helicobacter gen. nov. as Helicobacter pylori comb. nov. and Helicobacter mustelae comb. nov., respectively.* International Journal of Systematic and Evolutionary Microbiology, 1989. **39**(4): p. 397-405.

28.   *Infection with Helicobacter pylori.* IARC Monogr Eval Carcinog Risks Hum, 1994. **61**: p. 177-240.

29.   Brown, L.M., *Helicobacter pylori: epidemiology and routes of transmission.* Epidemiol Rev, 2000. **22**(2): p. 283-97.

30.   Hooi, J.K.Y., et al., *Global Prevalence of Helicobacter pylori Infection: Systematic Review and Meta-Analysis.* Gastroenterology, 2017. **153**(2): p. 420-429.

31.   Khalifa, M.M., R.R. Sharaf, and R.K. Aziz, *Helicobacter pylori: a poor man's gut pathogen?* Gut pathogens, 2010. **2**(1): p. 1-12.

32.   Awuku, Y.A., et al., *Prevalence of helicobacter pylori infection among children living in a rural setting in Sub-Saharan Africa.* BMC Public Health, 2017. **17**(1): p. 360.

33.   Kayali, S., et al., *Helicobacter pylori, transmission routes and recurrence of infection: state of the art.* Acta Biomed, 2018. **89**(8-S): p. 72-76.

34.   Zhang, Y.Y., et al., *Review article: 'true' re-infection of Helicobacter pylori after successful eradication--worldwide annual rates, risk factors and clinical implications.* Aliment Pharmacol Ther, 2009. **29**(2): p. 145-60.

35.   Cover, T.L. and M.J. Blaser, *Helicobacter pylori in health and disease.* Gastroenterology, 2009. **136**(6): p. 1863-73.

36.   Das, A., et al., *Gastric microbiome of Indian patients with Helicobacter pylori infection, and their interaction networks.* Sci Rep, 2017. **7**(1): p. 15438.

37.   Schreiber, S., et al., *The spatial orientation of Helicobacter pylori in the gastric mucus.* Proc Natl Acad Sci U S A, 2004. **101**(14): p. 5024-9.

38.   Bucker, R., et al., *Helicobacter pylori colonization critically depends on postprandial gastric conditions.* Sci Rep, 2012. **2**: p. 994.

39.   Behrens, W., et al., *Localisation and protein-protein interactions of the Helicobacter pylori taxis sensor TlpD and their connection to metabolic functions.* Scientific reports, 2016. **6**(1): p. 1-20.

40.   Oh, J.D., S.M. Karam, and J.I. Gordon, *Intracellular Helicobacter pylori in gastric epithelial progenitors.* Proc Natl Acad Sci U S A, 2005. **102**(14): p. 5186-91.

41.   Chu, Y.T., et al., *Invasion and multiplication of Helicobacter pylori in gastric epithelial cells and implications for antibiotic resistance.* Infect Immun, 2010. **78**(10): p. 4157-65.

42.   Huang, Y., et al., *Adhesion and Invasion of Gastric Mucosa Epithelial Cells by Helicobacter pylori.* Front Cell Infect Microbiol, 2016. **6**: p. 159.

43.   Morales-Espinosa, R., et al., *High expression of Helicobacter pylori VapD in both the intracellular environment and biopsies from gastric patients with severity.* PLoS One, 2020. **15**(3): p. e0230220.

44.   Beasley, D.E., et al., *The Evolution of Stomach Acidity and Its Relevance to the Human Microbiome.* PLoS One, 2015. **10**(7): p. e0134116.

45.   Meyer-Rosberg, K., et al., *The effect of environmental pH on the proton motive force of Helicobacter pylori.* Gastroenterology, 1996. **111**(4): p. 886-900.

46.   Sachs, G., et al., *Acid, protons and Helicobacter pylori.* Yale J Biol Med, 1996. **69**(3): p. 301-16.

47.   Morgan, D.R., et al., *Growth of Campylobacter pylori in liquid media.* J Clin Microbiol, 1987. **25**(11): p. 2123-5.

48.   Stingl, K., et al., *Energetics of Helicobacter pylori and its implications for the mechanism of urease-dependent acid tolerance at pH 1.* J Bacteriol, 2002. **184**(11): p. 3053-60.

49.   Mobley, H.L., M.D. Island, and R.P. Hausinger, *Molecular biology of microbial ureases.* Microbiol Rev, 1995. **59**(3): p. 451-80.

50.   Jones, M.D., Y. Li, and D.B. Zamble, *Acid-responsive activity of the Helicobacter pylori metalloregulator NikR.* Proc Natl Acad Sci U S A, 2018. **115**(36): p. 8966-8971.

51.   van Vliet, A.H., F.D. Ernst, and J.G. Kusters, *NikR-mediated regulation of Helicobacter pylori acid adaptation.* Trends Microbiol, 2004. **12**(11): p. 489-94.

52.   Weeks, D.L., et al., *A H+-gated urea channel: the link between Helicobacter pylori urease and gastric colonization.* Science, 2000. **287**(5452): p. 482-5.

53.   Takahashi-Kanemitsu, A., C.T. Knight, and M. Hatakeyama, *Molecular anatomy and pathogenic actions of Helicobacter pylori CagA that underpin gastric carcinogenesis.* Cellular & molecular immunology, 2020. **17**(1): p. 50-63.

54.   Scott, D.R., et al., *Mechanisms of acid resistance due to the urease system of Helicobacter pylori.* Gastroenterology, 2002. **123**(1): p. 187-95.

55.   Krishnamurthy, P., et al., *Helicobacter pylori containing only cytoplasmic urease is susceptible to acid.* Infect Immun, 1998. **66**(11): p. 5060-6.

56.   Phadnis, S.H., et al., *Surface localization of Helicobacter pylori urease and a heat shock protein homolog requires bacterial autolysis.* Infect Immun, 1996. **64**(3): p. 905-12.

57.   Dunn, B.E., et al., *Localization of Helicobacter pylori urease and heat shock protein in human gastric biopsies.* Infect Immun, 1997. **65**(4): p. 1181-8.

58.   Ha, N.-C. and B.-H. Oh, *The importance of the surface urease of Helicobacter pylori: a reconciling picture: Response from Ha and Oh.* TRENDS in Microbiology, 2001. **9**(11): p. 534.

59.   Sachs, G., et al., *The importance of the surface urease of Helicobacter pylori: fact or fiction?* TRENDS in Microbiology, 2001. **9**(11): p. 532-534.

60.   Stingl, K., K. Altendorf, and E.P. Bakker, *Acid survival of Helicobacter pylori: how does urease activity trigger cytoplasmic pH homeostasis?* Trends in microbiology, 2002. **10**(2): p. 70-74.

61.   Ha, N.C., et al., *Supramolecular assembly and acid resistance of Helicobacter pylori urease.* Nat Struct Biol, 2001. **8**(6): p. 505-9.

62.   Debowski, A.W., et al., *Helicobacter pylori gene silencing in vivo demonstrates urease is essential for chronic infection.* PLoS Pathog, 2017. **13**(6): p. e1006464.

63.   Sachs, G., D.R. Scott, and Y. Wen, *Gastric infection by Helicobacter pylori.* Curr Gastroenterol Rep, 2011. **13**(6): p. 540-6.

64.   Johansson, M.E., H. Sjovall, and G.C. Hansson, *The gastrointestinal mucus system in health and disease.* Nat Rev Gastroenterol Hepatol, 2013. **10**(6): p. 352-61.

65. Leal, J., H.D.C. Smyth, and D. Ghosh, *Physicochemical properties of mucus and their impact on transmucosal drug delivery.* Int J Pharm, 2017. **532**(1): p. 555-572.

66. Phillipson, M., et al., *The importance of mucus layers and bicarbonate transport in preservation of gastric juxtamucosal pH.* Am J Physiol Gastrointest Liver Physiol, 2002. **282**(2): p. G211-9.

67. Huang, J.Y., et al., *Multiple Acid Sensors Control Helicobacter pylori Colonization of the Stomach.* PLoS Pathog, 2017. **13**(1): p. e1006118.

68. Huang, J.Y., et al., *Chemodetection and Destruction of Host Urea Allows Helicobacter pylori to Locate the Epithelium.* Cell Host Microbe, 2015. **18**(2): p. 147-56.

69. Gu, H., *Role of Flagella in the Pathogenesis of Helicobacter pylori.* Curr Microbiol, 2017. **74**(7): p. 863-869.

70. Celli, J.P., et al., *Helicobacter pylori moves through mucus by reducing mucin viscoelasticity.* Proc Natl Acad Sci U S A, 2009. **106**(34): p. 14321-6.

71. Howitt, M.R., et al., *ChePep controls Helicobacter pylori Infection of the gastric glands and chemotaxis in the Epsilonproteobacteria.* mBio, 2011. **2**(4).

72. Kao, C.Y., et al., *Higher motility enhances bacterial density and inflammatory response in dyspeptic patients infected with Helicobacter pylori.* Helicobacter, 2012. **17**(6): p. 411-6.

73. Sycuro, L.K., et al., *Multiple peptidoglycan modification networks modulate Helicobacter pylori's cell shape, motility, and colonization potential.* PLoS Pathog, 2012. **8**(3): p. e1002603.

74. Sycuro, L.K., et al., *Peptidoglycan crosslinking relaxation promotes Helicobacter pylori's helical shape and stomach colonization.* Cell, 2010. **141**(5): p. 822-33.

75. Cover, T.L., et al., *Divergence of genetic sequences for the vacuolating cytotoxin among Helicobacter pylori strains.* J Biol Chem, 1994. **269**(14): p. 10566-73.

76. Alm, R.A., et al., *Comparative genomics of Helicobacter pylori: analysis of the outer membrane protein families.* Infect Immun, 2000. **68**(7): p. 4155-68.

77. Trust, T.J., et al., *High-affinity binding of the basement membrane proteins collagen type IV and laminin to the gastric pathogen Helicobacter pylori.* Infect Immun, 1991. **59**(12): p. 4398-404.

78. Oleastro, M. and A. Menard, *The Role of Helicobacter pylori Outer Membrane Proteins in Adherence and Pathogenesis.* Biology (Basel), 2013. **2**(3): p. 1110-34.

79. Ilver, D., et al., *Helicobacter pylori adhesin binding fucosylated histo-blood group antigens revealed by retagging.* Science, 1998. **279**(5349): p. 373-377.

80. Bugaytsova, J.A., et al., *Helicobacter pylori Adapts to Chronic Infection and Gastric Disease via pH-Responsive BabA-Mediated Adherence.* Cell Host Microbe, 2017. **21**(3): p. 376-389.

81. Kwok, T., et al., *Helicobacter exploits integrin for type IV secretion and kinase activation.* Nature, 2007. **449**(7164): p. 862-6.

82. Koniger, V., et al., *Helicobacter pylori exploits human CEACAMs via HopQ for adherence and translocation of CagA.* Nat Microbiol, 2016. **2**: p. 16188.

83. Moonens, K., et al., *Helicobacter pylori adhesin HopQ disrupts trans dimerization in human CEACAMs.* EMBO J, 2018. **37**(13).

84. Xu, C., et al., *Virulence of Helicobacter pylori outer membrane proteins: an updated review.* Eur J Clin Microbiol Infect Dis, 2020. **39**(10): p. 1821-1830.

85. Valkonen, K.H., T. Wadstrom, and A.P. Moran, *Interaction of lipopolysaccharides of Helicobacter pylori with basement membrane protein laminin.* Infect Immun, 1994. **62**(9): p. 3640-8.

86.   Edwards, N.J., et al., *Lewis X structures in the O antigen side-chain promote adhesion of Helicobacter pylori to the gastric epithelium.* Mol Microbiol, 2000. **35**(6): p. 1530-9.

87.   Horridge, D.N., et al., *Outer inflammatory protein a (OipA) of Helicobacter pylori is regulated by host cell contact and mediates CagA translocation and interleukin-8 response only in the presence of a functional cag pathogenicity island type IV secretion system.* Pathog Dis, 2017. **75**(8).

88.   Mahdavi, J., et al., *Helicobacter pylori SabA adhesin in persistent infection and chronic inflammation.* Science, 2002. **297**(5581): p. 573-8.

89.   Pang, S.S., et al., *The three-dimensional structure of the extracellular adhesion domain of the sialic acid-binding adhesin SabA from Helicobacter pylori.* J Biol Chem, 2014. **289**(10): p. 6332-6340.

90.   Noto, J.M. and R.M. Peek, Jr., *The Helicobacter pylori cag Pathogenicity Island.* Methods Mol Biol, 2012. **921**: p. 41-50.

91.   Tomb, J.F., et al., *The complete genome sequence of the gastric pathogen Helicobacter pylori.* Nature, 1997. **388**(6642): p. 539-47.

92.   Winans, S.C., D.L. Burns, and P.J. Christie, *Adaptation of a conjugal transfer system for the export of pathogenic macromolecules.* Trends in microbiology, 1996. **4**(2): p. 64.

93.   Christie, P.J., *The cag pathogenicity island: mechanistic insights.* Trends in microbiology, 1997. **5**(7): p. 264-265.

94.   Fischer, W., et al., *Four Chromosomal Type IV Secretion Systems in Helicobacter pylori: Composition, Structure and Function.* Front Microbiol, 2020. **11**: p. 1592.

95.   Jimenez-Soto, L.F., et al., *Helicobacter pylori type IV secretion apparatus exploits beta1 integrin in a novel RGD-independent manner.* PLoS Pathog, 2009. **5**(12): p. e1000684.

96.   Wessler, S. and S. Backert, *Molecular mechanisms of epithelial-barrier disruption by Helicobacter pylori.* Trends Microbiol, 2008. **16**(8): p. 397-405.

97.   Tegtmeyer, N., S. Wessler, and S. Backert, *Role of the cag-pathogenicity island encoded type IV secretion system in Helicobacter pylori pathogenesis.* FEBS J, 2011. **278**(8): p. 1190-202.

98.   Tegtmeyer, N., et al., *A small fibronectin-mimicking protein from bacteria induces cell spreading and focal adhesion formation.* J Biol Chem, 2010. **285**(30): p. 23515-26.

99.   Camorlinga-Ponce, M., et al., *Topographical localisation of cagA positive and cagA negative Helicobacter pylori strains in the gastric mucosa; an in situ hybridisation study.* J Clin Pathol, 2004. **57**(8): p. 822-8.

100.   Waskito, L.A., et al., *Distribution and clinical associations of integrating conjugative elements and cag pathogenicity islands of Helicobacter pylori in Indonesia.* Sci Rep, 2018. **8**(1): p. 6073.

101.   Kim, S.S., et al., *Helicobacter pylori in the pathogenesis of gastric cancer and gastric lymphoma.* Cancer Lett, 2011. **305**(2): p. 228-38.

102.   Alfarouk, K.O., et al., *The Possible Role of Helicobacter pylori in Gastric Cancer and Its Management.* Front Oncol, 2019. **9**: p. 75.

103.   Covacci, A., et al., *Molecular characterization of the 128-kDa immunodominant antigen of Helicobacter pylori associated with cytotoxicity and duodenal ulcer.* Proc Natl Acad Sci U S A, 1993. **90**(12): p. 5791-5.

104.   Odenbreit, S., et al., *Translocation of Helicobacter pylori CagA into gastric epithelial cells by type IV secretion.* Science, 2000. **287**(5457): p. 1497-500.

105.   Jungblut, P.R., et al., *Comparative proteome analysis of Helicobacter pylori.* Mol Microbiol, 2000. **36**(3): p. 710-25.

106. Jimenez-Soto, L.F. and R. Haas, *The CagA toxin of Helicobacter pylori: abundant production but relatively low amount translocated.* Sci Rep, 2016. **6**: p. 23227.

107. Naito, M., et al., *Influence of EPIYA-repeat polymorphism on the phosphorylation-dependent biological activity of Helicobacter pylori CagA.* Gastroenterology, 2006. **130**(4): p. 1181-90.

108. Takahashi-Kanemitsu, A., C.T. Knight, and M. Hatakeyama, *Molecular anatomy and pathogenic actions of Helicobacter pylori CagA that underpin gastric carcinogenesis.* Cell Mol Immunol, 2020. **17**(1): p. 50-63.

109. Higashi, H., et al., *EPIYA motif is a membrane-targeting signal of Helicobacter pylori virulence factor CagA in mammalian cells.* J Biol Chem, 2005. **280**(24): p. 23130-7.

110. Tammer, I., et al., *Activation of Abl by Helicobacter pylori: a novel kinase for CagA and crucial mediator of host cell scattering.* Gastroenterology, 2007. **132**(4): p. 1309-19.

111. Tsutsumi, R., et al., *Attenuation of Helicobacter pylori CagA· SHP-2 signaling by interaction between CagA and C-terminal Src kinase.* Journal of Biological Chemistry, 2003. **278**(6): p. 3664-3670.

112. Selbach, M., et al., *The Helicobacter pylori CagA protein induces cortactin dephosphorylation and actin rearrangement by c-Src inactivation.* EMBO J, 2003. **22**(3): p. 515-28.

113. Asahi, M., et al., *Helicobacter pylori CagA protein can be tyrosine phosphorylated in gastric epithelial cells.* J Exp Med, 2000. **191**(4): p. 593-602.

114. Selbach, M., et al., *Src is the kinase of the Helicobacter pylori CagA protein in vitro and in vivo.* J Biol Chem, 2002. **277**(9): p. 6775-8.

115. Poppe, M., et al., *Phosphorylation of Helicobacter pylori CagA by c-Abl leads to cell motility.* Oncogene, 2007. **26**(24): p. 3462-72.

116. Segal, E.D., et al., *Altered states: involvement of phosphorylated CagA in the induction of host cellular growth changes by Helicobacter pylori.* Proc Natl Acad Sci U S A, 1999. **96**(25): p. 14559-64.

117. Moese, S., et al., *Helicobacter pylori induces AGS cell motility and elongation via independent signaling pathways.* Infect Immun, 2004. **72**(6): p. 3646-9.

118. Moese, S., et al., *The Helicobacter pylori CagA protein disrupts matrix adhesion of gastric epithelial cells by dephosphorylation of vinculin.* Cell Microbiol, 2007. **9**(5): p. 1148-61.

119. Jones, K.R., J.M. Whitmire, and D.S. Merrell, *A Tale of Two Toxins: Helicobacter Pylori CagA and VacA Modulate Host Pathways that Impact Disease.* Front Microbiol, 2010. **1**: p. 115.

120. Salama, N.R., M.L. Hartung, and A. Muller, *Life in the human stomach: persistence strategies of the bacterial pathogen Helicobacter pylori.* Nat Rev Microbiol, 2013. **11**(6): p. 385-99.

121. Chmiela, M., N. Walczak, and K. Rudnicka, *Helicobacter pylori outer membrane vesicles involvement in the infection development and Helicobacter pylori-related diseases.* J Biomed Sci, 2018. **25**(1): p. 78.

122. Olofsson, A., et al., *Biochemical and functional characterization of Helicobacter pylori vesicles.* Mol Microbiol, 2010. **77**(6): p. 1539-55.

123. Shimoda, A., et al., *Exosomes as nanocarriers for systemic delivery of the Helicobacter pylori virulence factor CagA.* Sci Rep, 2016. **6**: p. 18346.

124. Leunk, R.D., et al., *Cytotoxic activity in broth-culture filtrates of Campylobacter pylori.* J Med Microbiol, 1988. **26**(2): p. 93-9.

125. Cover, T.L. and M.J. Blaser, *Purification and characterization of the vacuolating toxin from Helicobacter pylori.* J Biol Chem, 1992. **267**(15): p. 10570-5.

126. Atherton, J.C., et al., *Mosaicism in vacuolating cytotoxin alleles of Helicobacter pylori. Association of specific vacA types with cytotoxin production and peptic ulceration.* J Biol Chem, 1995. **270**(30): p. 17771-7.

127. Rhead, J.L., et al., *A new Helicobacter pylori vacuolating cytotoxin determinant, the intermediate region, is associated with gastric cancer.* Gastroenterology, 2007. **133**(3): p. 926-36.

128. Chung, C., et al., *Diversity of VacA intermediate region among Helicobacter pylori strains from several regions of the world.* J Clin Microbiol, 2010. **48**(3): p. 690-6.

129. Foegeding, N.J., et al., *An Overview of Helicobacter pylori VacA Toxin Biology.* Toxins (Basel), 2016. **8**(6).

130. Nguyen, V.Q., R.M. Caprioli, and T.L. Cover, *Carboxy-terminal proteolytic processing of Helicobacter pylori vacuolating toxin.* Infect Immun, 2001. **69**(1): p. 543-6.

131. Utsch, C. and R. Haas, *VacA's Induction of VacA-Containing Vacuoles (VCVs) and Their Immunomodulatory Activities on Human T Cells.* Toxins (Basel), 2016. **8**(6).

132. Ilver, D., et al., *Helicobacter pylori toxin VacA is transferred to host cells via a novel contact-dependent mechanism.* Cell Microbiol, 2004. **6**(2): p. 167-74.

133. Lupetti, P., et al., *Oligomeric and subunit structure of the Helicobacter pylori vacuolating cytotoxin.* J Cell Biol, 1996. **133**(4): p. 801-7.

134. Chambers, M.G., et al., *Structural analysis of the oligomeric states of Helicobacter pylori VacA toxin.* J Mol Biol, 2013. **425**(3): p. 524-35.

135. Cover, T.L., P.I. Hanson, and J.E. Heuser, *Acid-induced dissociation of VacA, the Helicobacter pylori vacuolating cytotoxin, reveals its pattern of assembly.* J Cell Biol, 1997. **138**(4): p. 759-69.

136. Yahiro, K., et al., *Activation of Helicobacter pylori VacA toxin by alkaline or acid conditions increases its binding to a 250-kDa receptor protein-tyrosine phosphatase beta.* J Biol Chem, 1999. **274**(51): p. 36693-9.

137. Sewald, X., W. Fischer, and R. Haas, *Sticky socks: Helicobacter pylori VacA takes shape.* Trends Microbiol, 2008. **16**(3): p. 89-92.

138. Fischer, W., et al., *Outer membrane targeting of passenger proteins by the vacuolating cytotoxin autotransporter of Helicobacter pylori.* Infection and immunity, 2001. **69**(11): p. 6769-6775.

139. McClain, M.S., et al., *Acid activation of Helicobacter pylori vacuolating cytotoxin (VacA) results in toxin internalization by eukaryotic cells.* Mol Microbiol, 2000. **37**(2): p. 433-42.

140. Szabo, I., et al., *Formation of anion-selective channels in the cell plasma membrane by the toxin VacA of Helicobacter pylori is required for its biological activity.* EMBO J, 1999. **18**(20): p. 5517-27.

141. Debellis, L., et al., *Helicobacter pylori cytotoxin VacA increases alkaline secretion in gastric epithelial cells.* Am J Physiol Gastrointest Liver Physiol, 2001. **281**(6): p. G1440-8.

142. Montecucco, C. and R. Rappuoli, *Living dangerously: how Helicobacter pylori survives in the human stomach.* Nat Rev Mol Cell Biol, 2001. **2**(6): p. 457-66.

143. Gauthier, N.C., et al., *Helicobacter pylori VacA cytotoxin: a probe for a clathrin-independent and Cdc42-dependent pinocytic pathway routed to late endosomes.* Mol Biol Cell, 2005. **16**(10): p. 4852-66.

144. Mashima, H., et al., *Involvement of vesicle-associated membrane protein 7 in human gastric epithelial cell vacuolation induced by Helicobacter pylori-produced VacA.* Infect Immun, 2008. **76**(6): p. 2296-303.

145. Suzuki, J., et al., *Dynamin is involved in human epithelial cell vacuolation caused by the Helicobacter pylori-produced cytotoxin VacA.* J Clin Invest, 2001. **107**(3): p. 363-70.

146. Hennig, E.E., et al., *Helicobacter pylori VacA cytotoxin interacts with fibronectin and alters HeLa cell adhesion and cytoskeletal organization in vitro.* FEMS Immunol Med Microbiol, 2005. **44**(2): p. 143-50.

147. Terebiznik, M.R., et al., *Effect of Helicobacter pylori's vacuolating cytotoxin on the autophagy pathway in gastric epithelial cells.* Autophagy, 2009. **5**(3): p. 370-9.

148. Yahiro, K., et al., *Low-density lipoprotein receptor-related protein-1 (LRP1) mediates autophagy and apoptosis caused by Helicobacter pylori VacA.* J Biol Chem, 2012. **287**(37): p. 31104-15.

149. Tsugawa, H., et al., *Reactive oxygen species-induced autophagic degradation of Helicobacter pylori CagA is specifically suppressed in cancer stem-like cells.* Cell Host Microbe, 2012. **12**(6): p. 764-77.

150. Necchi, V., et al., *Natural history of Helicobacter pylori VacA toxin in human gastric epithelium in vivo: vacuoles and beyond.* Sci Rep, 2017. **7**(1): p. 14526.

151. Akada, J.K., et al., *Helicobacter pylori CagA inhibits endocytosis of cytotoxin VacA in host cells.* Dis Model Mech, 2010. **3**(9-10): p. 605-17.

152. Baj, J., et al., *Helicobacter pylori Virulence Factors—Mechanisms of Bacterial Pathogenicity in the Gastric Microenvironment.* Cells, 2021. **10**(1): p. 27.

153. Servetas, S.L., D.R. Bridge, and D.S. Merrell, *Molecular mechanisms of gastric cancer initiation and progression by Helicobacter pylori.* Curr Opin Infect Dis, 2016. **29**(3): p. 304-10.

154. Correa, P. and M.B. Piazuelo, *The gastric precancerous cascade.* J Dig Dis, 2012. **13**(1): p. 2-9.

155. Piscione, M., et al., *Eradication of Helicobacter pylori and Gastric Cancer: A Controversial Relationship.* Front Microbiol, 2021. **12**: p. 630852.

156. Wroblewski, L.E. and R.M. Peek, *Helicobacter pylori, cancer, and the gastric microbiota.* Stem Cells, Pre-neoplasia, and Early Cancer of the Upper Gastrointestinal Tract, 2016: p. 393-408.

157. Alipour, M., *Molecular Mechanism of Helicobacter pylori-Induced Gastric Cancer.* J Gastrointest Cancer, 2021. **52**(1): p. 23-30.

158. Cai, X., et al., *Helicobacter felis eradication restores normal architecture and inhibits gastric cancer progression in C57BL/6 mice.* Gastroenterology, 2005. **128**(7): p. 1937-1952.

159. Fritz, E.L., et al., *Incidence of Helicobacter felis and the effect of coinfection with Helicobacter pylori on the gastric mucosa in the African population.* Journal of Clinical Microbiology, 2006. **44**(5): p. 1692-1696.

160. Zhang, X.Y., P.Y. Zhang, and M.A. Aboul-Soud, *From inflammation to gastric cancer: Role of Helicobacter pylori.* Oncol Lett, 2017. **13**(2): p. 543-548.

161. Lauren, P., *The Two Histological Main Types of Gastric Carcinoma: Diffuse and So-Called Intestinal-Type Carcinoma. An Attempt at a Histo-Clinical Classification.* Acta Pathol Microbiol Scand, 1965. **64**: p. 31-49.

162. Machlowska, J., et al., *Gastric Cancer: Epidemiology, Risk Factors, Classification, Genomic Characteristics and Treatment Strategies.* Int J Mol Sci, 2020. **21**(11).

163. Karaman, M.M., et al., *In vivo assessment of Lauren classification for gastric adenocarcinoma using diffusion MRI with a fractional order calculus model.* Eur Radiol, 2021.

164. Assumpcao, P.P., et al., *The diffuse-type gastric cancer epidemiology enigma.* BMC Gastroenterol, 2020. **20**(1): p. 223.

165.	Petryszyn, P., N. Chapelle, and T. Matysiak-Budnik, *Gastric Cancer: Where Are We Heading?* Dig Dis, 2020. **38**(4): p. 280-285.

166.	Berlth, F., et al., *Pathohistological classification systems in gastric cancer: diagnostic relevance and prognostic value.* World J Gastroenterol, 2014. **20**(19): p. 5679-84.

167.	Yin, X., et al., *Prognostic significance of serum inflammation indexes in different Lauren classification of gastric cancer.* Cancer Med, 2021. **10**(3): p. 1103-1119.

168.	Jimenez Fonseca, P., et al., *Lauren subtypes of advanced gastric cancer influence survival and response to chemotherapy: real-world data from the AGAMENON National Cancer Registry.* Br J Cancer, 2017. **117**(6): p. 775-782.

169.	Shi, Y., et al., *SIRT1-targeted miR-543 autophagy inhibition and epithelial–mesenchymal transition promotion in Helicobacter pylori CagA-associated gastric cancer.* Cell death & disease, 2019. **10**(9): p. 1-14.

170.	Lee, D.-G., et al., *Helicobacter pylori CagA promotes Snail-mediated epithelial–mesenchymal transition by reducing GSK-3 activity.* Nature communications, 2014. **5**(1): p. 1-13.

171.	Li, W., et al., *Molecular alterations of cancer cell and tumour microenvironment in metastatic gastric cancer.* Oncogene, 2018. **37**(36): p. 4903-4920.

172.	Kahroba, H., M.S. Hejazi, and N. Samadi, *Exosomes: from carcinogenesis and metastasis to diagnosis and treatment of gastric cancer.* Cell Mol Life Sci, 2019. **76**(9): p. 1747-1758.

173.	Huang, T., et al., *The roles of extracellular vesicles in gastric cancer development, microenvironment, anti-cancer drug resistance, and therapy.* Mol Cancer, 2019. **18**(1): p. 62.

174.	Chen, K.B., et al., *Exosome-mediated peritoneal dissemination in gastric cancer and its clinical applications.* Biomed Rep, 2018. **8**(6): p. 503-509.

175.	Ding, F., et al., *The role of the ubiquitin-proteasome pathway in cancer development and treatment.* Front Biosci (Landmark Ed), 2014. **19**: p. 886-95.

176.	Sun, T., Z. Liu, and Q. Yang, *The role of ubiquitination and deubiquitination in cancer metabolism.* Molecular Cancer, 2020. **19**(1): p. 1-19.

177.	Voutsadakis, I.A., *The ubiquitin–proteasome system and signal transduction pathways regulating epithelial mesenchymal transition of cancer.* Journal of biomedical science, 2012. **19**(1): p. 1-13.

178.	Tracz, M. and W. Bialek, *Beyond K48 and K63: non-canonical protein ubiquitination.* Cell Mol Biol Lett, 2021. **26**(1): p. 1.

179.	Deng, L., et al., *The role of ubiquitination in tumorigenesis and targeted drug discovery.* Signal Transduct Target Ther, 2020. **5**(1): p. 11.

180.	Swatek, K.N. and D. Komander, *Ubiquitin modifications.* Cell Res, 2016. **26**(4): p. 399-422.

181.	Ohtake, F., et al., *K63 ubiquitylation triggers proteasomal degradation by seeding branched ubiquitin chains.* Proc Natl Acad Sci U S A, 2018. **115**(7): p. E1401-E1408.

182.	Collins, G.A. and A.L. Goldberg, *The logic of the 26S proteasome.* Cell, 2017. **169**(5): p. 792-806.

183.	Tsvetkov, P., et al., *Oncogenic addiction to high 26S proteasome level.* Cell death & disease, 2018. **9**(7): p. 1-14.

184.	Alvarez, A., et al., *KCTD5 and Ubiquitin Proteasome Signaling Are Required for Helicobacter pylori Adherence.* Front Cell Infect Microbiol, 2017. **7**: p. 450.

185.	Lamb, A., et al., *Helicobacter pylori CagA activates NF-kappaB by targeting TAK1 for TRAF6-mediated Lys 63 ubiquitination.* EMBO Rep, 2009. **10**(11): p. 1242-9.

186.	Horvat, A., et al., *Helicobacter pylori pathogen regulates p14ARF tumor suppressor and autophagy in gastric epithelial cells.* Oncogene, 2018. **37**(37): p. 5054-5065.

187. Palrasu, M., et al., *Bacterial CagA protein compromises tumor suppressor mechanisms in gastric epithelial cells.* J Clin Invest, 2020. **130**(5): p. 2422-2434.

188. Tsang, Y.H., et al., *Helicobacter pylori CagA targets gastric tumor suppressor RUNX3 for proteasome-mediated degradation.* Oncogene, 2010. **29**(41): p. 5643-50.

189. Gu, H. and B. Jan Fada, *Specificity in Ubiquitination Triggered by Virus Infection.* Int J Mol Sci, 2020. **21**(11).

190. Chaugule, V.K. and H. Walden, *Specificity and disease in the ubiquitin system.* Biochem Soc Trans, 2016. **44**(1): p. 212-27.

191. Buetow, L. and D.T. Huang, *Structural insights into the catalysis and regulation of E3 ubiquitin ligases.* Nat Rev Mol Cell Biol, 2016. **17**(10): p. 626-42.

192. Wang, M., et al., *Functional roles of E3 ubiquitin ligases in gastric cancer.* Oncol Lett, 2020. **20**(4): p. 22.

193. Yong, X., et al., *Helicobacter pylori virulence factor CagA promotes tumorigenesis of gastric cancer via multiple signaling pathways.* Cell Commun Signal, 2015. **13**: p. 30.

194. Ong, J.Y. and J.Z. Torres, *E3 ubiquitin ligases in cancer and their pharmacological targeting*, in *Ubiquitin Proteasome System-Current Insights into Mechanism Cellular Regulation and Disease*2019, IntechOpen.

195. Piedade, W.P. and J.K. Famulski, *E3 ubiquitin ligase-mediated regulation of vertebrate ocular development; new insights into the function of SIAH enzymes.* Biochem Soc Trans, 2021. **49**(1): p. 327-340.

196. Gopalsamy, A., T. Hagen, and K. Swaminathan, *Investigating the molecular basis of Siah1 and Siah2 E3 ubiquitin ligase substrate specificity.* PLoS One, 2014. **9**(9): p. e106547.

197. Famulski, J.K., et al., *Siah regulation of Pard3A controls neuronal cell adhesion during germinal zone exit.* Science, 2010. **330**(6012): p. 1834-8.

198. Zhang, Q., et al., *The substrate binding domains of human SIAH E3 ubiquitin ligases are now crystal clear.* Biochimica et Biophysica Acta (BBA)-General Subjects, 2017. **1861**(1): p. 3095-3105.

199. Ma, B., et al., *The SIAH2-NRF1 axis spatially regulates tumor microenvironment remodeling for tumor progression.* Nat Commun, 2019. **10**(1): p. 1034.

200. Nakayama, K., J. Qi, and Z. Ronai, *The ubiquitin ligase Siah2 and the hypoxia response.* Mol Cancer Res, 2009. **7**(4): p. 443-51.

201. Baba, K. and T. Miyazaki, *Novel Function of E3 Ubiquitin Ligase Siah2 to Regulate ROS Metabolism.* Journal of Biochemistry and Molecular Biology Research, 2016. **2**(2): p. 152-156.

202. Kim, H., et al., *Fine-tuning of Drp1/Fis1 availability by AKAP121/Siah2 regulates mitochondrial adaptation to hypoxia.* Mol Cell, 2011. **44**(4): p. 532-44.

203. Le Moan, N., et al., *Oxygen-dependent cleavage of the p75 neurotrophin receptor triggers stabilization of HIF-1α.* Molecular cell, 2011. **44**(3): p. 476-490.

204. Scortegagna, M., et al., *Siah2 control of T-regulatory cells limits anti-tumor immunity.* Nat Commun, 2020. **11**(1): p. 99.

205. Ghosh, S., et al., *Siah2 modulates sex-dependent metabolic and inflammatory responses in adipose tissue to a high-fat diet challenge.* Biol Sex Differ, 2019. **10**(1): p. 19.

206. Burke, S.J., et al., *The Ubiquitin Ligase SIAH2 Negatively Regulates Glucocorticoid Receptor Activity and Abundance.* Biomedicines, 2021. **9**(1): p. 22.

207. Kim, H., et al., *Siah2 regulates tight junction integrity and cell polarity through control of ASPP2 stability.* Oncogene, 2014. **33**(15): p. 2004-10.

208. Handa, O., Y. Naito, and T. Yoshikawa, *Helicobacter pylori: a ROS-inducing bacterial species in the stomach.* Inflamm Res, 2010. **59**(12): p. 997-1003.

209.   Gobert, A.P. and K.T. Wilson, *Polyamine-and NADPH-dependent generation of ROS during Helicobacter pylori infection: a blessing in disguise.* Free Radical Biology and Medicine, 2017. **105**: p. 16-27.

210.   Willems, P.H., et al., *Redox Homeostasis and Mitochondrial Dynamics.* Cell Metab, 2015. **22**(2): p. 207-18.

211.   Panieri, E. and M.M. Santoro, *ROS homeostasis and metabolism: a dangerous liason in cancer cells.* Cell Death Dis, 2016. **7**(6): p. e2253.

212.   Ma, Q., *Role of nrf2 in oxidative stress and toxicity.* Annu Rev Pharmacol Toxicol, 2013. **53**: p. 401-26.

213.   Baba, K., H. Morimoto, and S. Imaoka, *Seven in absentia homolog 2 (Siah2) protein is a regulator of NF-E2-related factor 2 (Nrf2).* J Biol Chem, 2013. **288**(25): p. 18393-405.

214.   Tamura, M., et al., *Involvement of mitochondrial reactive oxygen species in gastric carcinogenesis.* J Gastrointest Digestive Syst, 2013. **3**: p. 150.

215.   Das, L., et al., *ETS2 and Twist1 promote invasiveness of Helicobacter pylori-infected gastric cancer cells by inducing Siah2.* Biochemical Journal, 2016. **473**(11): p. 1629-1640.

216.   Kokate, S.B., et al., *Testin and filamin-C downregulation by acetylated Siah2 increases invasiveness of Helicobacter pylori-infected gastric cancer cells.* The international journal of biochemistry & cell biology, 2018. **103**: p. 14-24.

217.   Qi, J., et al., *Regulators and effectors of Siah ubiquitin ligases.* Cell Biochem Biophys, 2013. **67**(1): p. 15-24.

218.   Kokate, S.B., et al., *Testin and filamin-C downregulation by acetylated Siah2 increases invasiveness of Helicobacter pylori-infected gastric cancer cells.* Int J Biochem Cell Biol, 2018. **103**: p. 14-24.

219.   Deshaies, R.J. and C.A. Joazeiro, *RING domain E3 ubiquitin ligases.* Annual review of biochemistry, 2009. **78**.

220.   Amemiya, Y., P. Azmi, and A. Seth, *Autoubiquitination of BCA2 RING E3 ligase regulates its own stability and affects cell migration.* Mol Cancer Res, 2008. **6**(9): p. 1385-96.

221.   Shah, M., et al., *Inhibition of Siah2 ubiquitin ligase by vitamin K3 (menadione) attenuates hypoxia and MAPK signaling and blocks melanoma tumorigenesis.* Pigment Cell Melanoma Res, 2009. **22**(6): p. 799-808.

222.   Chillappagari, S., et al., *SIAH2-mediated and organ-specific restriction of HO-1 expression by a dual mechanism.* Sci Rep, 2020. **10**(1): p. 2268.

223.   Kokate, S.B., et al., *Acetylation-mediated Siah2 stabilization enhances PHD3 degradation in Helicobacter pylori-infected gastric epithelial cancer cells.* FASEB J, 2018. **32**(10): p. 5378-5389.

224.   Xu, D. and C. Li, *Regulation of the SIAH2-HIF-1 Axis by Protein Kinases and Its Implication in Cancer Therapy.* Front Cell Dev Biol, 2021. **9**: p. 646687.

225.   Garcia-Limones, C., et al., *CHK2 stability is regulated by the E3 ubiquitin ligase SIAH2.* Oncogene, 2016. **35**(33): p. 4289-301.

226.   Grishina, I., et al., *SIAH-mediated ubiquitination and degradation of acetyl-transferases regulate the p53 response and protein acetylation.* Biochim Biophys Acta, 2012. **1823**(12): p. 2287-96.

227.   Perez, M., et al., *Mutual regulation between SIAH2 and DYRK2 controls hypoxic and genotoxic signaling pathways.* J Mol Cell Biol, 2012. **4**(5): p. 316-30.

228.   Khurana, A., et al., *Regulation of the ring finger E3 ligase Siah2 by p38 MAPK.* J Biol Chem, 2006. **281**(46): p. 35316-26.

229.   Sarkar, T.R., et al., *Identification of a Src tyrosine kinase/SIAH2 E3 ubiquitin ligase pathway that regulates C/EBPδ expression and contributes to transformation of breast tumor cells.* Molecular and cellular biology, 2012. **32**(2): p. 320-332.

230.   Das, L., et al., *ETS2 and Twist1 promote invasiveness of Helicobacter pylori-infected gastric cancer cells by inducing Siah2.* Biochem J, 2016. **473**(11): p. 1629-40.

231.   Pan, X.Y., Y.N. Zhang, and H.B. Shen, *Large-scale prediction of human protein-protein interactions from amino acid sequence based on latent topic features.* J Proteome Res, 2010. **9**(10): p. 4992-5001.

232.   Zhang, Y., et al., *PIWIL2 suppresses Siah2-mediated degradation of HDAC3 and facilitates CK2α-mediated HDAC3 phosphorylation.* Cell death & disease, 2018. **9**(4): p. 1-11.

233.   Blom, N., S. Gammeltoft, and S. Brunak, *Sequence and structure-based prediction of eukaryotic protein phosphorylation sites.* J Mol Biol, 1999. **294**(5): p. 1351-62.

234.   Ardito, F., et al., *The crucial role of protein phosphorylation in cell signaling and its use as targeted therapy.* International journal of molecular medicine, 2017. **40**(2): p. 271-280.

235.   Pichaud, F., R.F. Walther, and F. Nunes de Almeida, *Regulation of Cdc42 and its effectors in epithelial morphogenesis.* J Cell Sci, 2019. **132**(10).

236.   Unbekandt, M., et al., *Discovery of Potent and Selective MRCK Inhibitors with Therapeutic Effect on Skin Cancer.* Cancer Res, 2018. **78**(8): p. 2096-2114.

237.   Rose, C.M., et al., *Highly Multiplexed Quantitative Mass Spectrometry Analysis of Ubiquitylomes.* Cell Syst, 2016. **3**(4): p. 395-403 e4.

238.   Calzado, M.A., et al., *An inducible autoregulatory loop between HIPK2 and Siah2 at the apex of the hypoxic response.* Nature cell biology, 2009. **11**(1): p. 85-91.

239.   Zhou, H., et al., *Toward a comprehensive characterization of a human cancer cell phosphoproteome.* J Proteome Res, 2013. **12**(1): p. 260-71.

240.   Jain, U., K. Saxena, and N. Chauhan, *Helicobacter pylori induced reactive oxygen Species: A new and developing platform for detection.* Helicobacter, 2021: p. e12796.

241.   Butcher, L.D., et al., *Oxidative stress resulting from Helicobacter pylori infection contributes to gastric carcinogenesis.* Cellular and molecular gastroenterology and hepatology, 2017. **3**(3): p. 316-322.

242.   Kountouras, J., et al., *Impact of reactive oxygen species generation on Helicobacter pylori-related extragastric diseases: a hypothesis.* Free radical research, 2017. **51**(1): p. 73-79.

243.   Dauer, P., et al., *ER stress sensor, glucose regulatory protein 78 (GRP78) regulates redox status in pancreatic cancer thereby maintaining "stemness".* Cell Death Dis, 2019. **10**(2): p. 132.

244.   Teng, J., et al., *Down-regulation of GRP78 alleviates lipopolysaccharide-induced acute kidney injury.* Int Urol Nephrol, 2018. **50**(11): p. 2099-2107.

245.   Pizzino, G., et al., *Oxidative Stress: Harms and Benefits for Human Health.* Oxid Med Cell Longev, 2017. **2017**: p. 8416763.

246.   Butcher, L.D., et al., *Oxidative Stress Resulting From Helicobacter pylori Infection Contributes to Gastric Carcinogenesis.* Cell Mol Gastroenterol Hepatol, 2017. **3**(3): p. 316-322.

247.   Ibrahim, I.M., D.H. Abdelmalek, and A.A. Elfiky, *GRP78: A cell's response to stress.* Life Sci, 2019. **226**: p. 156-163.

248.   Suyama, K., et al., *GRP78 suppresses lipid peroxidation and promotes cellular antioxidant levels in glial cells following hydrogen peroxide exposure.* PLoS One, 2014. **9**(1): p. e86951.

249. Dauer, P., et al., *GRP 78-mediated antioxidant response and ABC transporter activity confers chemoresistance to pancreatic cancer cells.* Molecular oncology, 2018. **12**(9): p. 1498-1512.

250. Lai, K.G., et al., *Novel roles of folic acid as redox regulator: Modulation of reactive oxygen species sinker protein expression and maintenance of mitochondrial redox homeostasis on hepatocellular carcinoma.* Tumour Biol, 2017. **39**(6): p. 1010428317702649.

251. Wang, X., et al., *Glucose-regulated protein 78 is essential for cardiac myocyte survival.* Cell Death Differ, 2018. **25**(12): p. 2181-2194.

252. Lu, G., H. Luo, and X. Zhu, *Targeting the GRP78 Pathway for Cancer Therapy.* Front Med (Lausanne), 2020. **7**: p. 351.

253. Wang, Y., et al., *Endoplasmic reticulum proteostasis control and gastric cancer.* Cancer Lett, 2019. **449**: p. 263-271.

254. Namba, T., et al., *Suppression of expression of endoplasmic reticulum chaperones by Helicobacter pylori and its role in exacerbation of non-steroidal anti-inflammatory drug-induced gastric lesions.* J Biol Chem, 2010. **285**(48): p. 37302-13.

255. Baird, M., et al., *The unfolded protein response is activated in Helicobacter-induced gastric carcinogenesis in a non-cell autonomous manner.* Laboratory Investigation, 2013. **93**(1): p. 112-122.

256. Wang, X., et al., *NLRP6 suppresses gastric cancer growth via GRP78 ubiquitination.* Exp Cell Res, 2020. **395**(1): p. 112177.

257. Qian, Y., et al., *Sodium Channel Subunit SCNN1B Suppresses Gastric Cancer Growth and Metastasis via GRP78 Degradation.* Cancer Res, 2017. **77**(8): p. 1968-1982.

258. Sajja, R.K., K.N. Green, and L. Cucullo, *Altered Nrf2 signaling mediates hypoglycemia-induced blood-brain barrier endothelial dysfunction in vitro.* PLoS One, 2015. **10**(3): p. e0122358.

259. Kausar, S., F. Wang, and H. Cui, *The Role of Mitochondria in Reactive Oxygen Species Generation and Its Implications for Neurodegenerative Diseases.* Cells, 2018. **7**(12).

260. Liao, Z., D. Chua, and N.S. Tan, *Reactive oxygen species: a volatile driver of field cancerization and metastasis.* Mol Cancer, 2019. **18**(1): p. 65.

261. Carlucci, A., et al., *Proteolysis of AKAP121 regulates mitochondrial activity during cellular hypoxia and brain ischaemia.* EMBO J, 2008. **27**(7): p. 1073-84.

262. Sun, F.C., et al., *Localization of GRP78 to mitochondria under the unfolded protein response.* Biochem J, 2006. **396**(1): p. 31-9.

263. Li, N., et al., *GRP78 regulates clusterin stability, retrotranslocation and mitochondrial localization under ER stress in prostate cancer.* Oncogene, 2013. **32**(15): p. 1933-42.

264. Ni, M., Y. Zhang, and A.S. Lee, *Beyond the endoplasmic reticulum: atypical GRP78 in cell viability, signalling and therapeutic targeting.* Biochem J, 2011. **434**(2): p. 181-8.

265. Yu, T., J.L. Robotham, and Y. Yoon, *Increased production of reactive oxygen species in hyperglycemic conditions requires dynamic change of mitochondrial morphology.* Proc Natl Acad Sci U S A, 2006. **103**(8): p. 2653-8.

266. Hung, C.H., et al., *A reciprocal relationship between reactive oxygen species and mitochondrial dynamics in neurodegeneration.* Redox Biol, 2018. **14**: p. 7-19.

267. Jezek, J., K.F. Cooper, and R. Strich, *Reactive Oxygen Species and Mitochondrial Dynamics: The Yin and Yang of Mitochondrial Dysfunction and Cancer Progression.* Antioxidants (Basel), 2018. **7**(1).

268. Vasconcellos, L.R., et al., *Protein aggregation as a cellular response to oxidative stress induced by heme and iron.* Proc Natl Acad Sci U S A, 2016. **113**(47): p. E7474-E7482.

269. Luciani, A., et al., *Defective CFTR induces aggresome formation and lung inflammation in cystic fibrosis through ROS-mediated autophagy inhibition.* Nat Cell Biol, 2010. **12**(9): p. 863-75.

270. Casas, C., *GRP78 at the Centre of the Stage in Cancer and Neuroprotection.* Front Neurosci, 2017. **11**: p. 177.

271. Ouyang, Y.B., et al., *Overexpressing GRP78 influences Ca2+ handling and function of mitochondria in astrocytes after ischemia-like stress.* Mitochondrion, 2011. **11**(2): p. 279-86.

272. Sisalli, M.J., et al., *Knocking-out the Siah2 E3 ubiquitin ligase prevents mitochondrial NCX3 degradation, regulates mitochondrial fission and fusion, and restores mitochondrial function in hypoxic neurons.* Cell Commun Signal, 2020. **18**(1): p. 42.

273. Martinez-Reyes, I. and N.S. Chandel, *Mitochondrial TCA cycle metabolites control physiology and disease.* Nat Commun, 2020. **11**(1): p. 102.

274. Kim, I.J., et al., *Helicobacter pylori Infection Modulates Host Cell Metabolism through VacA-Dependent Inhibition of mTORC1.* Cell Host Microbe, 2018. **23**(5): p. 583-593 e8.

275. Jain, P., Z.Q. Luo, and S.R. Blanke, *Helicobacter pylori vacuolating cytotoxin A (VacA) engages the mitochondrial fission machinery to induce host cell death.* Proc Natl Acad Sci U S A, 2011. **108**(38): p. 16032-7.

276. Calvino Fernandez, M. and T. Parra Cid, *H. pylori and mitochondrial changes in epithelial cells. The role of oxidative stress.* Rev Esp Enferm Dig, 2010. **102**(1): p. 41-50.

277. Rodriguez-Gonzalez, A., et al., *Role of the aggresome pathway in cancer: targeting histone deacetylase 6-dependent protein degradation.* Cancer Res, 2008. **68**(8): p. 2557-60.

278. van Dam, L. and T.B. Dansen, *Cross-talk between redox signalling and protein aggregation.* Biochem Soc Trans, 2020. **48**(2): p. 379-397.

279. Levy, E., et al., *Causative Links between Protein Aggregation and Oxidative Stress: A Review.* Int J Mol Sci, 2019. **20**(16).

280. Kopito, R.R., *Aggresomes, inclusion bodies and protein aggregation.* Trends in cell biology, 2000. **10**(12): p. 524-530.

281. Qin, S., C. Jiang, and J. Gao, *Transcriptional factor Nrf2 is essential for aggresome formation during proteasome inhibition.* Biomed Rep, 2019. **11**(6): p. 241-252.

282. Taylor, J.P., et al., *Aggresomes protect cells by enhancing the degradation of toxic polyglutamine-containing protein.* Hum Mol Genet, 2003. **12**(7): p. 749-57.

283. Olzmann, J.A., L. Li, and L.S. Chin, *Aggresome formation and neurodegenerative diseases: therapeutic implications.* Curr Med Chem, 2008. **15**(1): p. 47-60.

284. Zhang, C., et al., *p38delta MAPK regulates aggresome biogenesis by phosphorylating SQSTM1 in response to proteasomal stress.* J Cell Sci, 2018. **131**(14).

285. Hillert, E.K., et al., *Proteasome inhibitor b-AP15 induces enhanced proteotoxicity by inhibiting cytoprotective aggresome formation.* Cancer Lett, 2019. **448**: p. 70-83.

286. Yehia, M., et al., *Association of Aggresomes with Survival Outcomes in Pediatric Medulloblastoma.* Sci Rep, 2019. **9**(1): p. 12605.

287. An, H. and A.V. Statsyuk, *An inhibitor of ubiquitin conjugation and aggresome formation.* Chem Sci, 2015. **6**(9): p. 5235-5245.

288. Yu, C.C., et al., *VCP phosphorylation-dependent interaction partners prevent apoptosis in Helicobacter pylori-infected gastric epithelial cells.* PLoS One, 2013. **8**(1): p. e55724.

289. Carija, A., et al., *Protein aggregation into insoluble deposits protects from oxidative stress.* Redox Biol, 2017. **12**: p. 699-711.

290. Rogers, A.B. and J.G. Fox, *Inflammation and Cancer I. Rodent models of infectious gastrointestinal and liver cancer.* American Journal of Physiology-Gastrointestinal and Liver Physiology, 2004. **286**(3): p. G361-G366.

291. Houghton, J. and T.C. Wang, *Helicobacter pylori and gastric cancer: a new paradigm for inflammation-associated epithelial cancers.* Gastroenterology, 2005. **128**(6): p. 1567-1578.

292. Schindelin, J., et al., *Fiji: an open-source platform for biological-image analysis.* Nature methods, 2012. **9**(7): p. 676-682.

293. Towbin, H., T. Staehelin, and J. Gordon, *Electrophoretic transfer of proteins from polyacrylamide gels to nitrocellulose sheets: procedure and some applications.* Proceedings of the National Academy of Sciences, 1979. **76**(9): p. 4350-4354.

294. Bruder, S.P., N. Jaiswal, and S.E. Haynesworth, *Growth kinetics, self-renewal, and the osteogenic potential of purified human mesenchymal stem cells during extensive subcultivation and following cryopreservation.* Journal of cellular biochemistry, 1997. **64**(2): p. 278-294.

295. Greenwood, S.K., et al., *Population doubling: a simple and more accurate estimation of cell growth suppression in the in vitro assay for chromosomal aberrations that reduces irrelevant positive results.* Environmental and molecular mutagenesis, 2004. **43**(1): p. 36-44.

296. Petrenko, Y., et al., *A comparative analysis of multipotent mesenchymal stromal cells derived from different sources, with a focus on neuroregenerative potential.* Scientific reports, 2020. **10**(1): p. 1-15.

LIST OF PLASMIDS USED

Plasmid	Source
pcDNA3.1+	Cat. No. V79020, Invitrogen
siah2	Cat. No. RG203802, Origene
pEGFP-N1-Cdc42BPB (*mrckβ*)	Cat. No. 50759, Addgene, USA
pEGFP-N1	Gifted by Prof. Naoki Mochizuki, National Cerebral and Cardiovascular Center, Osaka, Japan.
pcDNA3.1(+)-GRP78/BiP	Cat. No. 32701; Addgene
pDsRed2-Mito	Cat. No. 632421; Clontech, USA
siah2 S6A	Generated from *siah2* plasmid
siah2 T275A	Generated from *siah2* plasmid
siah2 T279A	Generated from *siah2* plasmid
siah2 S282A	Generated from *siah2* plasmid

APPENDIX II

LIST OF siRNAs USED

Name	Source
Human *siah2* siRNA	Cat. No. SR304370, Origene
Human negative control siRNA	Cat. No. SR30004, Origene
Human *mrckβ* siRNA	Cat. No. sc-60064, Santa Cruz Biotechnology
Human *grp78* siRNA	Cat. No. sc-29338, Santa Cruz Biotechnology
Human negative control siRNA	Cat. No. sc-37007, Santa Cruz Biotechnology

APPENDIX III

LIST OF PRIMARY ANTIBODIES USED

Antibody	Dilution used	Source
Phospho-Threonine	1:1000	Cat. No. 9386S, Cell Signaling Technology (CST), USA
Phospho-Serine	1:200	Cat. No. P5747, Sigma-Aldrich, USA
Siah2	1:200 , 1:50 (IF), 1:100 (IP)	Cat. No. sc-5507, Santa Cruz Biotechnology
GAPDH	1:2000	Cat. No. 10-10011; ABGENEX Pvt. Ltd., India
MRCKβ	1:400 , 1:100 (IF)	Cat. No. sc-374597, Santa Cruz Biotechnology
Ubiquitin	1:1000	Cat. No. 3936P, CST
P-Ser^6-Siah2	1:250 , 1:100 (IF)	Custom synthesized from Bioklone Biotech Private Limited, India
P-Thr^{279}-Siah2	1:200 , 1:100 (IF)	Custom synthesized from Bioklone Biotech Private Limited, India
GRP78	1:300 , 1:100 (IF)	Cat. No. ab21685; Abcam, USA
Cox IV	1:1000	Cat. No. 4850S, CST

Normal goat IgG	1:1000 (IP)	Cat. No. sc2028, Santa Cruz Biotechnology

WB: Western blot   IF: Immunofluorescence   IP: Immunoprecipitation

Sequence used for generation of Siah2 customized antibodies

Antibody	Peptide used
P-Ser[6]-Siah2	MSRPS<u>S</u>TGPSA
P-Thr[279]-Siah2	EA<u>T</u>PRSIHDGVAAAIMN

The highlighted amino acids in the sequences were phosphorylated.

APPENDIX IV

LIST OF SECONDARY ANTIBODIES USED

Antibody	Conjugate	Dilution used	Source
Anti-mouse	HRP-conjugated	1:2000	Cat. No. 7076S, CST
Anti-rabbit	HRP-conjugated	1:2000	Cat. No. 7074S, CST
Anti-goat	HRP-conjugated	1:2000	Cat. No. ab6741, Abcam
Anti-mouse	Alexa flour 488	1:500	Cat. No. A-11001, Thermo Fisher Scientific
Anti-mouse	Alexa flour 594	1:500	Cat. No. A-11005, Thermo Fisher Scientific
Anti-rabbit	Alexa flour 488	1:500	Cat. No. A-21206, Thermo Fisher Scientific
Anti-rabbit	Alexa flour 594	1:500	Cat. No. A-11012, Thermo Fisher Scientific
Anti-goat	Alexa flour 488	1:500	Cat. No. A-11055, Thermo Fisher Scientific
Anti-goat	Alexa flour 594	1:500	Cat. No. A-11058, Thermo Fisher Scientific

APPENDIX V

PRIMERS USED FOR *SIAH2* SITE-DIRECTED MUTAGENESIS

Mutation	Primer sequence
siah2 S6A	5' CATGAGCCGCCCGTCCGCCACCGGCCCCAGCGC 3'
siah2 T275A	5' GGGAACCGGCGGAGATTGGCCTGGGAGGCCACGCCCC 3'
siah2 T279A	5' AGATTGACCTGGGAGGCCGCGCCCCGTTCGATTCATG 3'
siah2 S282A	5' TGGGAGGCCACGCCCCGTGCGATTCATGACGGTGTGG 3'